THE DEVELOPMENT OF A RADIAL ACTIVE MAGNETIC BEARING

J.D. NEL

Dissertation submitted in partial fulfilment of the requirements for the degree Magister Ingeneriae in Electrical and Electronic Engineering at the North-West University

Supervisor: Prof. G. van Schoor

2004

Potchefstroom

SUMMARY

This dissertation presents the development of a radial active magnetic bearing (AMB). With AMBs the rotor of a machine can be suspended in the air without any direct contact between the stator and the rotor. This makes it a frictionless bearing and eliminates the need for lubrication. The AMB system implements a feedback control system to control the position of the rotor.

The aim of this project is to develop a radial AMB with an air gap of 1 mm and a rotation speed of 3000 rpm. Through this project basic knowledge of magnetic suspension is gained and expertise is established at the Engineering Faculty. The model can be used for further studies and as a demonstration model to illustrate the concept of AMBs.

The model constitutes one radial AMB and one conventional ball bearing supporting a rigid shaft. The AMB system constitutes 1) electromagnets, 2) power amplifiers, 3) position sensors and 4) a control system. Inductive sensors measure the air gap between the shaft and the stator in the vertical and horizontal axis. The sensor signal is fed back to a controller that provides a control signal to the power amplifiers. The power amplifiers control the current through the electromagnets that apply a force on the shaft. The shaft is then suspended in the air. An air pressure turbine is used to propel the shaft up to 3000 rpm.

A homopolar AMB configuration is implemented using mild steel for the electromagnets. The four electromagnets used in the system are designed in terms of a required force. Linear power amplifiers are designed to activate the electromagnets and to eliminate possible noise problems on the sensors. Inductive position sensors are implemented producing a dc voltage proportional to the size of the air gap.

dSpace® software is used to implement the controller. A position sensor value is read in through an analog-to-digital converter channel and subtracted from a reference signal for the position. The error signal is then the input of the controller. The controller sends a control signal via the digital-to-analog converter to the power amplifiers. A PID controller is created in Simulink®. With the aid of dSpace® software the controller is downloaded onto the dSpace card.

Different tests are performed to characterise the system. The step responses in both axes are measured and the percentage overshoots and settling times are determined. Impulse disturbance tests at different speeds are used to calculate the dynamic stiffness and damping of the system. Stable suspension was achieved with the final AMB system at rotation speeds of 3000 rpm. The maximum deviation was found to be less than 0.11 mm from the centre position. The settling time was less than 0.4 s and with no steady state error.

The developed AMB system has a relatively low dynamic stiffness. Future studies can be done to find the effect that each PID parameter has on the dynamic stiffness. It is recommended that the controller be implemented on an embedded microcontroller to eliminate the computer and the dSpace® card.

OPSOMMING

In die verhandeling word die ontwikkeling van 'n radiale Aktiewe Magnetiese Laer (AML) voorgelê. Met AMLs kan die rotor van 'n masjien gesuspendeer word sonder enige fisiese kontak tussen die stator en rotor. Dit is dus 'n wrywinglose laer en elimineer smering. 'n AML maak gebruik van 'n terugvoer-beheer-stelsel om die rotor se posisie te beheer.

Die doel van die projek is om 'n radiale AML te ontwikkel met 'n luggaping van 1 mm en 'n rotasiespoed van 3000 opm. Basiese kennis van magnetiese suspensie word verkry en kundigheid word gevestig in die Fakulteit Ingenieurswese. Die model kan gebruik word vir verdere studies en as 'n demonstrasiemodel om die konsep van AMLs te illustreer.

Die model bestaan uit een AML en een konvensionele koeëllaer wat 'n as ondersteun. Die AML stelsel bestaan uit 1) elektromagnete 2) kragversterkers 3) posisiesensors en 'n 4) beheerstelsel. Induktiewe sensors meet die grootte van die luggaping in die vertikale en horisontale as. Die sensorsein word teruggevoer na 'n beheerder wat 'n beheersein verskaf aan die kragversterkers. Die kragversterkers beheer die stroom deur die elektromagnete wat dan 'n krag op die as uitoefen. Die as word dan in die lug gesuspendeer. 'n Lugdrukturbine word gebruik om die as te laat roteer tot by 3000 opm.

'n Homopolêre konfigurasie is gebruik met elektromagnete wat uit sagte staal vervaardig is. Die vier elektromagnete is ontwerp i.t.v. 'n verlangde krag. Lineêre kragversterkers is ontwerp om die elektromagnete te aktiveer en sodoende ook moontlike geraasprobleme op die sensors te elimineer. Induktiewe posisiesensors is geïmplementeer wat 'n gelykstroomspanning lewer, direk eweredig aan die grootte van die luggaping.

dSpace® sagteware is gebruik om die beheerder te implementeer. Die posisiesensor-uitset word ingelees deur 'n analoog-na-digitaal omsetterkanaal en word afgetrek van 'n verwysingsein vir die posisie. Die foutsein is dan die inset van die beheerder. Die beheerder stuur beheer sein via 'n digital-na-analoog omsetter na die kragversterker. 'n PID beheerder is geskep in Simulink®. Die beheerder word gelaai op die dSpace® kaart met behulp van dSpace® sagteware.

Verskeie toetse is uitgevoer om die stelsel te karakteriseer. Die trapresponse in albei asse is gemeet en die persentasie verbyskiet en vestigingstye is bepaal. Impuls-steuringstoetse by verskillende snelhede is gebruik om die dinamiese styfheid en demping van die stelsel te bepaal. Stabiele suspensie is verkry met die finale AML stelsel by 'n spoed van 3000 opm. Die maksimum afwyking is minder as 0.11 mm. Die vestigngstyd is minder as 0.4 s en daar is geen bestendige toestand fout.

Die ontwikkelde AML stelsel het 'n relatiewe lae styfheid. Verdere studies kan gedoen word om die effek van elke PID parameter op die dinamiese styfheid te bepaal. Dit word aanbeveel om die beheerder te implementeer op 'n ingebedde mikro-beheerder om sodoende die rekenaar en die dSpace® kaart te elimineer.

ACKNOWLEDGEMENTS

I gratefully acknowledge the assistance, guidance and contribution provided by the following people in the light of my project:

- Prof. George van Schoor for his guidance and enthusiasm
- M Tech Industrial for the financial support
- Mr. J. Roberts for his advice and inputs regarding the rotor dynamics
- my parents and Myra for their loyalty and love
- Zebedee and Eugén for their support and friendship

As die Here die huis nie bou nie,
swoeg dié wat daaraan bou, tevergeefs.
As die Here die stad nie beskerm nie,
waak dié wat dit beskerm tevergeefs.-Psalm 127

TABLE OF CONTENTS

LIST OF FIGURES

LIST OF TABLES

LIST OF ABBREVIATIONS

A/D	analogue to digital conversion
ac	alternating current
AMBs	Active Magnetic Bearings
CTR	current transfer ration
D/A	digital to analogue conversion
dc	direct current
GUI	graphical user interface
I/O	input/output
mmf	magnetic motive force
PBMR	Pebble Bed Modular Reactor
PM	phase margin
PWM	pulse width modulation
rpm	revolutions per minute

LIST OF SYMBOLS

ζ	damping factor
η	power amplifier efficiency
θ	one half of the journal sector
μ_0	permeability of free space
μ_r	relatively permeability of the material
τ	time constant
ϕ	magnetic flux
ω_n	natural frequency
ω	rotation speed

A_{iron}	area of the electromagnet pole
A_{window}	window area of the electromagnet
A_{wire}	area of the wire
B	magnetic flux density
b_{eq}	dynamic damping
c	length of electromagnet leg
c_v	viscous damping
e	eccentricity
f_i	force-current constant
F_{max}	total carrying force of the electromagnet
f_0	force at nominal current
G	imbalance quality grade
H	magnetic field intensity
h	height of the coil window
i	current in the coil
I_d	current density
i_0	nominal current
k	actuator constant
K_d	differential gain
k_{eq}	dynamic stiffness
K_i	integral gain
K_p	proportional gain
k_s	stiffness
L_0	nominal coil inductance of a sensor
m	mass
N	amount of coil turns in the electromagnet
N_1	primary windings
N_2	secondary windings
P_{coil}	active power dissipated in the coil
pf	coil packing factor
$R_{\theta cs}$	case to sink thermal resistance
$R_{\theta jc}$	junction to case thermal resistance
$R_{\theta sa}$	sink to ambient thermal resistance
R_{coil}	coil resistance

r_p	radius of the electromagnet
r_{shaft}	shaft raduis
R_{source}	resistance of the source resistor
V_{cc}	supply voltage
V_{ds}	voltage across the drain source of a MOSFET
V_{gs}	voltage across the gate source of a MOSFET
w	width of electromagnet leg
W_m	potential energy stored in a magnetic field wm
x_0	nominal air gap

Chapter 1

Introduction

The aim of this project is to develop a radial Active Magnetic Bearing (AMB) system. The project was initiated by the Pebble Bed Modular Reactor (PBMR) project to establish a knowledgebase in the field of AMB technology. This chapter discusses background on AMBs, the purpose of research, issues to be addressed and the research methodology followed. An overview of the dissertation is also given.

1.1. AMBs and the PBMR

The PBMR is a helium-cooled reactor that uses the Brayton thermodynamic gas cycle to convert nuclear energy into electrical energy [1]. The nuclear energy is generated in the reactor core by nuclear fusion. Helium gas will be used to transfer the energy from the reactor to a turbo-generator unit that will generate electrical power. Figure 1.1 gives a schematic diagram of the PBMR system layout [2]. The fundamental concept of the design is aimed at achieving a plant that has no physical process that could cause a radiation hazard beyond its site boundary. This means that all possible sources of nuclear contamination to the environment must be eliminated.

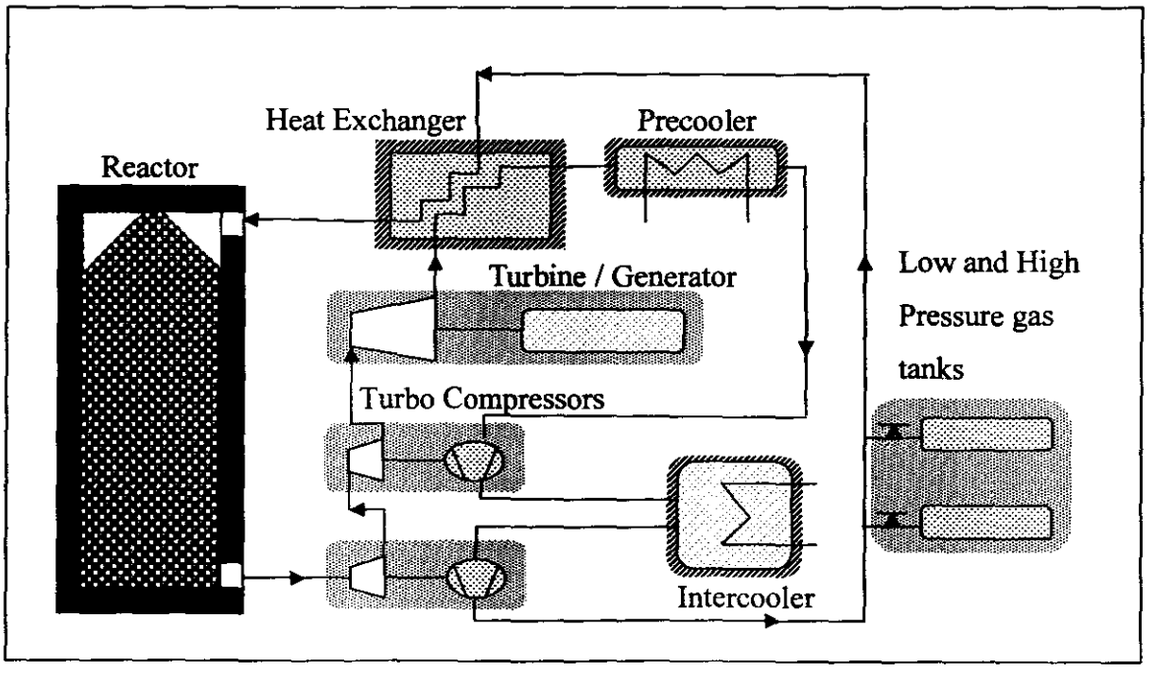

Figure 1.1: PBMR System Layout [3]

To prevent nuclear contamination to the environment helium gas is used as coolant because it is chemically and radiologically inert. If for some reason the helium would escape from the system into the atmosphere it will not hold a contamination risk for the environment. The only other possible source of nuclear contamination in the gas cycle would be oil from the oil film bearings of the compressors, power turbine and generator. For this reason bearings that do not use any kind of lubrication are used.

Magnetic bearings work on the principle that an electromagnet attracts ferromagnetic material. Figure 1.2 shows the basic construction of an AMB. The rotor, made out of ferromagnetic material, can be supported by an electromagnet in the stator of a machine. The purpose of the electromagnet is to apply a force on the rotor to keep a constant air gap between the rotor and the stator. This electromagnet and rotor system is a classical example of an unstable system [3]. Without some kind of feedback the rotor will be attracted to the electromagnet and the two bodies will collide.

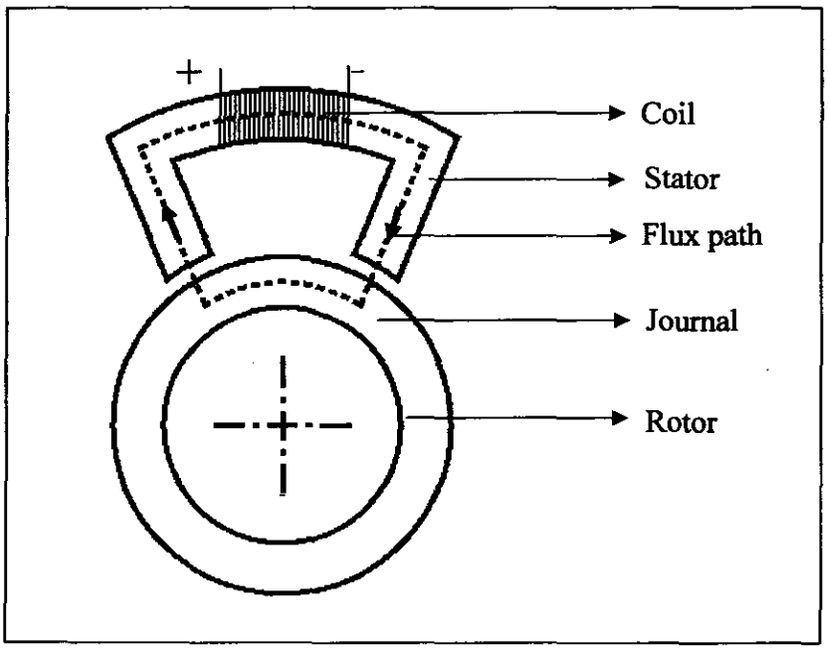

Figure 1.2: Basic principle of magnetic bearings [4]

When feedback is implemented, the position of the rotor or shaft is actively being controlled. Such a system is called an active magnetic bearing system. It constitutes four components: 1) electro-magnets, 2) position sensors, 3) a control system and 4) power amplifiers [5]. There are two types of magnetic bearings: a radial and axial bearing. A typical machine would consist out of two radial

bearings and an axial bearing. The axial bearing prevents movement of the rotor along its own axis and the radial bearings will prevent rotor movement perpendicular to the rotor axis.

AMBs are implemented only in systems where they provide superior value compared to other types of bearings [6]. At present magnetic bearings have a much higher installation cost than other types of bearings. The initial installation cost is possibly its greatest disadvantage. Therefore AMBs are not found in commercial induction motors and standard turbines or generators. Every magnetic bearing is especially designed for its specific application. Two world leading manufacturers of AMB systems are Revolve Magnetic Bearings Inc. and Waukesha Bearings Corporation. They implement AMBs in compressors, pumps, turbo expanders, steam turbines, gas turbines, motors and centrifuges. AMB research is also done extensively by the University of Virginia in the USA.

1.2. Problem Statement

A radial AMB needs to be developed. This model will help establish an AMB research facility in the Faculty of Engineering. The radial model must be designed in such a way that the design process and principles are clear and so that it can be used by students for further studies in the field of AMBs. There are three issues that have to be addressed: 1) electromechanical design, 2) power amplifier and sensors design and 3) the control system.

1.2.1. Electromechanical design

There are only two initial specifications for the AMB. Firstly the air gap between the stator and rotor must be 1 mm and the secondly the system must be stable at rotation speeds of up to 3000 rpm. The electromechanical design constitutes the design of the shaft and the electromagnets. There are two types of radial AMBs: a heteropolar and a homopolar configuration. The best suited configuration must be chosen. There are a few different design options. A logical design sequence must be found to calculate the size of the shaft and the electromagnets.

When the design is finished, drawings must be made to manufacture the AMB. The model must be built in such a way that the electromagnets are firmly in position and care must be taken to ensure a uniform air gap of 1 mm. Sensors, a back-up bearing and an air pressure turbine must be included on the model.

1.2.2. Power amplifiers and sensors

The power amplifiers must be developed in-house. Therefore the correct specifications must be found in terms of the rated voltage and current. This may not be the only specifications and other requirements must be investigated and quantified. There are also different types of power amplifiers. The best suitable type must be chosen.

The sensors must also be developed in-house. Factors such as linearity, noise sensitivity and costs must be considered. There are numerous types of sensors available and the best suited type must be chosen.

1.2.3. Control system

The control system must constitute a computer workstation, dSpace® software, and a dSpace® card. A basic understanding of the software is necessary. The interaction between the different components of dSpace® must be understood. ControlDesk® software is also part of dSpace® and the program must be learned because it will be used for the graphical user interface of the system. Linear or non-linear control techniques can be implemented.

1.3. Proposed Methodology

This project will be conducted in six phases: 1) Detail background study of AMB design and control, 2) electromechanical design of the AMB, 3) AMB simulation, 4) power amplifier and sensor design, 5) system integration and 6) system characterization. Figure 1.3 shows the AMB components that will be designed in phases 2 - 5.

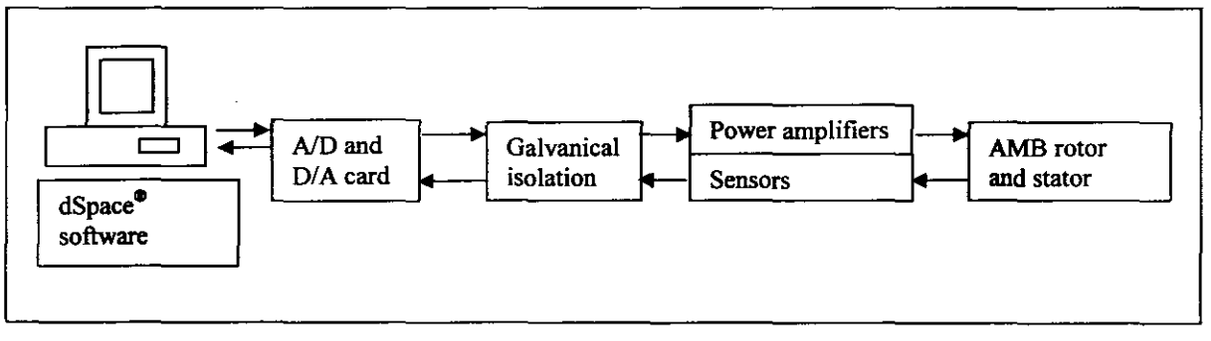

Figure 1.3: Basic components of the AMB system

1.3.1. Background study

A detail study on AMBs will be done. The basic principles of AMBs and the equations describing its behaviour will be investigated. An important aspect is rotor dynamic principles that will be used

to design the shaft of the AMB. Special attention will be given to a radial type bearing and how to design it. Power amplifiers and sensors will also form part of the background study, the different types, their advantages and disadvantages.

1.3.2. Electromechanical design

The electromagnetic design is the most challenging part of the project. Before the electromagnetic design can really start the dimensions of the shaft and the required force must specified. The shaft must be a rigid body and the required force must be calculated from the imbalance specifications of the shaft. Once this is done the electromagnetic design can be conducted.

The electromagnet configuration must be chosen. The pole area and number of windings is then calculated. Once the design is completed it must be verified with finite element analysis methods. The proposed AMB system will have one radial AMB and one conventional ball bearing as shown in Figure 1.4.

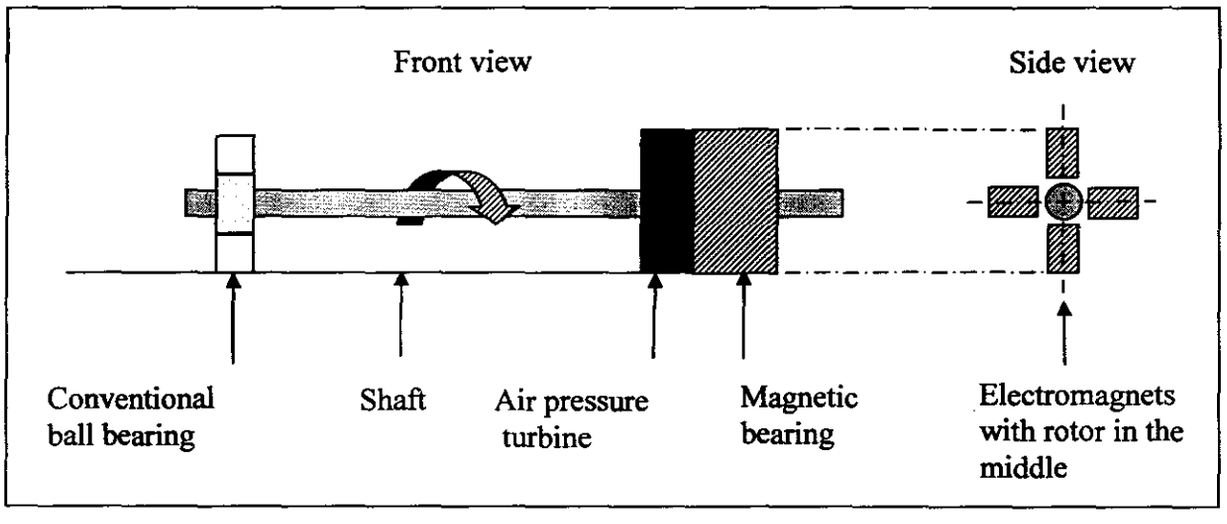

Figure 1.4: Simplified radial bearing

1.3.3. Simulation

The AMB will be simulated in Matlab®. Results of the electromagnetic design will be used and a controller will be implemented. Centrifugal forces due to shaft imbalance will form part of the simulation. Important characteristics such as power amplifier specifications and control parameters will be obtained from the simulation.

1.3.4. Power amplifier and sensors

The type of power amplifier and sensor must be chosen. Different options must be considered in terms of cost, linearity, and noise sensitivity. The power amplifier will be designed according to the results of the simulation. A simulation of the power amplifier will be done in CircuitMaker® and the characteristics of the power amplifier will also be built into the Matlab® simulation of the AMB.

1.3.5. System integration

All the components of the AMB must be integrated to form the final AMB system. The sensors and the power amplifiers must be connected to the computer through dedicated I/O channels. An optical speed sensor will be used to measure the speed and this value will be read in through a bit I/O channel. A graphical interface will be created in ControlDesk® to monitor the position of the shaft.

1.3.6. System evaluation

The last phase of the project will be to characterize the system. A step response test will be done and the results will be compared with the expected results from the simulation. The stability of the system will be tested at rotational speeds of up to 3000 rpm. The dynamic stiffness and damping of the system will be calculated.

1.4. Overview of the dissertation

The background study on AMBs is discussed in Chapter 2. A non-linear model and a linear model are derived. The equivalent stiffness and damping of AMBs are given. Then the different components are discussed. Basic theory on rotor dynamics is given.

In Chapter 3 the electromagnetic design of the AMB is done. A certain design procedure is used to design the shaft and the electromagnets. An electromagnet configuration is chosen. The shaft and electromagnet are dimensioned and the design is verified with finite element analyses. The manufacturing of the AMB is discussed and drawings of the AMB are shown.

Chapter 4 discusses the simulation of the AMB in Matlab®. The simulation is done using a mathematical model for the actuator. The simulation is done only in the vertical axis of the AMB. A centrifugal force is introduced to simulate the rotation of the shaft in the presence of an unbalance. The results of the simulation are used to design the power amplifier. The optimum PID controller parameters are found through iteration.

The power amplifier and sensor design are done in Chapter 5. Firstly the power amplifier is discussed. The specification for the power amplifier is given and the type of power amplifier is chosen. A simulation of the power amplifier circuit is done. Actual results of the final power amplifier are given. The type of sensor is chosen and a simulation of the circuit is also done.

All the components are integrated to form the complete AMB system. In Chapter 6 the integration of the power amplifiers and sensors with dSpace® is discussed. Different D/A and A/D channels are used to connect the power amplifiers and the sensors with the dSpace® card. The graphical user interface forms part of the integration process and the different layouts of the interface are explained.

The final AMB system is characterized in Chapter 7. The step responses of the system are measured and the percentage overshoots and settling times are calculated. The results are compared to the simulation. The behaviour of the system at different rotation speeds is investigated. The dynamic stiffness and damping is calculated.

In Appendix A the critical frequency of the shaft is calculated. Appendix B is a derivation of the force that an electromagnet with a bowed surface can exert on the shaft. The result is used in Chapter 3 to design the electromagnet more accurately. Appendix C is a table of rotor imbalance grades. Typical examples of rotors of a certain grade are given. The electromagnetic design as done in MathCad® is given in Appendix C. Appendix D is the complete Cadkey® drawings of the AMB. Photos of the AMB system are given in Appendix E.

The included CD in Appendix F contains: MS Word® format of this dissertation, Matlab® simulation, MathCad® electromagnetic design, QuickField® finite analyses and dSpace® experiment files.

Chapter 2

Background on active magnetic bearings

Basic background on active magnetic bearings (AMBs) is given in this chapter. This chapter gives insight in the control of AMBs. Non-linear and linear models are derived. The stiffness and damping of an AMB is determined in terms of model and control parameters. The components of the AMB are discussed as well as different power amplifiers and sensor types. Rotor dynamics forms an important part of AMB design and important aspects of rotor dynamics are explained.

2.1. Introduction to Active Magnetic Bearings

AMBs are used to suspend a rotor of a machine in the air in a stable condition. The term *active* means that the system must be actively controlled by implementing a feedback controller. The most important advantage is that there is no friction between the rotor and the stator. This eliminates the need for lubrication and also allows the machine to spin at very high speeds, the only limitation being the strength of the rotor material. The disadvantage is that the bearing is larger, with a large initial cost.

An AMB constitutes four basic components: 1) electromagnets or the magnetic actuators, 2) a control system, 3) power amplifiers and 4) position sensors. Figure 2.1 shows a basic block diagram of a typical AMB [7].

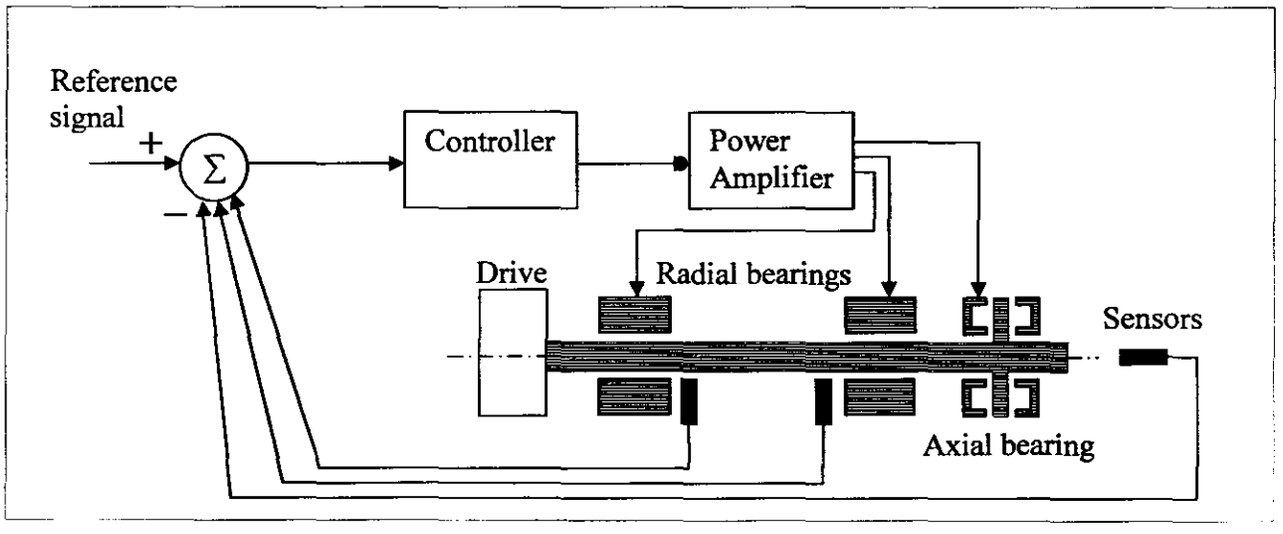

Figure 2.1: Block diagram of a basic AMB

The sensors measure the position of the rotor. This sensor signal is fed back and subtracted from a required reference value. The error signal is then the input to the controller. The controller is typically a digital controller implemented on an imbedded microcontroller. The output of the controller is connected to the power amplifiers. The power amplifiers control the current in the coils. Voltage mode or current mode power amplifiers can be used. The electromagnets apply a force on the rotor and the rotor is suspended in the air.

2.2. Non-linear model of AMBs

A theoretical model is derived to determine the force that an electromagnet exerts on a rotor [6][8]. The following assumptions are made: 1) the flux levels in the material of the electromagnet and rotor are below its saturation level, 2) the deviation of the shaft is small in comparison to the nominal air gap between the rotor and the stator, 3) flux distribution is uniform in the stator and flux leakage is small. The relation between magnetic field intensity ($\boldsymbol{H}$) and the enclosed current or magnetomotive force (mmf) is given by Ampere's law in (2.1) where $\boldsymbol{dl}$ is a differential length along the closed path of integration L. $\boldsymbol{H}$ and $\boldsymbol{dl}$ are printed in bold because they are vectors.

$$\oint \boldsymbol{H} \bullet \boldsymbol{dl} = I_{enc} = \Im \text{ (mmf)} \tag{2.1}$$

When the uniform $\boldsymbol{H}$ field is parallel to the path of integration for a coil of N turns and current i, the relation is given by:

$$\oint \boldsymbol{H} \bullet \boldsymbol{dl} = HL = Ni = \Im \text{ (mmf)} \tag{2.2}$$
$$\therefore \mathrm{H} = \mathrm{Ni/L}$$

The relation between the field intensity and magnetic flux density (B_{air}) in air is given by

$$B_{air} = \mu_o H \tag{2.3}$$

When working with magnetic circuits with an air gap, most of the magnetic energy is concentrated in the air gap and a small portion of the energy is located in the magnetic material of the magnet. A linear relationship between B and H also applies in the material. This relationship is only valid for values of B below the magnetic saturation point of the material and is given by

$$B = \mu_o \mu_r H \tag{2.4}$$

where μ_r is the relative permeability of the material. Typical ferromagnetic materials have a relative permeability between 1000 to 5000.

The basic principle and geometry of a magnetic bearing is illustrated in Figure 2.2. Each electromagnet has N windings with a current i and the pole area (area of one air gap) is A_g. The magnetic flux (ϕ) through the area A_g is given by definition as:

$$\phi = \int \boldsymbol{B}_{air} \bullet d\boldsymbol{a} \tag{2.5}$$

When $\boldsymbol{B}$ is perpendicular on $d\boldsymbol{a}$ the flux is:

$$\phi = B_{air} A_g \tag{2.6}$$

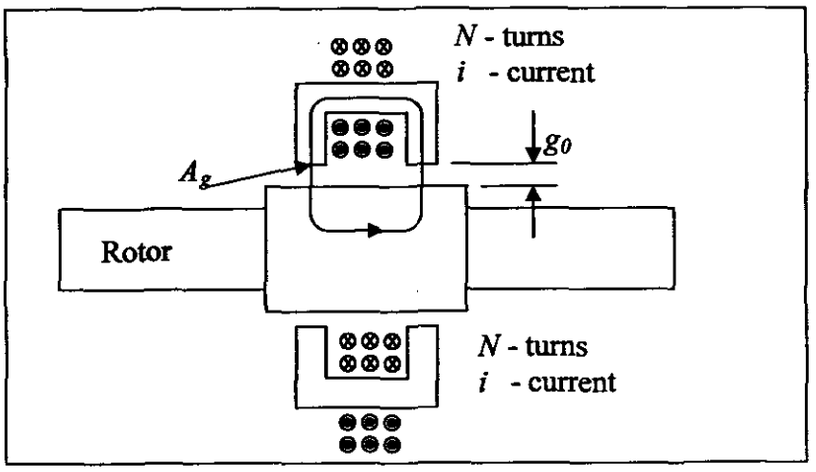

Figure 2.2: Basic magnetic bearing

Since $\mu_r >> 1$ in the iron the magnetization of the iron is neglected. Therefore only the path length of the two air gaps are considered. The flux density in each air gap is the same and B_{air} is found by using (2.2) to (2.6) and substituting the length (L) with 2 times the air gap g_0:

$$H = Ni / L$$

$$\frac{B_{air}}{\mu_0} = Ni / L$$

and $L = 2g_0$

$$\therefore B_{air} = \frac{\mu_0 Ni}{2g_0} \tag{2.7}$$

The potential energy stored in a magnetic field in a certain volume is given by:

$$W_m = \frac{1}{2} \int_{vol} \boldsymbol{B}_{air} \bullet \boldsymbol{H}\, dv \tag{2.8}$$

In the air gap of a magnetic circuit the energy stored can be expressed as

$$W_{air} = \frac{1}{2}(B_{air}H)Vol = \frac{1}{2}\frac{B_{air}^2}{\mu_0}Vol \tag{2.9}$$

Working with one pole of the electromagnet the incremental change in volume is $d(Vol) = A\ dg$. From the definition of work, the energy in the air gap is:

$$dW_{air} = \boldsymbol{F} \bullet d\boldsymbol{l} = F\ dg$$

$$\frac{1}{2}\left(\frac{B_{air}^2}{\mu_0}\right)A\ dg = F\ dg \tag{2.10}$$

Thus the pulling force on the rotor per pole of electromagnet is then given by

$$F = \frac{1}{2}\left(\frac{B_{air}^2}{\mu_0}\right)A_g \tag{2.11}$$

and the total force per magnet is then multiply by two for two poles per magnet so that the total force is

$$F = \left(\frac{B_{air}^2}{\mu_0}\right)A_g \tag{2.12}$$

Equation (2.7) is substituted into (2.12) so that the force is in terms of the coil current, turns and the area of the air gap:

$$F = \left(\frac{\mu_0\ Ni}{2g_0}\right)^2\left(\frac{1}{\mu_0}\right)A_g = \frac{1}{4}\mu_0 N^2 A_g\frac{i^2}{g_0^2}$$

The area (A_g) and the number of turns (N) are fixed and therefore can be replaced by a constant k so that

$$k = \frac{1}{4}\mu_0 N^2 A_g$$

$$\therefore F = k\frac{i^2}{g_0^2} \tag{2.13}$$

The interpretation of equation (2.13) gives very good insight in the operation of an AMB. The current is the variable that is adjusted to produce the force. The force is proportional to the square of the current and inversely proportional to the square of the air gap. This makes the system non-linear and naturally unstable. The force equation can be approximated by a linear function at the working point of the AMB. This will be discussed in the following section.

The complete AMB system model is shown in Figure 2.3. The coil current and the position signal are used to calculate the force. By subtracting the weight and dividing with the mass the acceleration ($\ddot{x}$) of the shaft is obtained. The position x is found by integrating the acceleration. Note that x indicates the position.

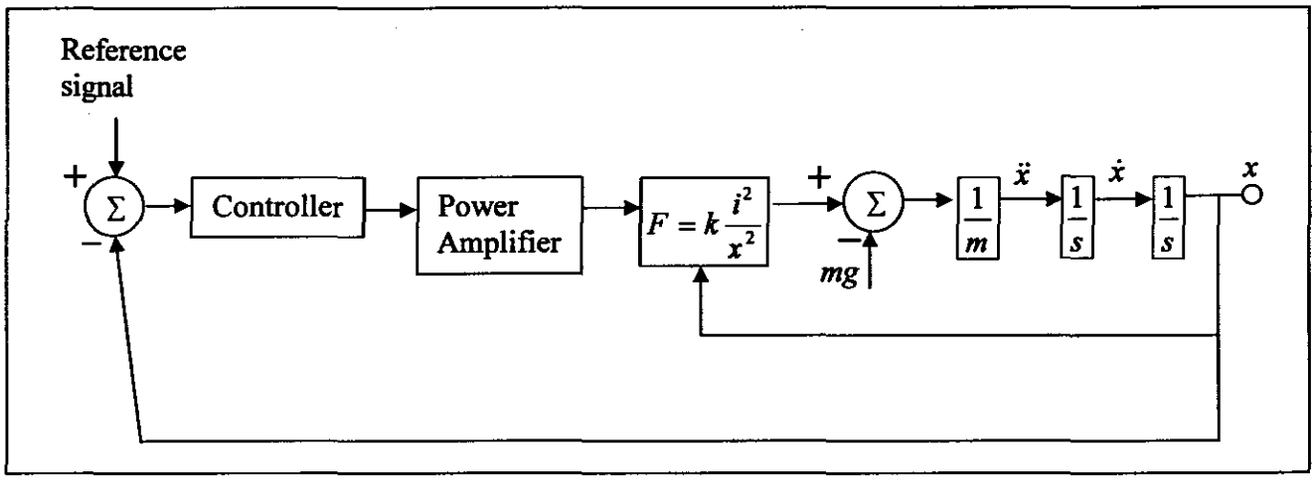

Figure 2.3: Non-linear AMB system model

2.3. Linear model of the AMB

The force (f) that the electromagnet exerts on the suspended body decreases with an increase in displacement. This instantly destabilises the system [9]. The relationship is illustrated in Figure 2.4. The derivative of the force displacement curve is negative and the value is the mechanical stiffness of the suspension denoted with the variable k_s.

AMBs are controlled to suspend the rotor at a certain nominal point. At the nominal point the resultant force on the rotor is by definition zero. In control design it is sufficient to use a linear model at the operating point. This is a straight line with a negative gradient k_s. When deriving such a linear model for AMBs it is assumed that the deviation around the operating point is very small. Deviations are due to rotor imbalance or external load disturbances.

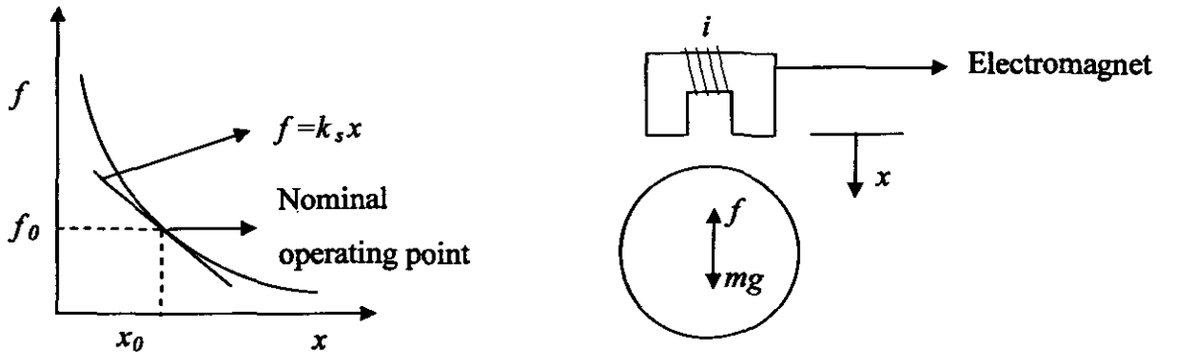

f	–	force exerted by the electromagnet on the body
mg	–	gravitation force
x	–	displacement between electromagnet and suspending body
i_0	–	bias current in the coil
f_0	–	force at nominal operating point
x_0	–	position at nominal operating point

Figure 2.4: Force-displacement relationship

The force in the electromagnet is controlled by controlling the current in the electromagnet coil. The current in the coil comprises two components: a steady-state component (i_0) and a control current (Δi). The steady-state current provides the attraction force at the nominal operating point while the control current provides attraction force for variations around the operating point [3]. From (2.13) it is shown that the force is also proportional to the square of the current. This force-current relationship is also used in the linear model of AMBs. The relationship is shown in Figure 2.5. The derivative at the operating point is the force-current factor k_i. The values k_i and k_s are used as constants in the linear model of AMBs.

The relationship between force, current and displacement can be illustrated on a single graph (Figure 2.6) for better insight [3]. The force-displacement relationship graph in Figure 2.4 can be expanded to include different curves for different bias currents (i_0).

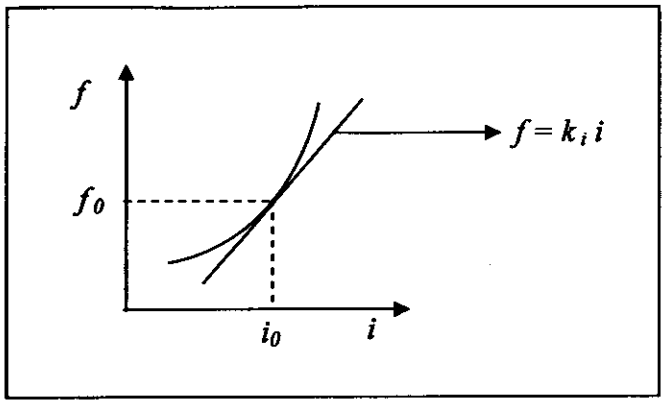

Figure 2.5: Force-current relationship

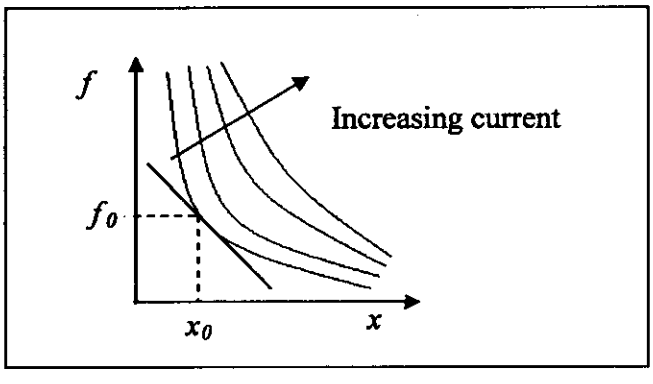

Figure 2.6: Expanded force-displacement graph

To derive a linear model for AMBs the differential driving mode must be used [3]. In this mode two opposing electromagnets are used so that the resulting force can be negative or positive. A bias current is added to each of the two control signals as shown in Figure 2.7. The resulting force is then given by (2.14).

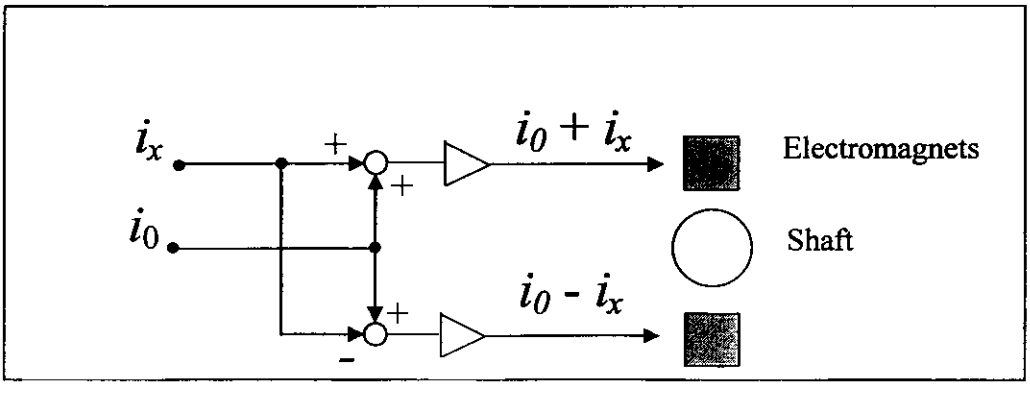

Figure 2.7: Differential driving mode

$$
\begin{aligned}
f_r &= f_+ - f_- \\
&= k\frac{(i_0 + i_x)^2}{(x_0 + \Delta x)^2} - k\frac{(i_0 - i_x)^2}{(x_0 - \Delta x)^2}
\end{aligned}
\tag{2.14}
$$

with:

f_r	–	resulting force on the rotor
f_+	–	upward force
f_-	–	downward force
k	–	electromagnet constant
i_x	–	control current
Δx	–	deviation position from the centre

By differentiating (2.14) with respect to current and position at the operating point (x_0,i_0) the deviation in force is obtained:

$$
\begin{aligned}
\Delta f_r &= \frac{4ki_0}{x_0^2} i_x + \frac{4ki_0}{x_0^3} \Delta x \\
&= k_i i_x + k_s \Delta x
\end{aligned}
\tag{2.15}
$$

The constant values k_i and k_s are the stiffness and force-current factors respectively. As shown, the values can be calculated explicitly from the physical parameters of the AMB. This model is used with good results for many applications according to [3]. In the extreme cases where: the rotor and stator is in contact, or saturation of the material occurs or where the control current is in the order of the steady-state current this model will not work.

2.4. An AMB model in terms of stiffness and damping

2.4.1. Stiffness and damping

The stiffness (k_{eq}) of a spring is its ability to resist deformation [10]. A simple spring-mass-damper system is shown in Figure 2.8. The force of the spring can exert is approximately proportional to the displacement (x). A damping force referred to as viscous damping (b_{eq}) produces a damping force proportional to the velocity of the mass (m). An electromagnet that suspends a body is equivalent to the spring-mass-damper system [11].

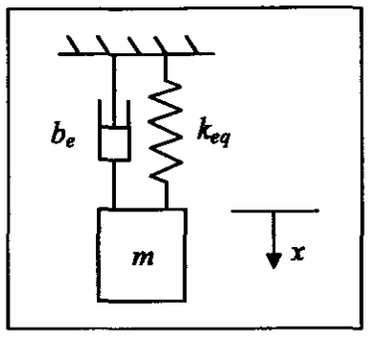

Figure 2.8: Spring-mass-damper system

Using Newton's second law a differential equation that describes the unforced motion of the above system yields:

$$m\ddot{x} + b_{eq}\dot{x} + k_{eq}x = 0 \tag{2.16}$$

For constant coefficients of (2.16) the characteristic equation in the s plane is

$$ms^2 + b_{eq}s + k_{eq}s = 0 \tag{2.17}$$

The natural oscillating frequency (ω_n) of the system is defined [12] as

$$\omega_n = \sqrt{\frac{k_{eq}}{m}} \tag{2.18}$$

2.4.2. Equivalent model

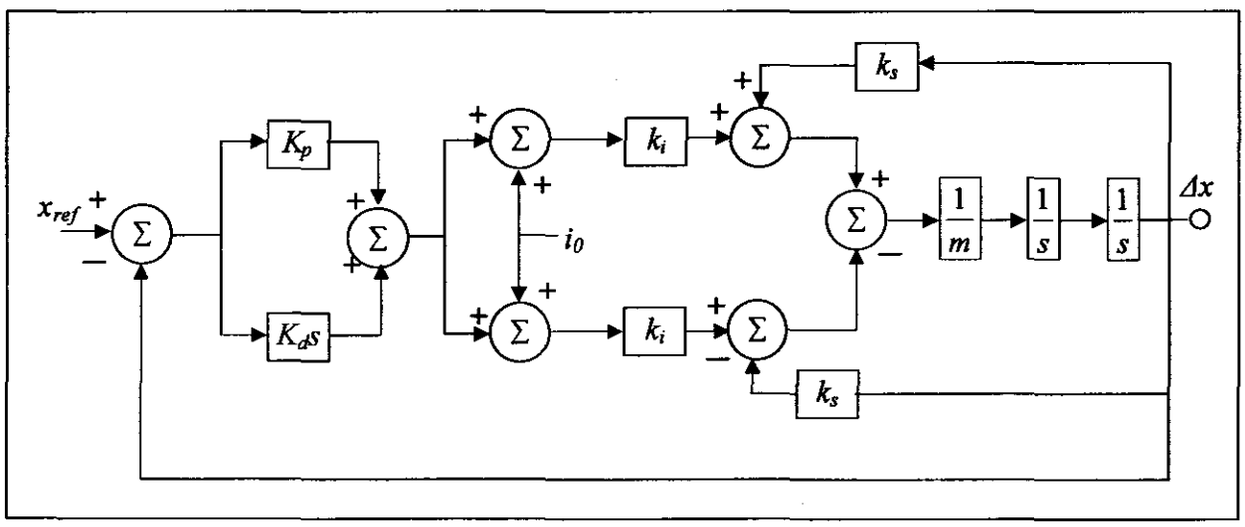

Figure 2.9: Equivalent block diagram

To determine the stiffness and damping of an AMB the block diagram in Figure 2.9 is used. A PD controller is used. The controller has two terms: a proportional (K_p) and derivative term (K_d). Two opposing electromagnets are used. From [13] the transfer function of the system shown in Figure 2.9 is:

$$T(s) = \frac{2K_pK_i + 2K_dK_is}{ms^2 + 2K_dK_is + (2K_pK_i - 2K_s)} \tag{2.19}$$

This equation can be compared to (2.17) to find the equivalent stiffness and damping of the AMB. From the characteristic equation the equivalent stiffness and damping is given in (2.21).

$$\begin{aligned} q(s) &= ms^2 + 2K_dk_is + (2K_pk_i - 2k_s) \\ &= s^2 + \frac{b_{eq}}{m}s + \frac{k_{eq}}{m} \end{aligned} \tag{2.20}$$

$$\begin{aligned} b_{eq} &= 2K_dk_i \\ k_{eq} &= 2K_pk_i - 2k_s \end{aligned} \tag{2.21}$$

2.5. Components of AMBs

2.5.1. The electromagnet

Electromagnets can be classified in two different configurations based on the type of suspension. A radial configuration prevents movement of the rotor perpendicular to the rotor axis while an axial configuration prevents movement of the rotor parallel to the rotor axis.

An axial bearing is shown in Figure 2.10. The magnetic flux flows from the stator through the runner and back to the stator to complete the loop. There are usually two axial bearings in a machine, one on each end. The magnetic polarity of the runner does not change. This means that the eddy current losses because of a changing magnetic field in the runner are very small. An axial bearing is therefore usually not laminated [14].

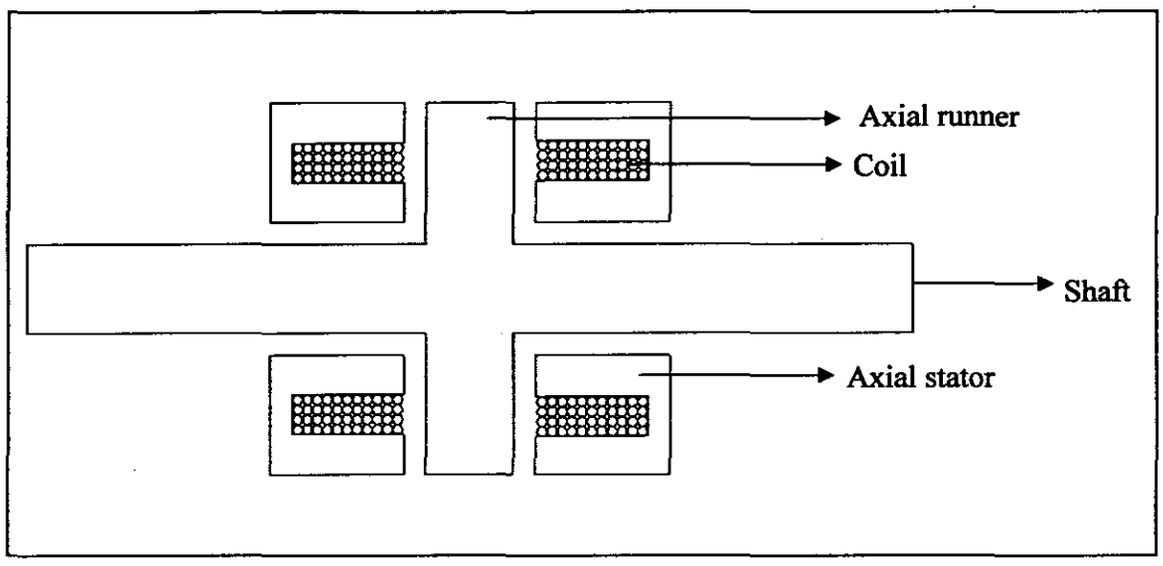

Figure 2.10: AMB axial bearing

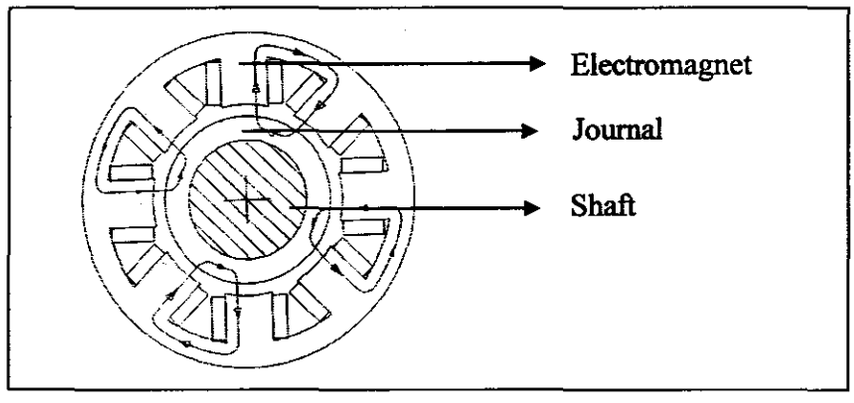

Figure 2.11: AMB radial bearing

The radial AMB shown in Figure 2.11 has eight electromagnets or poles and is most commonly used. The minimum number of poles to achieve a force in all directions is three [7]. A radial bearing can have a heteropolar or homopolar structural shape. With a heteropolar bearing the magnetic flux in the rotor is perpendicular to the rotor axis and with a homopolar bearing the flux is parallel to the rotor axis as illustrated in Figure 2.12. The reason for these two different configurations is because of the iron losses in the rotor. The homopolar magnet has lower eddy current losses than the heteropolar magnet [10]. This can be explained by observing the north – south positions of the magnet at the air gap. When rotating the rotor of the homopolar magnet will not change polarity from north to south, but for the heteropolar rotor, any specific point of the rotor will change polarity

4 times in one revolution. This change in polarity induces eddy currents in the rotor and produces i^2R losses.

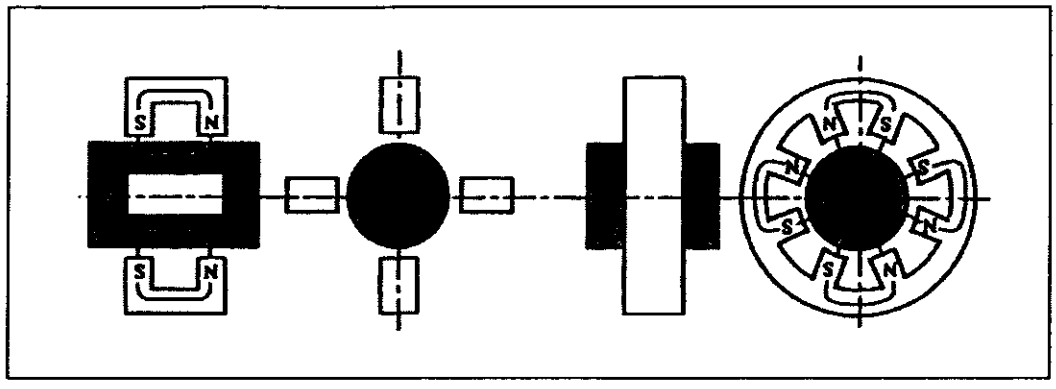

Figure 2.12: Homopolar and heteropolar radial AMB [6]

In general there are two types of magnetic materials: 1) soft and 2) hard magnetic materials. The soft magnetic materials can easily be magnetized and demagnetized. This property makes it the ideal material for AMBs. Soft magnetic materials are commonly used in transformer cores as well as in rotors and stators of motors. Hard magnetic materials are used for permanent magnets in speakers and telephone receivers. To make the best material selection the following factors must be considered: permeability, saturation flux density, electrical resistivity, mechanical strength and ease of manufacturing [15].

Permeability of a material is the ratio of the magnetic flux density (B) to the magnetic field intensity (H). This is an indication of the ease of excitation. Using the highest permeability alloys such as nickel-iron alloys is not justifiable because of the air gap present in the magnetic path. The air gap must be kept to a minimum to gain maximum advantage of using such alloys.

Electrical resistivity is an important factor to reduce eddy currents. A higher resistivity will reduce eddy currents and reduce losses which are proportional to the square of the current (i^2R). Magnetic saturation is probably the most important factor to consider because the force increases with the square of the flux density (see (2.12)). Selecting a material with a high saturation level such as an iron-cobalt alloy with a saturation level of 2.4 T will reduce the physical size of the magnet.

Mechanical strength is important for laminated rotors. The material must be heat treated to increase its strength, but this decreases its permeability and increases the hysteresis losses. There is therefore a definite trade off between magnetic and mechanical properties. The ease of manufacturing does

not pose great problems since the alloys can be machined or stamped in laminations. The most difficult alloys to machine are 3-4% silicon-iron because of its brittleness.

2.5.2. Power amplifiers

There are two basic types of power amplifiers: linear and switched mode. Each can have different configurations with its advantages and disadvantages [16]. Swithed mode amplifiers are used more commonly in the industry especially in applications with a large power requirement. In this section both types are discussed.

A power amplifier receives a control signal from the controller and according to the value of that signal it controls the level of current in the coil. The control signal is normally a voltage signal between 0 and 5 V or 10 V. The power amplifier has a current feedback signal of ensure that the desired current in the coil is maintained.

There are basically two requirements that a power amplifier must satisfy: 1) current rating and 2) slew rate. An AMB designer specifies the rms current and the peak current that is necessary to produce a required force. The peak current is only required for short time periods in case of a sudden external disturbance. The power amplifier must be able to deliver the rms current continuously without overheating.

The slew rate of an AMB is specified in Newton per second and the required rate of change of the force with respect to time. This requirement is due to imbalance in the rotor; the force that an electromagnet must exert to counter the centrifugal force changes with time. For the force to change quickly, the current must change quickly. The rate that the current can change with respect to time is determined by the supply voltage. Therefore care must be taken to use power amplifiers with high enough supply voltages to achieve specific slew rate requirements. A linear amplifier controls the current in the coil in such a way that the switching element is operated in its active region. This means that the voltage across the coil and the gate or base signal of the switching element is continuous. Figure 2.13 shows a graph of an n-channel MOSFET's current-voltage characteristics [16]. The voltage across the drain-source (V_{ds}) of the MOSFET is on the x- axis and the current through the MOSFET (i) on the y-axis. The different curves are for different values of the gate source voltage (V_{gs})

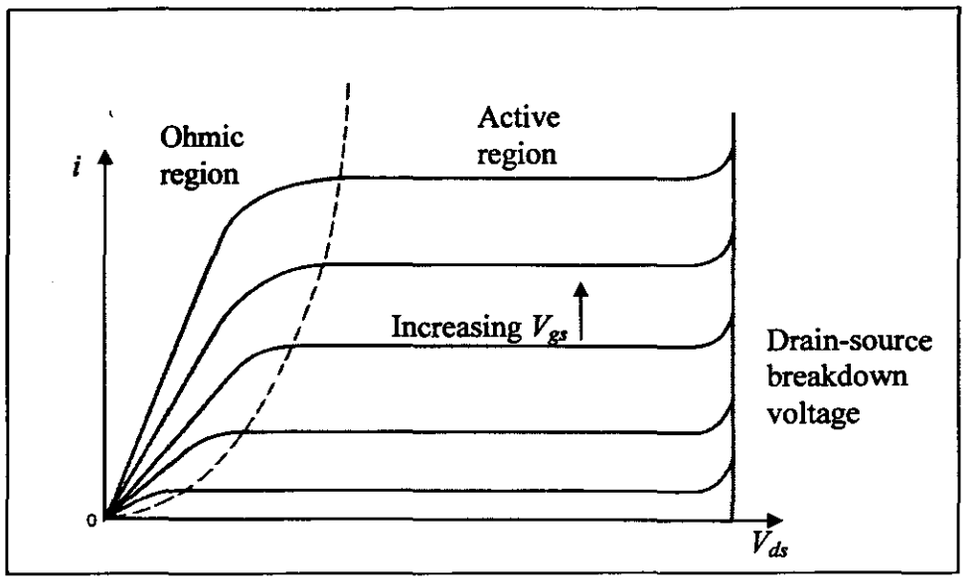

Figure 2.13: Current-voltage characteristics of an n–channel MOSFET

Linear power amplifiers are known for their poor efficiency because most of the power is dissipated in the switching element and not in the load. The efficiency can be calculated as shown in the following example: Consider a 1.5 Ω coil that must carry 5 A with a supply voltage of 50 V. The inductance of the coil is neglected because the current can be approximated as a dc current. The power dissipated in the coil is:

$$\begin{aligned} P_{coil} &= i^2 R \\ &= 5^2 (1.5)\,\text{W} \\ &= 37.5\ \text{W} \end{aligned}$$

This means that the power dissipated in the power amplifiers must be the total power minus the power in the coil which is:

$$\begin{aligned} P_a &= V_{cc} i - P_{coil} \\ &= (50)(5) - 37.5\,\text{W} \\ &= 221.5\ \text{W} \end{aligned}$$

The power amplifier efficiency is then:

$$\begin{aligned} \eta &= \frac{P_{coil}}{V_{cc} i} \frac{100}{1} \\ &= \frac{37.5}{250} \frac{100}{1} \\ &= 15\% \end{aligned}$$

The one big advantage that a linear amplifier has is its low noise. There is no sudden and large change in the voltage across the coils therefore not much noise is generated. A typical linear

amplifier configuration is shown in Figure 2.14 [6]. Two switching elements are used. The npn element is used to increase the current and pnp element to change the direction of the current. It is sometimes necessary to change the current direction to keep the current continuous. When working with currents close to zero, current and voltage are measured and fed back to the mixer. The mixer can select the controlled variable, current or voltage. This means that the voltage or the current can be the controlled variable. The output signal of the mixer is subtracted from control input signal.

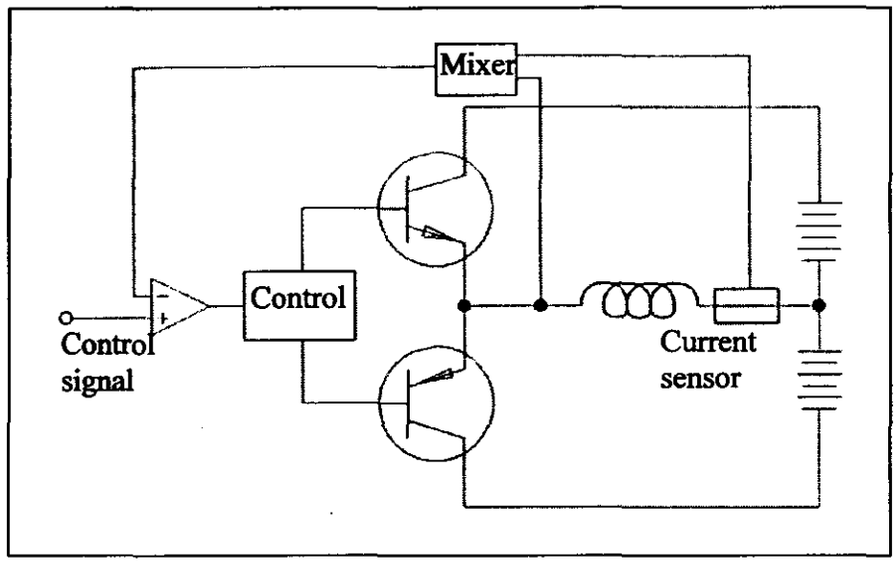

Figure 2.14: Linear power amplifier

Switching amplifiers are most commonly used for AMBs because of their efficiency and controllability. There are numerous types of switching amplifiers but they work on the same principle; to switch the voltage across the coil at a certain frequency. By varying the duty cycle of the voltage, the level of current can be controlled. The current then has a ripple component that can be used for self-sensing AMBs (self–sensing AMBs use the gradient of the current to estimate the position of the rotor). The disadvantage of swithed mode amplifiers is that it generates substantial noise. The forward converter and H-bridge configurations will be discussed.

A forward converter is shown in Figure 2.15 [17]. The converter constitutes a switching element, step down transformer and LC filter on the output. The switch S1 can be a MOSFET and the switching of the MOSFET can be done with a PWM (pulse width modulation) signal. The voltage and current waveforms are shown in Figure 2.16.

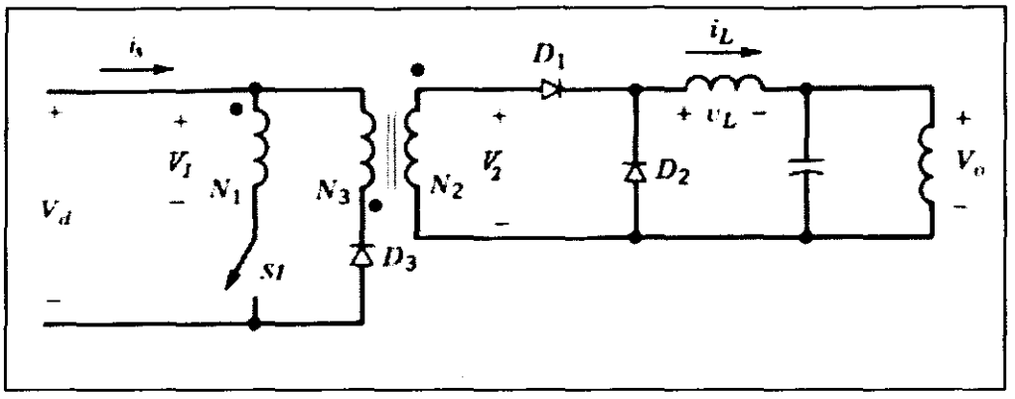

Figure 2.15: Forward converter [16]

When S1 is closed, diode D1 becomes forward biased and D2 is reversed biased. The load current will then increase. During this time (t_{on}) energy is transferred to the load or electromagnet coil. The voltage on the secondary winding of the transformer is then given by

$$v_2 = \frac{N_2}{N_1} V_d \tag{2.22}$$

The output voltage across the coil is then:

$$V_o = \frac{N_2}{N_1} V_d - V_L \tag{2.23}$$

When S1 is opened (t_{off}) the current (i_L) circulates through D_2. The transformer has to demagnetise through N3 and D3 which becomes forward biased. N3 has the same number of turns as N1 but is wound in the opposite direction. The transformer must demagnetise before the next cycle can begin. Therefore from [16] it is shown that this requires the same time as t_{on} and that the maximum duty cycle for this type of converter is 50 %. The current in the coil will decrease and the output voltage is then:

$$V_o = -V_L \tag{2.24}$$

An H-bridge configuration is shown in Figure 2.17. It constitutes four switching elements and a load represented by a resistor and an ideal coil. With this configuration a higher slew rate is possible because energy can be extracted very fast by closing switches 2 and 3. The resultant voltage across the coil is then the negative of the supply voltage and current will quickly decrease. The current can be increased by closing switches 1 and 4.

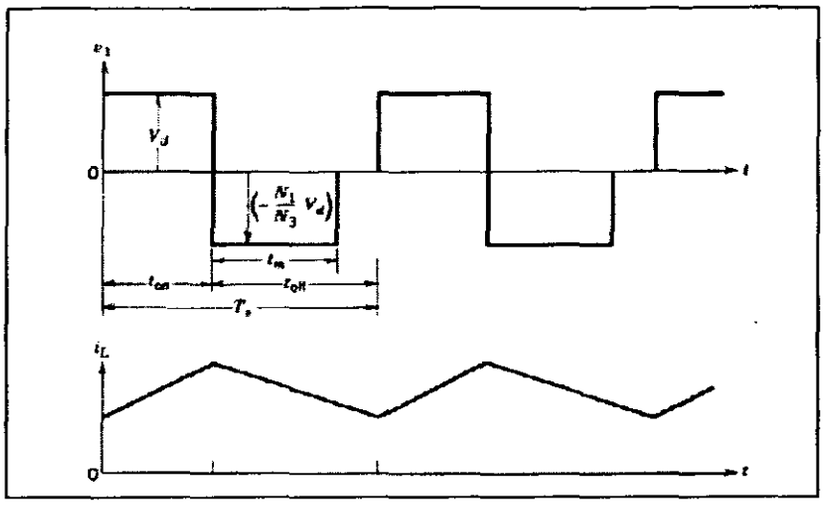

Figure 2.16: Primary voltage and load current of a forward converter [16]

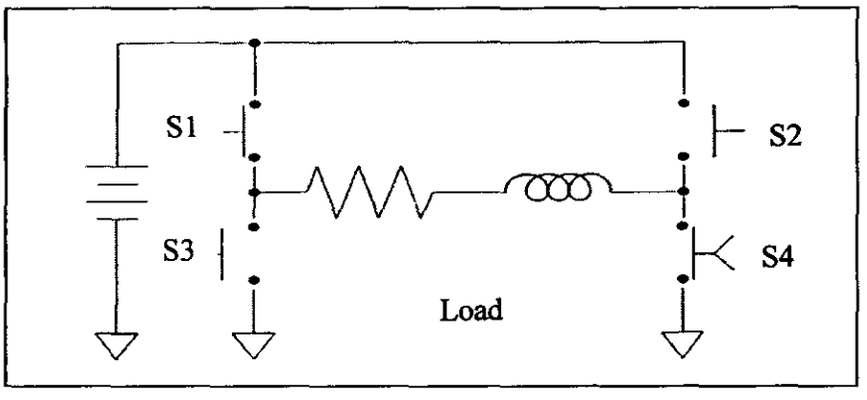

Figure 2.17: H- bridge power amplifier

A schematic representation of the control structure of a switching power amplifier is shown in Figure 2.18. The PWM logic gives the PWM output to the H-bridge. The duty cycle of the PWM signal is proportional to the input signal from the error amplifier. The switching frequency is determined by the RC time constant. The mixer can select current or voltage mode control.

Current mode control is more common than voltage mode control for AMBs [11]. To measure the current, a sensing resistor or a Hall Effect device can be used. The sensing resistor is the simplest method but has the disadvantage of high power dissipation in the resistor and there is no isolation from the load voltage.

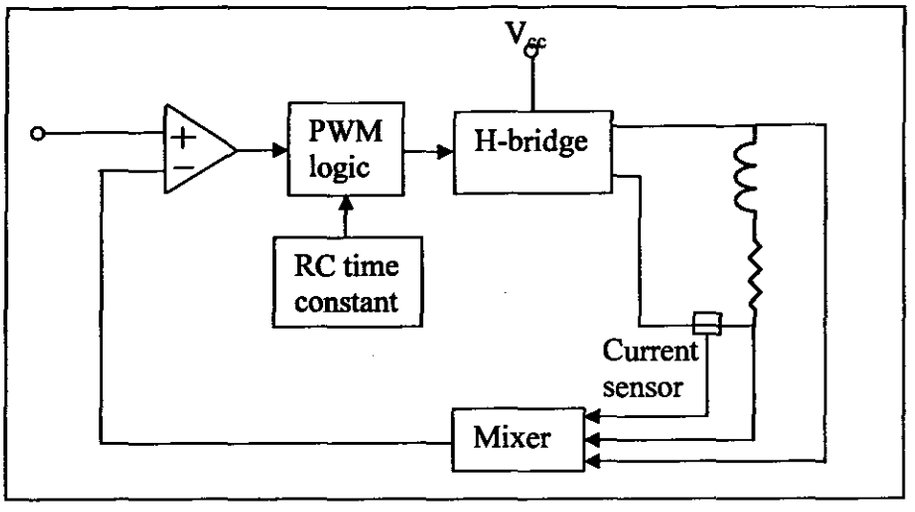

Figure 2.18: Control structure of a switching power amplifier

2.5.3. Sensors

Sensors are critical in AMBs. The system can only be controlled as good as the sensors can measure. Therefore much thought must be given to sensors when designing an AMB. Usually the AMB designer does not design the sensor itself but only buys a specific type from the shelf. The type of sensor depends on the type of application and the characteristics that need to be measured. Sensors are compared on the following characteristics: gap requirements, bandwidth, linearity and noise susceptibility. Common characteristics of all sensors are that they are not in contact with the suspended rotor, and that their bandwidth must exceed that of the amplifier and actuator [18].

Commonly in industrial applications the gap between the sensitive portion of the probe and the sensed target is filled with a process gas, fluid or even dirt particles. The properties of this intervening material may have an effect on what type of sensor to use. The bandwidth of a sensor describes the maximum frequency of motion which the sensor can accurately measure. For high speed rotors it is important to have a higher bandwidth than for lower speed applications. Working in the linear range of a sensor is important because sensors are not absolute linear devices. The linear range of a specific sensor is normally given.

Noise susceptibility has a significant impact on the performance of sensors. The physical placement of the sensors is important so that it is isolated from possible noise sources. The main source of magnetic noise is from leakage flux of the AMB coils and 50 Hz signals from the main power network.

There are numerous types of sensors available: ultrasonic, capacitive, optical, eddy current and inductive sensors to name only a few. The eddy current and variable reluctance probes will be discussed in more detail.

Eddy current probes constitute an ac signal generator, an excitation coil and a search coil (Figure 2.19). The ac current in the excitation coil generates a changing magnetic field in the rotor. This changing magnetic field induces eddy currents in the rotor which depends on the size of the air gap.

These sensors require a non conducting material in the air gap and the target to be measured must have a constant electrical conductivity. The advantage of these sensors is their good linearity and sensitivity. They are relatively expensive but widely used in the industry, not only in AMBs.

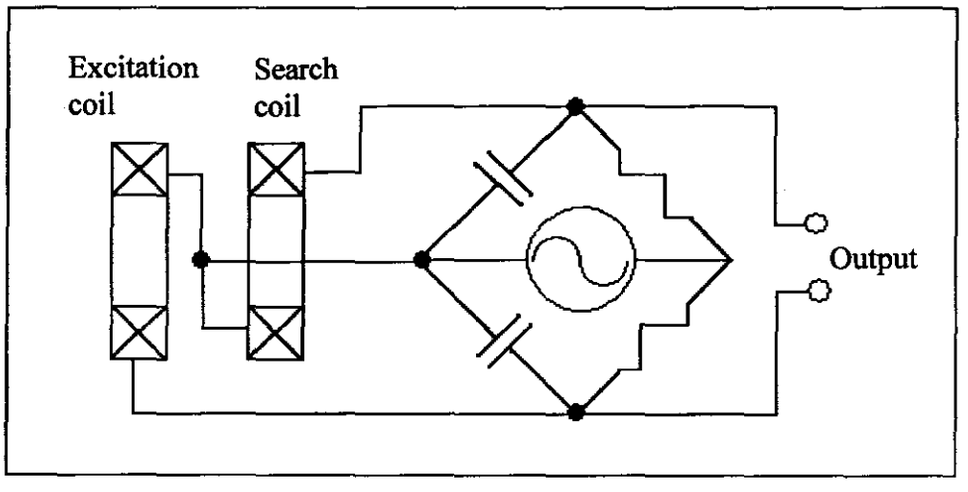

Figure 2.19: Eddy current probes [6]

Inductive sensors work in pairs. Two small coils are placed on the opposite side of a rotor (Figure 2.20). The coils are excited by a high frequency ac signal. If the air gap changes the impedances of the coils also change. The two coils are connected in series and used in a voltage divider configuration so that the change in inductance can be measured as shown in Figure 2.21. The signal is passed through a band-pass filter to eliminate noise. It is then rectified and converted to a dc signal. This dc signal is proportional to the air gap size.

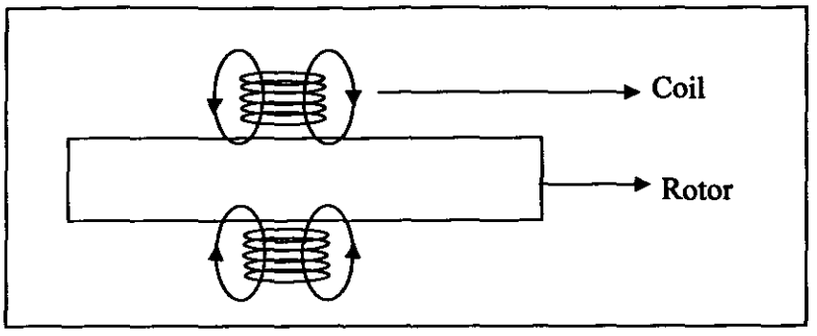

Figure 2.20: Placement of inductive sensors

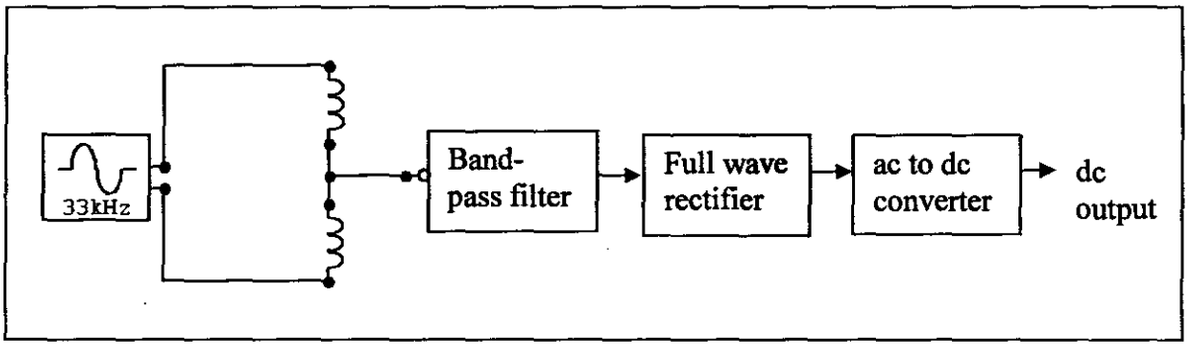

Figure 2.21: Inductive sensor connection

2.5.4. Control system

Different control systems have been implemented in AMBs. Examples of non-linear controllers are fuzzy logic, sliding-mode and H_∞ controllers. Despite the fact that this is a non-linear system, linear control techniques have been implemented successfully. A PID controller is very good example of a robust linear control system.

The PID controller has three parameters: proportional gain, integral gain and derivative gain. This type of controller is very popular because of its robust performance and functional simplicity [19]. PID controllers have been implemented effectively in AMBs where the system operation is maintained near the design conditions and deviation in the air gap is relatively small ($x << x_0$). The general transfer function for a PID controller is:

$$G_{PID} = K_p + \frac{K_i}{s} + K_d s \tag{2.25}$$

with

K_p – proportional gain

K_i – integral gain

K_d – derivative gain

To design such a controller values for the three parameters must be found. This can be done on trial-and error basis but do not always give the desired performance characteristics. One method to calculate the parameters is discussed in [19] by using the ITAE performance index. This index takes the integral of time multiplied by the absolute error. Three PID coefficients are selected to minimise the ITAE performance index.

AMBs can be controlled using only PD control. The integral term is left out. The force that the bearing exerts constitutes 2 parts: a force proportional to the displacement of the journal and a force proportional to the journal velocity (the time derivative of the position error). This control is equivalent to a spring-mass-damper system. An unsuspended AMB has a negative stiffness. When the feedback and the PD control system are implemented the system's overall stiffness must be positive. Both terms has an effect on the stiffness and damping as seen from (2.21) where the stiffness and damping are expressed in terms of K_p, K_d, k_s and k_i. The proportional constant K_p is selected to match the desired bearing stiffness whereas the constant K_s is selected to match the required bearing damping.

2.6. Rotor dynamics of a radial AMB

2.6.1. Basic terms of rotor dynamics

In the design of AMBs the dynamics of the rotor play a very important role. Therefore knowledge of rotor dynamics is necessary. Any rotor has a certain amount of imbalance that causes the rotor to vibrate. These vibrations can reach a maximum at a certain speed called the critical speed [12]. At this speed the rotor can be damaged or it can fail. The field of rotor dynamics can get very complicated because of mathematical differential equations that have to be solved to predict rotor behaviour. In the industry finite element software packages are used to determine the critical speeds of rotors. However the most basic terms must still be understood. This section gives an introduction to the field of rotor dynamics.

2.6.2. Rotor imbalance

A rotor is held in position with bearings so that it can rotate around a fixed axis. At low rotational speeds the rotation axis is the same as the geometrical axis shown in Figure 2.22. The centre of mass of the rotor is defined as the point that moves as though all the mass were concentrated at that

point. All the external forces work in on that point. Ideally the centre of mass must be on the geometrical axis. This is however not possible because of imperfections in the shape of the rotor and the material. The centre of mass is therefore located at a certain distance from the geometrical axis. This is called an imbalance in the rotor.

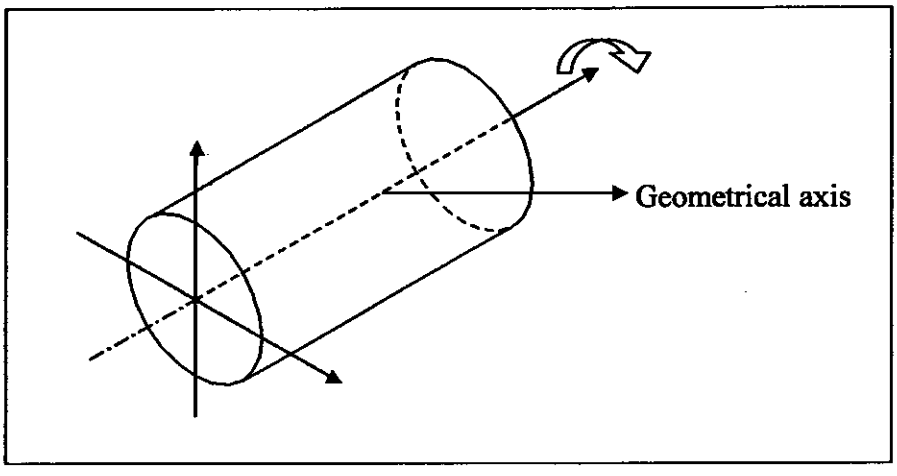

Figure 2.22: Rotation axis of a rotor

An imbalance can be static or dynamic. If the imbalance is in the middle of the rotor (exactly between the two bearings) it is a static imbalance. When the imbalance is not in the middle of the rotor it can create a moment around the bearing. This is a dynamic imbalance. It can only be detected when the rotor is in rotation. It is possible to balance a rotor in such a way to reduce the static and dynamic imbalances. Figure 2.23 is a schematic drawing of a shaft illustrating when the imbalance would be static or dynamic. The force indicated in the figure is the centrifugal force that will be explained in the next section. With dynamic imbalance the force is in opposite directions.

The distance that the centre of mass is located from the rotation axis is called the eccentricity (e) of the centre of mass [20]. The value of e is normally a very small number and measured in millimetres. Rotors can be balanced to reduce the imbalance to a certain specification. ISO 1940 contains such balance quality grades. These grades are determined by taking the product of the nominal operating speed (ω) of the rotor and a maximum value for the eccentricity (e). The grades are indicated by the preceding letter G, for example G630 means the product of (e x ω) is equal to 630 mm/s. Note that for a specific ω and grade, the eccentricity is only an upper limit for the rotor. Its actual eccentricity can be less than this limit.

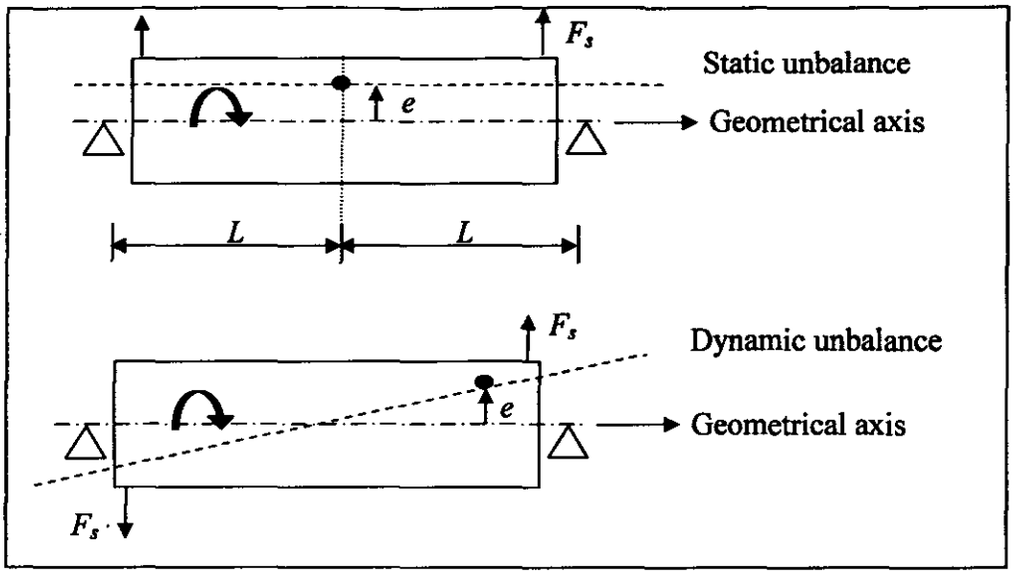

Figure 2.23: Static and dynamic imbalances

The letter G is also used in calculations to calculate eccentricity. A G630 also means that G = 630 mm/s and e can then be calculated from (2.26) with ω the nominal operating speed. The smallest grade is G0.4 and the largest grade is G4000. The grades are separated by a factor of 2.5. Different machines have different grades for example gas and steam turbines have a grade of G2.5 while car wheels have a grade of G40.

$$G = \omega e \tag{2.26}$$

with

e	–	eccentricity of the rotor
ω	–	rotational speed
M	–	centre of mass of the rotor

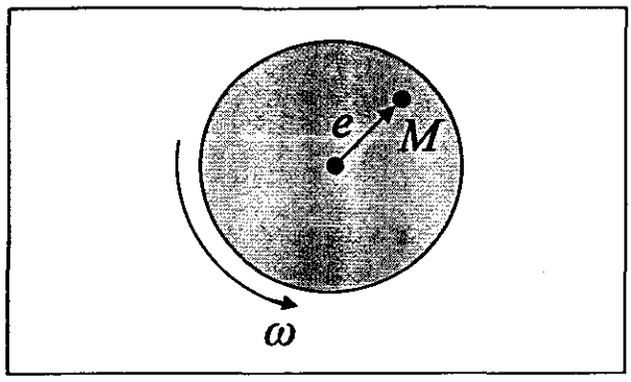

Figure 2.24: Rotor imbalance

2.6.3. Centrifugal force

An important effect of imbalance in rotors is that it produces a centrifugal force. This centrifugal force is very important because it gives an indication of the force the AMB must be able to exert to keep the rotor stable. If the quality grade of the rotor is known the force can be calculated using (2.27). This centrifugal force is outwards and a vibrating or oscillating force. The force is proportional to the mass and proportional to the square of the rotational speed as shown in (2.27). This indicates that high speed application rotors must be well balanced to minimise the centrifugal force.

$$F_c = m\omega^2 e \tag{2.27}$$

with

F_c – centrifugal force
m – rotor mass

2.6.4. Critical speeds

At certain speeds a rotor will experience excessive vibration, much larger than the calculated centrifugal force. These speeds are called the critical frequencies of the shaft. If the shaft is not strong enough the vibrations can damage the machine and the shaft. This is because at this speed the axis of rotation changes from its geometrical axis to an axis through its centre of gravity [12]. There are an infinite number of critical frequencies but for a typical turbo-machine only the lowest three or four falls within its operating speed range [21].

The vibration of a rotor can produce different types of motions that can be seen as whirl orbits around a centre axis. The orbits can be circular, elliptical or in a straight line at an angle to the x-

axis. A graph of whirl amplitude versus shaft speed clearly demonstrates what happens at a critical speed. Vibration at this speed can be reduced by increasing the damping of the system. For some simple rotors the first critical speed can be approximated by using (2.18) from the spring-mass-damper system.

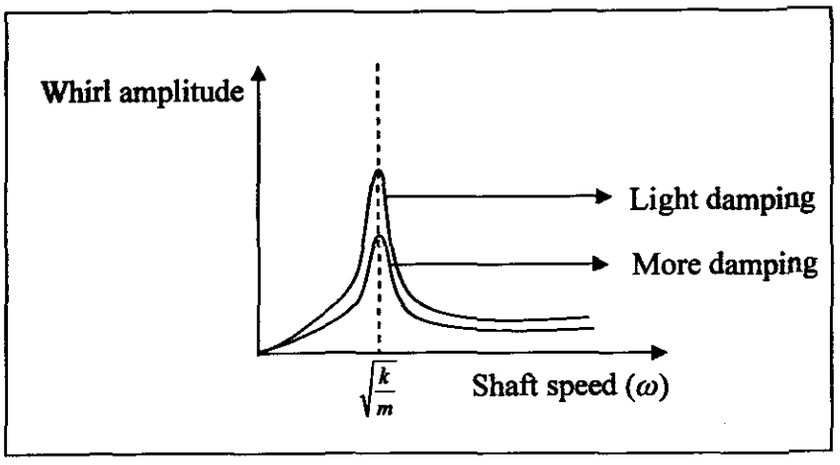

Figure 2.25: Typical imbalance response of rotor

At a natural frequency the rotor is bowed into a certain shape associated with that particular mode [12]. A mode is the first, second, third etc., critical frequency of the shaft. For the first two modes there is negligible bending in the shaft and they are called the cylindrical and conical modes respectively as shown in Figure 2.26. This figure indicates the shaft deflection at the first two modes. At the third mode the shaft starts to bend.

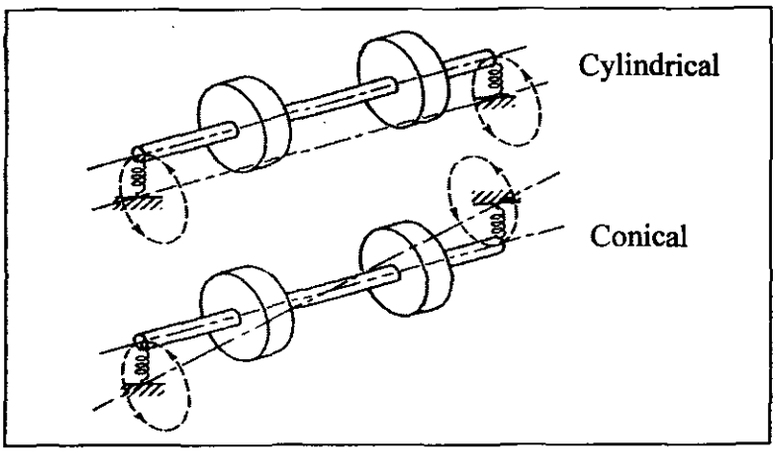

Figure 2.26: First two rigid-rotor modes of a symmetrical shaft [12]

When designing a rotor the nominal working speed of the machine must not be near a critical frequency. The reason is obvious from the above discussion that it could lead to rotor damage. With

steam turbines and turbo compressors the rotation speed often needs to be higher than a critical speed. Therefore the machine must pass the critical speed. In such a case the machine can be quickly accelerated through the critical speed without subjecting it to the high vibrations. Vibration increase with time and before the vibration gets too high the machine passes the critical speed [22].

2.7. Conclusion

In this chapter the reader is introduced to AMBs, its operating principles, its different components and its control. Non-linear and linear models are derived. The stiffness and damping of AMBs are expressed in terms of control and model parameters. There are two types of AMBs: a radial and an axial bearing. Both are necessary for a fully suspended rotor. Different types of power amplifiers and sensors can be used for AMBs each with its advantages and disadvantages.

From the force of the electromagnet it is clear that an AMB is a non-linear system. The force of the electromagnet is proportional to the square of the current and inversely proportional to the square of the air gap size. A suspended AMB works on the same principle as a spring-damper system. Linear and non-linear and control techniques exist for AMBs. Rotor dynamics forms an important part of AMB design. The natural frequency of the shaft and the shaft imbalance must be taken into consideration when designing an AMB.

Chapter 3

Electromagnetic design

3.1. The importance of a good design

The mechanical design is probably the single most important component of an AMB design. Once the bearing has been built and thousands of rands have been spent, there is no turning back and changes or corrections to the mechanical setup cannot easily be made. The design must consider a wide range of variables from mechanical vibrations to slew rates of the power amplifiers.

There are numerous ways in which to conduct the design from very basic approximations to finite element simulations to optimise the design. The complexity of the design is determined by the type of application and the time and money available for the design. The AMB design explained in this dissertation is a radial configuration where only one AMB is used and one conventional bearing to support a shaft.

In order to design the system basic knowledge of rotor dynamics and electromagnetism is required. Fundamental magnetic and rotor dynamic principles are used to gain insight in the operation of the bearing and the different design variables. The design was done with the help of MathCad® software. The complete MathCad® worksheet is included on the CD in Appendix F.

3.2. Design problem

The mechanical system constitutes one radial AMB and one conventional roller bearing. These two bearings must support a rigid shaft. The shaft will be subjected to variable levels of imbalance and will have a maximum rotational speed of 3000 rpm. The AMB must have an air gap between the shaft and the stator of 1 mm and a back-up bearing with half the air gap of 0.5 mm. The back-up bearing must prevent the shaft from damaging the electromagnets.

The starting point in this design is to choose a shaft diameter and to make an estimation of the forces that the radial bearing must be able to support. The AMB must support the weight of the shaft as well as centrifugal forces of the shaft due to imbalance. Secondly the critical frequency of the shaft must be calculated so that the shaft can be treated as a rigid body. The rigid shaft simplifies the control system of the AMB. There are no initial dimensional specifications, but the model is designed to be a small and compact test rig that can be used for future studies.

3.3. Design steps

The design is done in a logical sequence. Each step is explained and the necessary calculation and formulas are given. An iterative approach is followed, so that if the system characteristics are not satisfactory, the dimensions and system parameters are changed to obtain the desired values. Assumptions are made to simplify the design process where necessary. Figure 3.1 shows the design process that is followed.

The first step is to specify the dimensions of the shaft. This can be done because there is no restriction on the size of the model except that the shaft must be a rigid body to simplify the control and the position sensing of the AMB. This basically means that at 3000 rpm the shaft must still be a rigid body. Any shaft becomes flexible at some rotation speed. This property of the shaft is explained in Chapter 2.

The next step is to make an estimation of the force on the shaft. This is mainly a centrifugal force of the shaft which is proportional to the square of the rotational speed and proportional to the imbalance grade of the shaft. By using the amount of force and the rotation speed the required slew rate of the power amplifier is calculated. The AMB actuator is then designed for this specified force and the slew rate is used in the power amplifier design.

It was decided to use a homopolar electromagnet configuration as discussed in section 3.6. The pole area of the electromagnet is calculated from the force specification. Once again in this case there are a few ways to determine the width and length of the pole. It can be chosen the same so that the pole is square as in [6] for a heteropolar design. For this design it is decided to divide the shaft circumference into eight equal sectors of 45°. The width of each of the four electromagnets will then cover one sector of the shaft as explained in section 3.6.

The last step in this design procedure is to calculate the window area and the number of windings. The current of the power amplifier and the maximum magnetic flux are specified and the amount of turns is calculated. The window area is calculated by assuming a certain wire packing factor and an allowable current density in the coils is chosen.

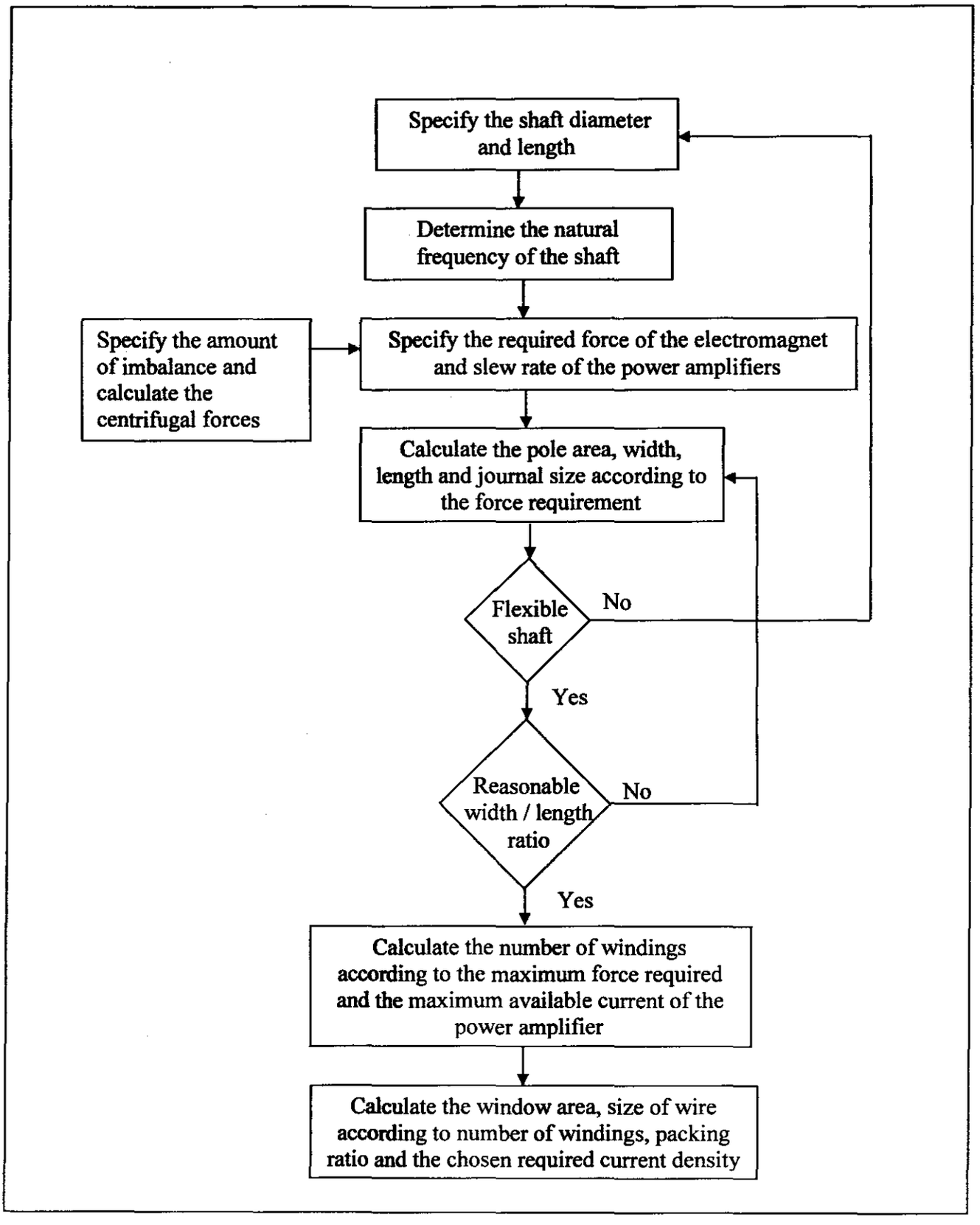

Figure 3.1: Design sequence

3.4. Shaft design

An important characteristic of the shaft for the purpose of this design is that it must be considered as a rigid body. This depends on the working speed of the shaft and its critical frequency. A rotating body have more than one critical speed of which the third critical frequency is its first bending mode. Due to imbalance a rotating body will not rotate around its geometric centre but rotate about an axis through its centre of gravity. At the critical frequency the vibration because of imbalance is a maximum.

The vibrations of the shaft can be classified into two types: synchronous and non-synchronous whirl. Shaft imbalance will always produce whirling which is synchronous with shaft speed. There are three ways to reduce the synchronous whirl: 1) balance the shaft, 2) change the speed or dimensions of the shaft and 3) add damping to the system. It was decided to use the second option for this design. The speed is 3000 rpm and the dimensions of the shaft will be changed. The normal operating speed must generally be 20% lower than the critical speed for safe operation. Therefore the minimum critical speed is: 3000/0.8 = 3750 rpm.

For the AMB shaft the critical frequency is calculated using the spring-damper-mass model. The total shaft basically consists out of two cylinders; one thin long rod and the AMB journal. Both effect the critical frequency. Obtaining the dimensions for the shaft is an iterative process. The diameter of the shaft is firstly specified. Then the size of the journal is calculated and the critical frequency is calculated. The critical frequency speed must be greater than 3750. The calculations are shown in Appendix A and the critical speed is calculated as 6000 rpm.

3.5. Required force

The required force of an AMB is the force that the electromagnets can exert on the shaft. When standing still the only force that must be overcome is the weight of the shaft. When the shaft rotates there are centrifugal forces present because of shaft imbalance. These forces can be calculated if the grade of imbalance is known. There are other external forces that also work in on the shaft for example load vibrations or the driving method. An air pressure turbine is used in this AMB and the wind will blow in on the top and the bottom part of the shaft so that is does not cause imbalanced forces. The shaft will not have a load attached to it. Therefore only the weight and centrifugal forces will be taken into consideration.

The shaft will be a homogenous body (not laminated) and it is therefore assumed that the shaft will have a very small imbalance. The centrifugal force that the bearing must be able to support is therefore very small. To expand the characteristics of the AMB system it was decided to make provision for larger centrifugal forces. The shaft contains four holes where imbalance weights can be added in the form of screws. The weights will increase or decrease the centrifugal force dramatically. This makes the model more versatile for imbalance tests and rotor dynamic analyses.

The ISO 1940 standard contains imbalance quality grades. This standard classifies rotors into different imbalance grades according to the amount of imbalance of the rotor. Every grade has a number that corresponds to the product of the eccentricity and the operating speed of the rotor as explained in Chapter 2. Typical grades are given in Appendix C. If the imbalance grade is known the centrifugal force can be calculated.

In this design a specific maximum imbalance grade is chosen and the centrifugal force for this imbalance is calculated. This imbalance grade will then represent the highest possible allowable imbalance on the shaft for stable suspension. The force is the maximum centrifugal force of the shaft.

To calculate the centrifugal force an imbalanced grade of G100 is used. The eccentricity for the shaft rotating at 3000 rpm is then determined.

The centrifugal force for the shaft of mass m is:

$$G = e_{imbalance}\,\omega_{radians/s} \tag{3.1}$$

$$e_{imbalance} = G\frac{60}{N_{shaft}\,2\pi}$$

$$= 0.31831 \text{ mm}$$

with

G	- imbalance grade in mm/s (G = 100 mm/s)
$e_{imbalance}$	- eccentricity of the shaft
$\omega_{radians/s}$	- rotation speed in rad/s
N_{shaft}	- rotation speed in rpm (N_{shaft} = 3000 rpm)

The centrifugal force is then:

$$F_{cen} = (\omega_{rad/s})^2 e_{imbalance} m_{shaft} \approx 63\text{N} \tag{3.2}$$

with

m_{shaft} - shaft mass ($m_{shaft} = 2$ kg)

Note that the mass of the shaft is the total mass including the journal. Although the size of the journal is not yet known in this stage of the design, this value represents an approximation for the total mass. It is decided to choose the required force at 100 N. This means that the bearing is over designed in terms of force and imbalance specifications. This is done because losses in the material of the AMB are not accounted for in this design. In [6] a correction factor of 1.25 is used for radial AMB design to account for losses. With this force specification the electromagnets can then be designed.

3.6. Electromagnet configuration

A homopolar configuration with four electromagnets is chosen as shown in Figure 3.2. The polarity of the legs in one electromagnet can be made the same as the polarity of the corresponding legs in the other electromagnets. When the shaft rotates and move from one electromagnet to the next the polarity in the shaft at a certain point does not change for example from positive to negative, but only changes from positive to zero and back to positive. Therefore the losses in the rotor can be made lower if the polarities of the corresponding legs are the same. This configuration makes it possible to use electromagnets and a shaft with no laminations.

More than four electromagnets can be used with three magnets the minimum to ensure a stable system. Designs where there are more than four electromagnets are mostly optimised for physical size and losses. A basic sketch of the bearing is shown in Figure 3.2. Appendix C shows the detail drawings done in Cadkey®.

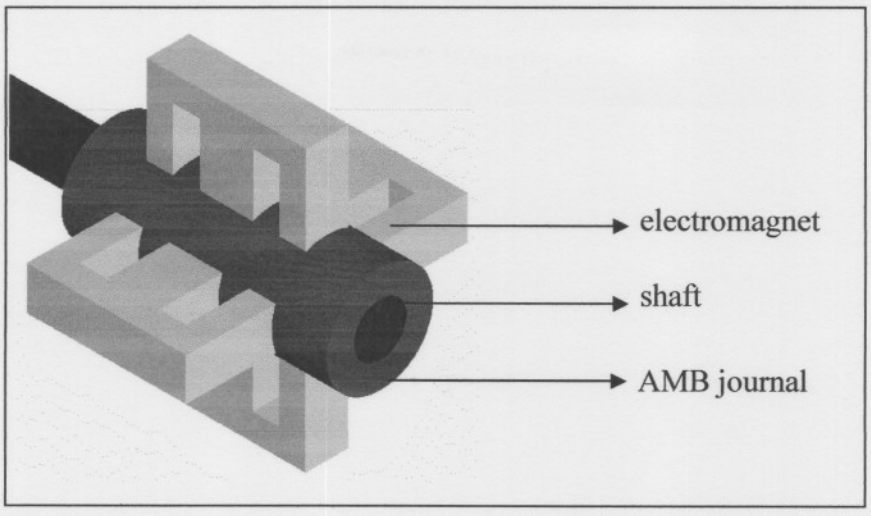

Figure 3.2: Homopolar radial AMB

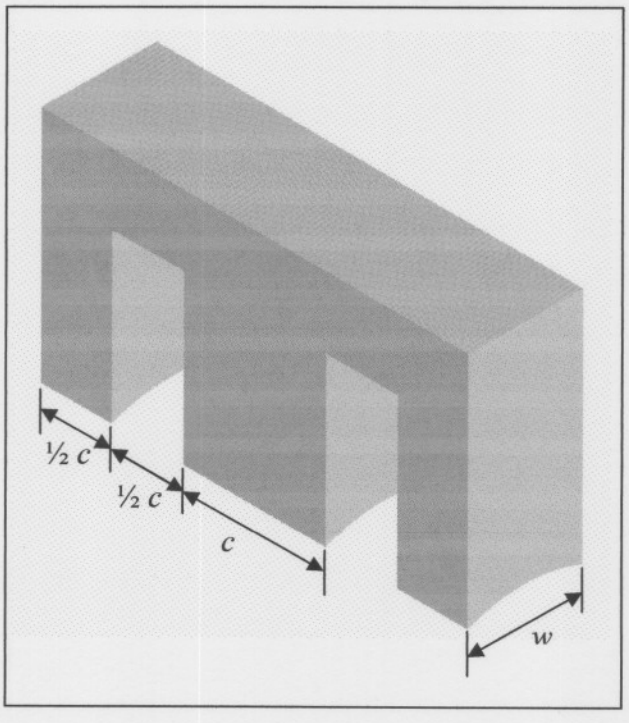

Figure 3.3: The electromagnet

The pole area of the AMB is the area of the centre leg of the AMB shown in Figure 3.3. The design is done so that area of the side legs is half that of the centre leg. The values for w and c are calculated in the next section. The coil is wound around the centre leg and a bobbin is used to fit the coil precisely on the leg. A front view of the electromagnets is shown in Figure 3.4. The circumference of the shaft is divided in eight equal sectors of 45° each. The angle θ as used in (3.3) is half of the sector angle and is equal to 22.5°.

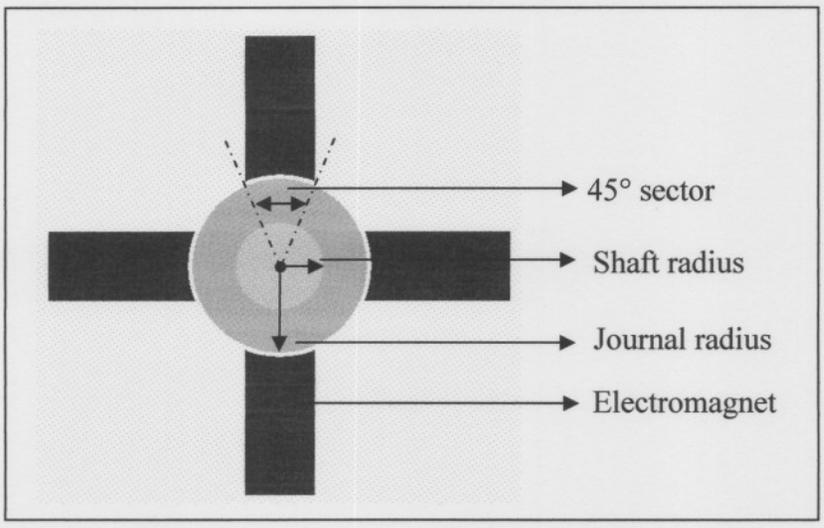

Figure 3.4: Front view of the radial AMB

3.7. Pole area

To calculate the pole area (3.3) is used. The force and flux density are specified. A maximum magnetic flux density (B_{iron}) of 1 Tesla is chosen in the iron. Commercially available mild steel will be used. This kind of steel is used because there are no special requirements in terms of very high saturation levels or low losses. The steel can also be easily machined. A maximum force of 100 N is used as calculated in the previous section.

$$F_{\max} = \left(\frac{B_{iron}^2}{\mu_0}\right)\left(\frac{\sin\theta}{\theta}\right)^2 A_{iron} \tag{3.3}$$

$$A_{iron} = 270\,\text{mm}^2$$

with

F_{max} - the specified maximum force

B_{iron} - magnetic flux density in the iron

θ - half the angle of one sector of the electromagnet (22.5°)

μ_0 - permeability of air

A_{iron} - pole area

The $\sin(\theta)/\theta$ factor is a correction factor used because the electromagnet is not a flat surface. The mathematical derivation is given in Appendix.B

The next step is to calculate the radius of the journal. This can be done by writing w and c in terms of the total radius and then substitute it into:

$$A_{iron} = c.w \tag{3.4}$$

To prevent the saturation of the journal the journal has a thickness of ½ c. Therefore the total radius is now the shaft radius plus the ½ c plus the 1 mm air gap:

$$\begin{aligned} r_p &= \frac{1}{2}c + r_{shaft} + g_0 \\ \therefore c &= \left(r_p - r_{shaft} - g_0\right)2 \end{aligned} \tag{3.5}$$

with

g_0 - the 1 mm air gap between the shaft and stator

r_{shaft} - radius of the shaft

r_p - total radius including the air gap

Note the difference between the radius of the shaft and the radius of the journal in Figure 3.4. To obtain the width w in terms of the total radius the trigonometric relation between the total radius and the angle θ is used:

$$w = 2r_p \sin\theta \tag{3.6}$$

Equation (3.5) and (3.6) is substituted in to (3.4) and then the total radius r_p is given by:

$$\begin{aligned} r_p &= \frac{r_{shaft} + g_0 + \sqrt{\left(r_{shaft} + g_0\right)^2 + \dfrac{A_{iron}}{\sin\theta}}}{2} \\ &\approx 20 \text{ mm} \end{aligned} \tag{3.7}$$

The value r_p includes the air gap of 1 mm but it is decided to make the journal radius 20 mm and the total radius (r_p) is then 21 mm. The journal radius is then exactly twice the radius of the shaft. The distance w and c is now calculated quite easily by using (3.5) and (3.6).

$$\begin{aligned} w &\approx 15 \text{ mm} \\ c &\approx 18 \text{ mm} \end{aligned} \tag{3.8}$$

3.8. Number of turns

The number of turns is chosen so that the peak amplifier current would not saturate the electromagnet material. The amplifiers for this project are linear current amplifiers that can supply 2.5 A, 50 V dc with a peak current capability of 2.8 A (I_{max}). The number of windings is then:

$$N = \frac{B_{sat} g_0}{\mu_0 I_{\max}} \approx 400 \text{ windings} \tag{3.9}$$

To determine the window area needed for the coil a current density of 4 A/mm^2 in the copper is used with a packing factor of 0.55. The window area is then:

$$A_{window} = \frac{NI_{rms}}{(4\,000\,000)0.55} = 581.8\,\text{mm}^2 \tag{3.10}$$

The height (h) of the window is then:

$$A_{window} = 0.5c\,h \quad \therefore h \approx 64\,\text{mm} \tag{3.11}$$

The desired size of the copper wire is calculated from:

$$A_{window}\,0.55 = (\pi r_{wire}^2)N \quad \therefore r_{wire} = 0.48\,\text{mm} \quad \therefore A_{wire} = 0.726\,\text{mm}^2 \tag{3.12}$$

with

A_{window}	- the window area
r_{wire}	- radius of the wire
A_{wire}	- area of the wire

The standard wire size with a diameter of 1 mm is chosen.

3.9. Finite element analysis

To verify the magnetic design QuickField® finite element analysis software is used. The package is a student version with a limit of 200 nodes that can be used. The analysis is only in two dimensions

with a default depth of 1 m. Thus the electromagnet cannot have a curved pole area and a flat pole area must be used. This the will result in an error of 2.55 % according to the correction factor used in (3.3).

In QuickField® the properties of each material must be specified. QuickField® has built in libraries for some common known materials. The B-H curve for the material is included in the library. Steel is chosen for the electromagnet and the shaft. The B-H curve shows that the saturation flux density is approximately 1.6 T. The curve for steel is shown in Figure 3.5. The magnetic field intensity is specified for the coil area as 2.8 A x 400 turns which is 1120. The outer boundaries of the electromagnet was specified with Dirichlet boundary conditions with a magnetic potensial of zero.

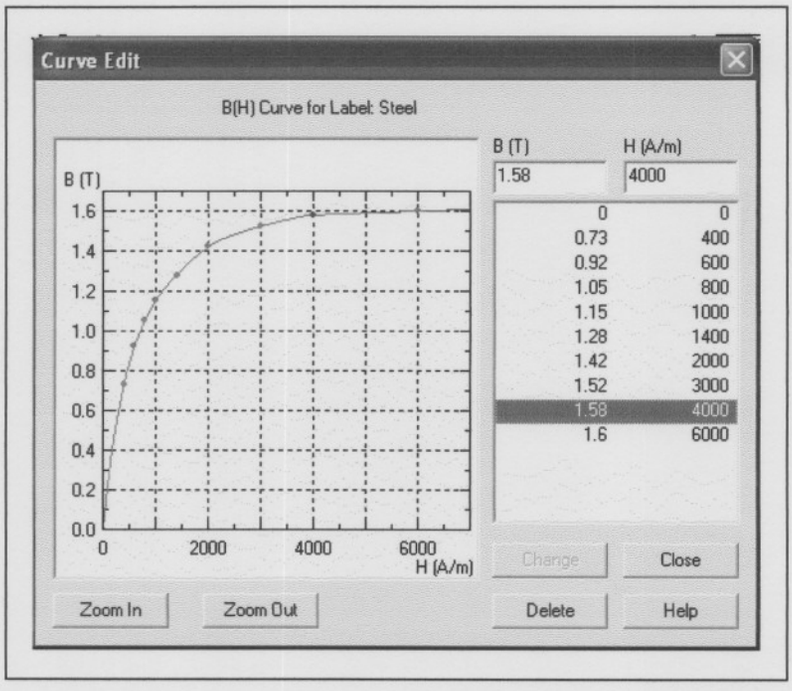

Figure 3.5: B-H curve for steel

The 200 node limit makes it difficult to accuratly analise the electromagnet. If too few nodes are used the force value is very low and inaccurate. If more nodes are used the force value and the accuracy increase. The number of nodes in each materiaal can be selected so that the part where the accuracy is very important has more nodes than the rest of the system. A Mesh is created using the nodes as shown in Figure 3.6. The outline of the electromagnet is made bold to distinguish between the mesh and the model. Upon analysis the flux lines are distrubuted shown as in Figure 3.7. With the help of the QuickField® calculator function the force on the shaft can be calculated.

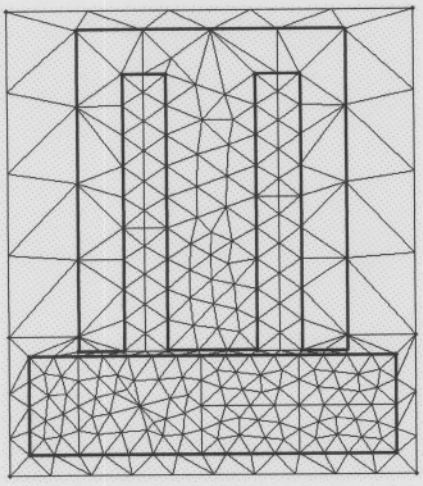

Figure 3.6: The Mesh of the electromagnet model

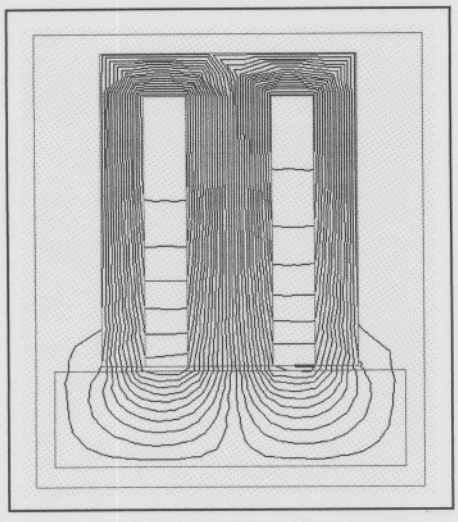

Figure 3.7: Electromagnet flux lines in QuickField®

At 200 nodes the value for the force is between 5539 N and 5959 N for various node densities. This value must still be converted because the depth of the system is by default 1 m and the depth of the electromagnet is 15 mm. The force is then found to be between 83 and 89 N. Note that the initial electromagnet is designed for 100 N but that this value is an overdesign to compensate for losses as discussed in section 3.5. The actual required force is 63 N. This means that the electromagnet design is still within specification and that the design has been verified.

3.10. Drawings and manufacturing

Once the design is completed drawings are done to manufacture the AMB. The drawings are done in Cadkey® and are given in Appendix D. The aim of this section is to explain how the different components are put together. The AMB constitutes four electromagnets, a shaft, sensors, an air pressure turbine and a ball bearing.

The complete drawing is shown in Figure 3.8. In this figure the ball bearing is situated at the back and the AMB in front. The air pressure turbine is at the rear side of the AMB. The four electromagnets are on the inside of the housing made of aluminium. Aluminium is used to prevent flux coupling between the electromagnets. In front of the AMB are the four cylindrical sensors. The holes in the shaft at the front end are where the imbalance weight can be added. The housing and the back-up bearing are shown in Figure 3.9. The housing is cut away to position the electromagnets in exactly the right place. The electromagnets are fastened by two bolts.

Two end plates are used to cover the electromagnets on both sides of the housing. The end plates houses the sensor and the turbine respectively. The end plates are manufactured with a small shoulder so that it fits precisely into the housing. A slot is machined in this shoulder so that the electromagnets fit into these slots. This is to keep the electromagnets in place when the centre hole for the shaft is machined.

To ensure that the air gap is exactly 1 mm, the housing is first made and the electromagnets and the end plates are fitted. The electromagnets are also made a small bit longer. The housing is then aligned and the 42 mm centre hole is machined with a laithe. The back-up bearing is then inserted onto the rear end plate.

The air pressure turbine is shown in Figure 3.10. Two air nozzles are made and fitted onto a turbine mount on one of the end plates. There are 18 holes in the journal with a diameter of 12 mm. The nozzles are alined so that the centre of the nozzle and the flat surface of the hole are on the same line.

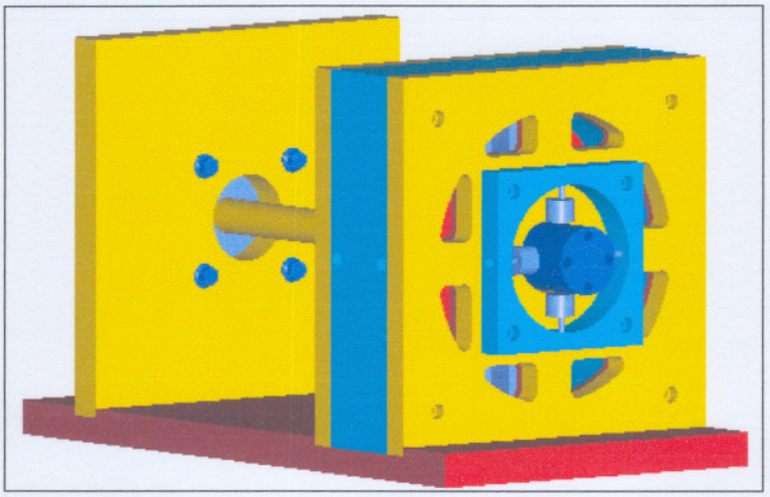

Figure 3.8: Complete AMB drawing

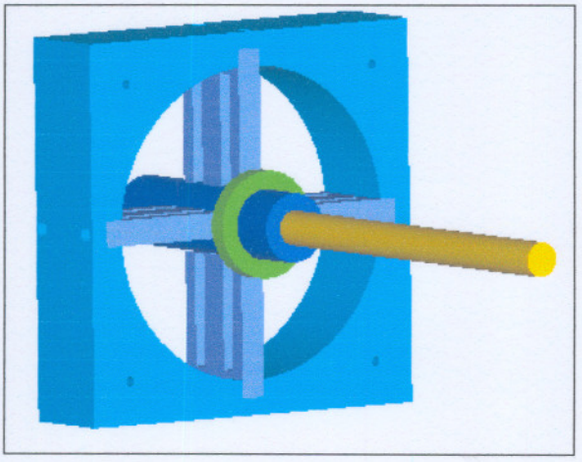

Figure 3.9: Drawing of the housing and back-up bearing

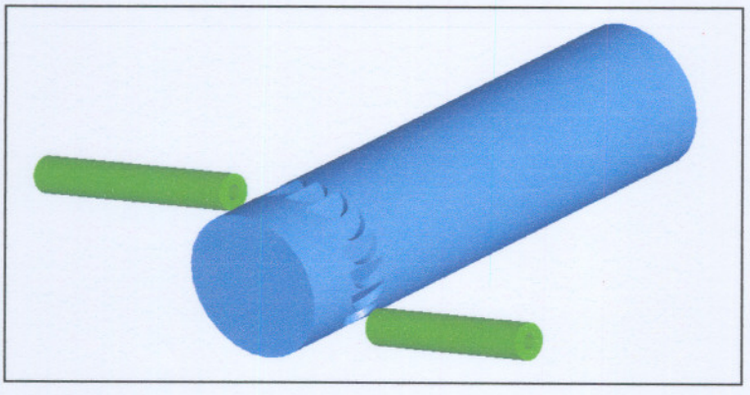

Figure 3.10: Air turbine on the journal

3.11. Conclusion

In this chapter the electromagnetic design is discussed. The design is done in a logical sequence: shaft design, required force and electromagnet design. A rigid shaft is designed and the shaft will have a rotation speed of 3000 rpm. An imbalance grade is specified for the shaft and the centrifugal force due to the imbalance is calculated. The electromagnet is then designed for that force. A homopolar electromagnet configuration is chosen. The AMB will not have any laminations.

The design is verified with finite element analysis and the results correspond to the electromagnet design. Drawings are done in Cadkey® for manufacturing. The AMB constitutes electromagnets, aliminium housing, air pressure turbine, a shaft and sensors. The turbine and back-up bearing are fitted on the rear endplate and the sensors are fitted on the front endplate. The complete set of drawings is shown in Appendix D.

Chapter 4

Simulation

The objective of this chapter is to discuss the simulation of the AMB system. The simulation of the complete system constituting the actuators, power amplifiers and control system is done in Matlab®. From the simulation results the specifications for the power amplifier and control system were obtained. The results will also be compared with the actual results of the implemented AMB in Chapter 7. The properties of the electromagnet designed in Chapter 3 are used in the simulation. The Matlab® code for the simulation is given on the CD in Appendix F.

4.1. Simulation components

The following components of the AMB were included in the simulation: actuator, power amplifier and controller. Only the vertical plane is simulated as shown in Figure 4.1. The top and bottom electromagnets work together to suspend the rotor in the vertical axis. The electromagnets on the left and right hand side were assumed to have no effect on the position in the y-axis. The centre position for the rotor is -1 mm as indicated in Figure 4.1. The position of the rotor is a value between -0.5 mm and -1.5 mm because the back-up bearing prevents the shaft from coming closer than 0.5mm to the electromagnet. The position value is scaled to a value between -0.9 and +0.9. This represents the sensor value that is used in Simulink® of the actual system. This conversion factor is explained in more detail in Chapter 6. The centre position is represented by the value 0 in Simulink®.

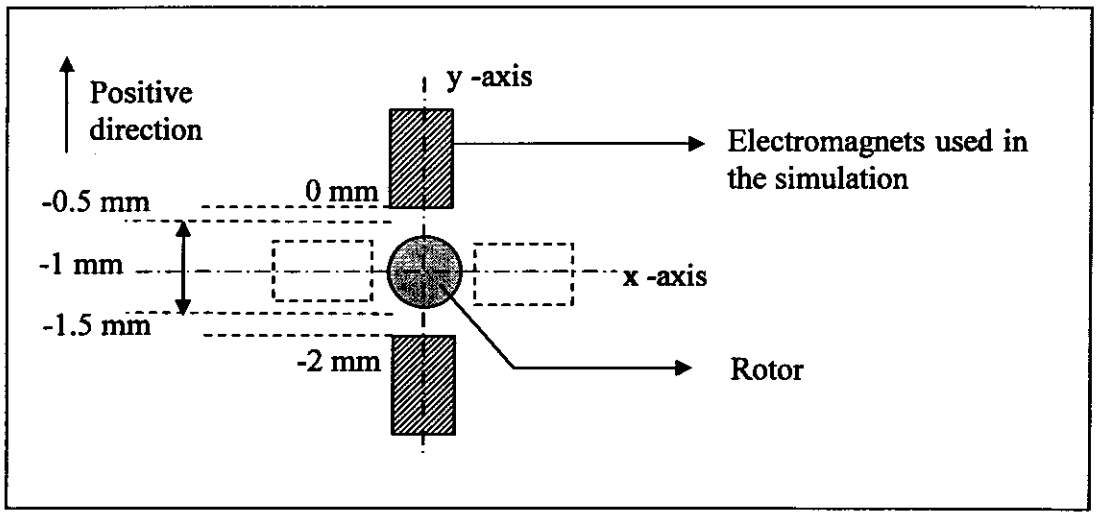

Figure 4.1: Side view of the AMB showing the four electromagnets

The power amplifiers are very important components of the AMB. To design the correct amplifier correctly, the results of the simulation are used. This includes the current, voltage and slew rate specifications. Each electromagnet has its own power amplifier. In the simulation two electromagnets opposing each other are used, each with its own power amplifier.

A PID controller is used to control the AMB system. A differential driving mode will be used as discussed in Chapter 2 and again shown in Figure 4.2. One controller is used to control the current in two opposing electromagnets. The control signal is added to the bias current for the top electromagnet. The same control signal is subtracted from bias current for the bottom electromagnet.

The parameters K_p (proportional gain), K_i (integral gain) and K_d (differential gain) obtained in the simulation are used in the actual control system. The effect of each parameter on the system's behaviour will also be investigated.

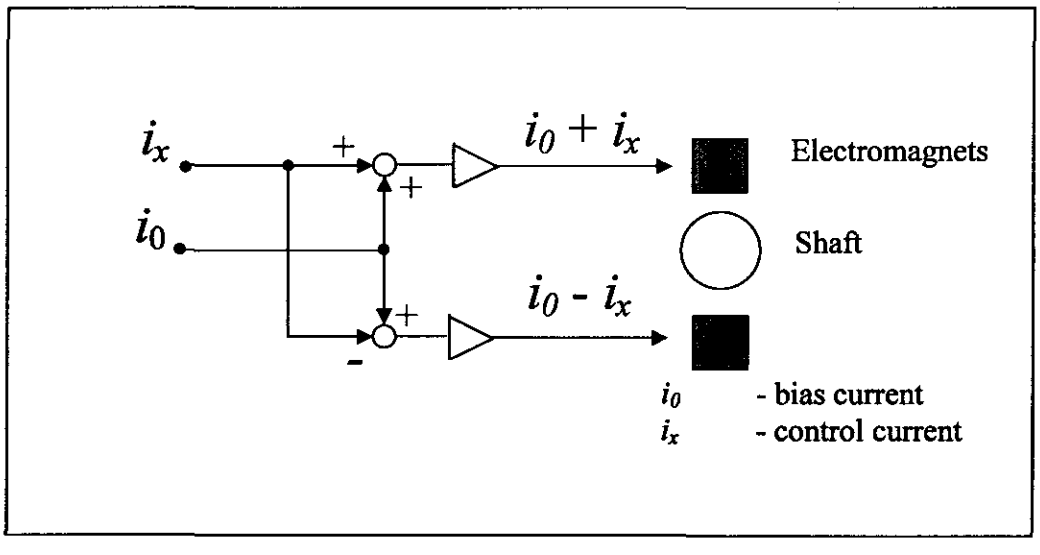

Figure 4.2: Differential driving mode

4.2. The position model

To simulate the force on the rotor the force equation from Chapter 2 is used. To calculate the force, the current and the position must be known. The initial condition for the current was zero and for the position was -1 mm, representing the centre position. The force equation is given in (4.1) with

$$k = \frac{1}{4}\mu_0 N^2 A_g \tag{4.1}$$

The next step in the simulation is to calculate the position of the rotor. Newton's second law is used to calculate the acceleration of the rotor. The double integral of the acceleration is then the position. The total force on the rotor is given by

$$F_{res} = F_1 - F_2 - mg \tag{4.2}$$

with

F_{res}	–	the resultant force on the rotor
F_1	–	the force exerted by the top electromagnet
F_2	–	the force exerted by the bottom electromagnet
mg	–	the weight of the rotor

The acceleration and position is then given by:

$$\begin{aligned} m\ddot{x} &= F_{res} \\ &= F_1 - F_2 - mg \\ \therefore \ddot{x} &= \frac{F_1 - F_2 - mg}{m} \\ \therefore x &= \iint a\,dt \end{aligned} \tag{4.3}$$

with

x	–	the position between -0.5 and -1.5 mm of the shaft.

The integration calculation in Matlab® was done numerically as given by (4.4):

$$x(k) = \dot{x}(k)dt + x(k-1) \tag{4.4}$$

with

$x(k)$	–	k^{th} position value
$x(k-1)$	–	$(k-1)^{th}$ position value
$\dot{x}(k)$	–	k^{th} velocity value
dt	–	step time of the simulation

4.3. The power amplifier

It is decided to use a linear amplifier to reduce the noise as will be explained in Chapter 5. The linear amplifier is a current mode amplifier and is also included in the simulation. This is also an iterative process between the simulation and the design of the power amplifier. The response of the simulated power amplifier and the actual one is nearly the same to ensure an accurate simulation of the AMB system. A simplified circuit of the power amplifier is shown in Figure 4.3. The current through the coil is sensed using a sense resistor (R_4). This signal is fed back to a difference amplifier that subtracts the actual current feedback signal from the desired current signal. The difference amplifier has a unity gain.

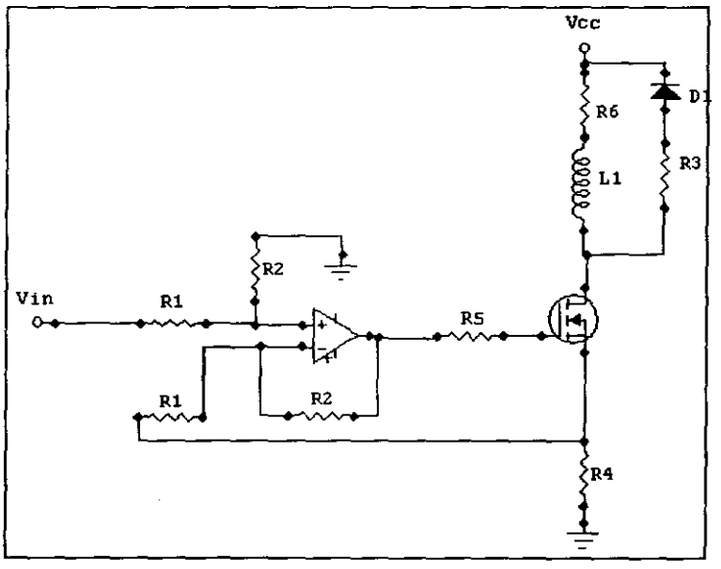

Figure 4.3: Simplified power amplifier

The power amplifier has two different states of operation: when the MOSFET is turned on in its linear region and when the MOSFET is turned off. With the linear operation of the amplifier the MOSFET will be in the on state most of the time, only when an impulse disturbance is applied the MOSFET will turn off quickly to reduce the current. The equivalent circuits for on and off states are shown in Figure 4.4 and Figure 4.5 respectively.

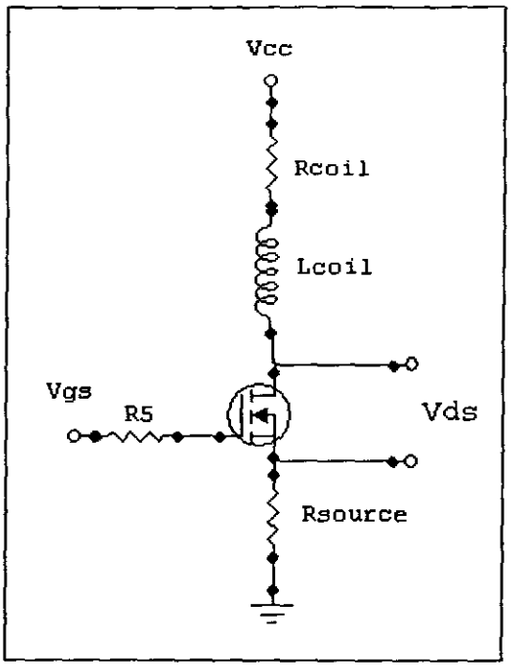

Figure 4.4: Equivalent circuit in the on state

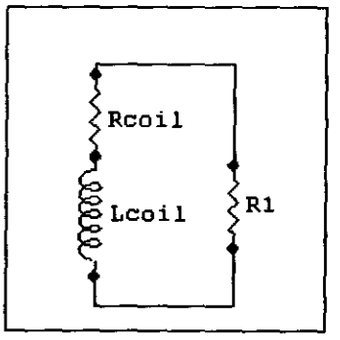

Figure 4.5: Equivalent circuit in the off state

To find the current through the coil in the on state the derivative of the current is first calculated and the result is then integrated. In the on state the sum of the voltages must be zero:

$$V_{cc} = i(R_{coil} + R_{source}) + L\frac{di}{dt} + V_{ds} \tag{4.5}$$

with

V_{cc}	–	dc supply voltage
i	–	current through the coil
R_{coil}	–	coil resistance
R_{source}	–	resistor between the MOSFET's source and ground

L – coil inductance

V_{ds} – voltage across the drain and source of the MOSFET

The derivative of the current is then:

$$\frac{di}{dt} = \frac{V_{cc} - i(R_{coil} + R_{source}) - V_{ds}}{L} \tag{4.6}$$

It is however necessary to get (4.6) in terms of the gate-source voltage (V_{gs}) of the MOSFET since this is the control signal. V_{gs} is inverse proportional to V_{ds}. If V_{gs} is at its maximum the MOSFET is turned on and V_{ds} is approximately zero. If V_{gs} is zero, the MOSFET is turned off and V_{ds} is equal to V_{cc}. Although the relationship is not exactly linear, it is found that it is still a good approximation. V_{ds} then becomes:

$$V_{ds} = V_{cc} - K_{fet} V_{gs} \tag{4.7}$$

with

K_{fet} - the gain ratio between V_{gs} and V_{ds}

If the MOSFET is off the describing differential equation is given by:

$$i(R_{coil} + R_1) + L\frac{di}{dt} = 0$$
$$\frac{di}{dt} = \frac{-i(R_{coil} + R_1)}{L} \tag{4.8}$$

4.4. The controller

The PID controller used constitutes three components: proportional (K_p), integral (K_i) and derivative (K_d) gain. The output of each component is added to obtain the control signal. A Simulink® block diagram of the controller is shown in Figure 4.6. The controller is implemented in Matlab® code and numerical integration and differentiation are used in the calculations.

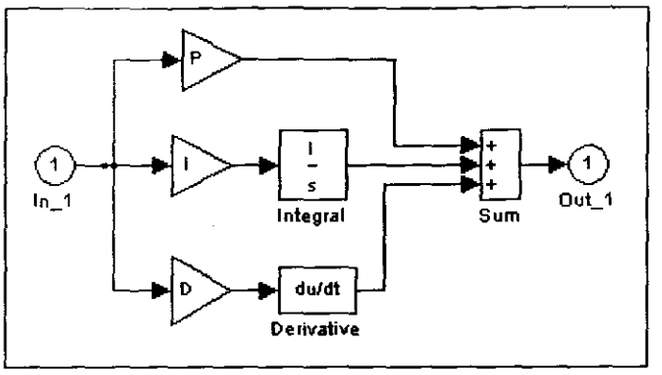

Figure 4.6: Controller block diagram

4.5. Simulation results

The following simulations are done

- Stable suspension with rotor not rotating
- Step response
- Effect of the PID parameters on the step response
- Imbalanced forces on the shaft

4.5.1. Stable suspension

A stable suspension without any imbalance forces is simulated and the results are shown in Figure 4.7. The position and the currents in the two coils are shown. The values of the control parameters are: $K_d = 0.9$, $K_i = 4$ and $K_d = 0.015$. The system settles in 0.7 s and is then stably suspended. The integral term ensures that there is no steady state error. The bias current in the top electromagnet is 0.92 A and 0.78 A in the bottom electromagnet. The top electromagnet has to overcome the weight of the rotor and therefore has a higher bias current.

4.5.2. Step response

A step of 0.045 mm is given to the system. The position and currents are shown in Figure 4.8. The percentage overshoot for an upwards step is 44 % and for a downwards step is 89 %. The settling time is 0.3 s and 0.4 s respectively. The momentum of the rotor causes the overshoot and the slower settling time for the downwards step. There is once again no steady state error.

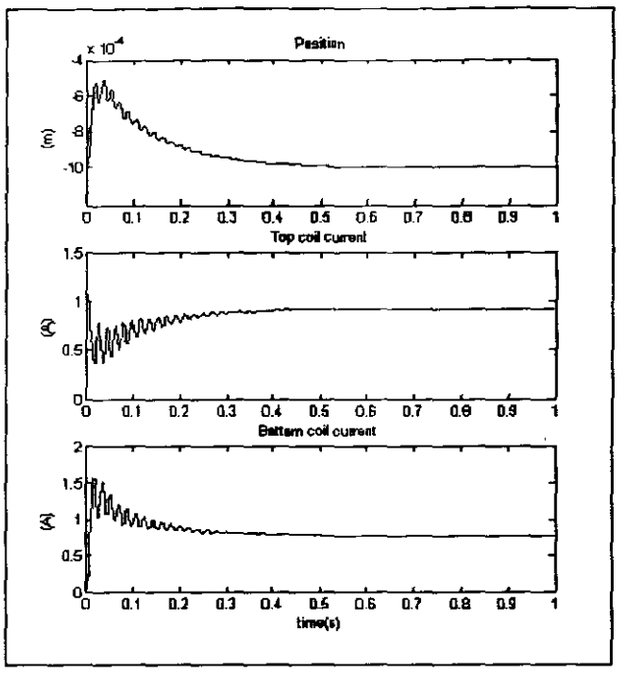

Figure 4.7: Stable suspension with no imbalance forces

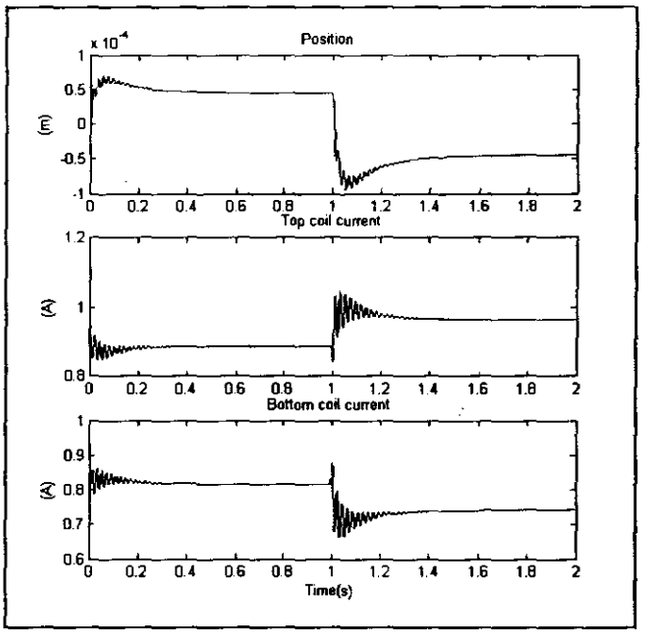

Figure 4.8: Simulation step response

Each PID control parameter has an important effect on the system. To investigate the effect each parameter is made significantly small and the step response is measured. The values used are shown in Table 4.1. Only one value is changed at a time and the other two are kept at its original value.

Value	Original value	Lower value
K_p	0.9	0.5
K_i	4	0
K_p	0.015	0.009

Table 4.1: PID values of the simulation

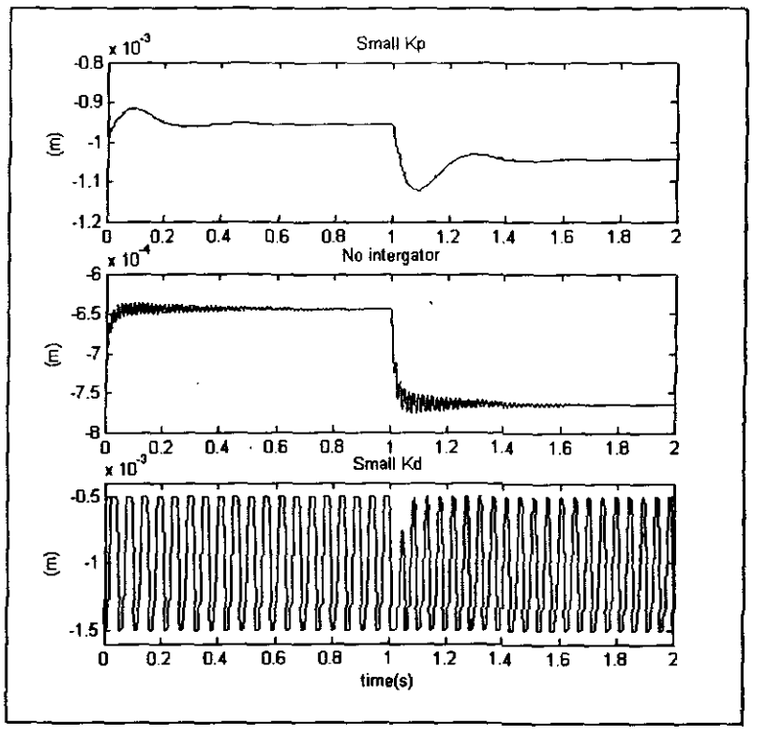

Figure 4.9: Effect of the PID parameters

A lower K_p value increases the overshoot of the system and this leads to decreased stiffness. The system is still stable but can become unstable if the value is too low. With no integration ($K_i = 0$) in the control system there is a steady-state error as shown in Figure 4.9. The most important parameter of the three is K_d. The system becomes unstable with a lower value. The system cannot be suspended successfully without this parameter because the AMB is a non-linear naturally unstable system.

4.5.3. Imbalance force

To simulate the rotation of the rotor a sinusoidal imbalance force is added on the shaft. The frequency of the force is 50 Hz which represents 3000 rpm. The imbalance force represents the centrifugal force during the rotation of the rotor. The centrifugal force on the rotor is calculated as

63 N in Chapter 3. The imbalance force is only activated after 1 s to give the AMB time to reach a stable position. Results are shown in Figure 4.10. The deviation in position is 0.5 mm peak to peak.

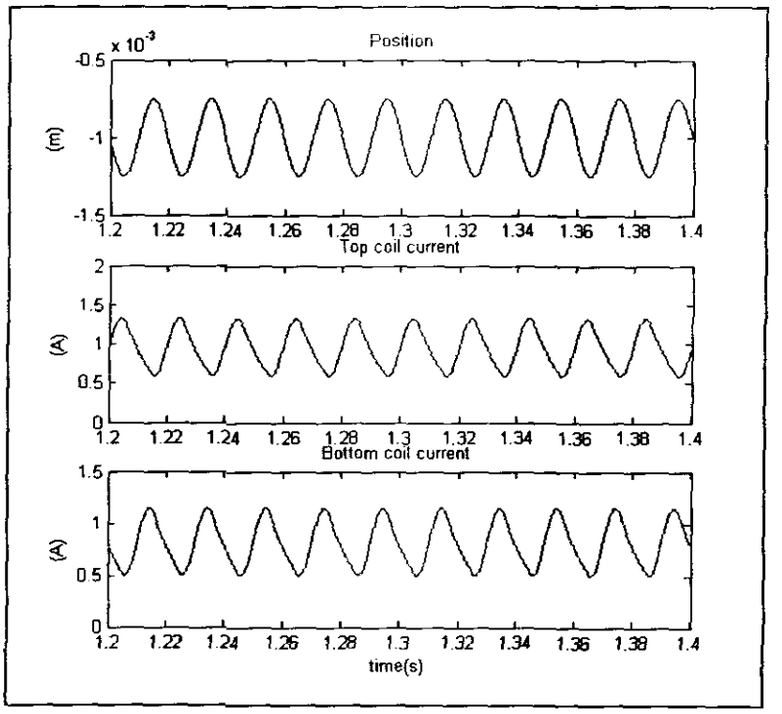

Figure 4.10: Suspension with an imbalance force

4.6. Conclusion

In this chapter the simulation of the AMB is discussed. The simulation makes use of differential equations to describe the behaviour of the AMB. The power amplifier is also included to find its proper specifications. The results of the simulation are given and stable suspension is achieved in the presence of a 63 N imbalance force. In the next chapter the results of the simulation will be used to design the power amplifier.

Chapter 5

Power amplifier and sensor design

The aim of this chapter is to explain the design of the power amplifier and the sensor. A linear power amplifier is chosen instead of a switched mode power amplifier because of noise considerations. The specification for the amplifiers is found from the results of the Matlab® simulation. CircuitMaker® is used to simulate the power amplifier. An inductive sensor is used to sense the position. This sensor proved to have a linear response and a high enough bandwidth. The cost of the sensor is also relatively low.

5.1. The power amplifier

The fundamental role of the power amplifier in AMBs is to control the level of magnetic energy stored in the coils and air gap so that it matches the desired energy. This means it controls the voltage across the coils (voltage mode) or the current in the coils (current mode). In AMBs the type and size of the amplifier is very important. This section constitutes: the design, simulation and actual results of a linear amplifier.

5.1.1. Type of power amplifier

The first decision to make is whether to use a switched mode amplifier or a linear amplifier. Both have their advantages and disadvantages. The decision is strongly influenced by the desired characteristics of the AMB itself. Factors like noise, efficiency, cooling, size and cost are probably the most important ones.

For this project the noise is the most important factor. Inductive type sensors are used to determine the position and were found to be very noise sensitive. The switched mode power supply generates noise at its switching frequency and this interferes with the sensor signal. Laboratory tests were done with a switched mode power amplifier and inductive sensors and the noise problem was significant.

The disadvantage of a linear amplifier is its low efficiency. Optimisation for power efficiency is however not part of the scope of this project. The problem with the low efficiency is that a huge amount of heat needs to be dissipated. To address the problem a detailed thermal design is necessary.

5.1.2. Specifications

Basic specifications of a power amplifier are in terms of rated voltage, rated rms current and slew rate. The rated voltage is the maximum voltage across the switching element when it is completely turned off and the rated rms current is the current that the amplifiers must continuously deliver to the coil. It is important to choose a switching element that can withstand the voltage and current ratings. The slew rate requirement is determined by the maximum change in force with respect to time that is necessary for a stable suspension in the presence of rotor imbalance. The specifications for the amplifier are obtained through an iterative process of simulation and fundamental calculation. The specifications for the linear amplifiers are:

- rms current: 2.5 A
- maximum output voltage: 50 V
- slew rate: 187.5 x 10^3 N/s

The power amplifiers have different stages: optical isolation, error amplifier, switching element and current sensing. A block diagram of the stages is shown Figure 5.1. The optical isolation protects the dSpace® card from dangerous voltage spikes that can damage the card and the computer. A current feedback signal is subtracted from the desired signal in the error amplifier. The output of the error amplifier represents the control signal of the power amplifier. The coil shown in Figure 5.1 is the coil of the electromagnet.

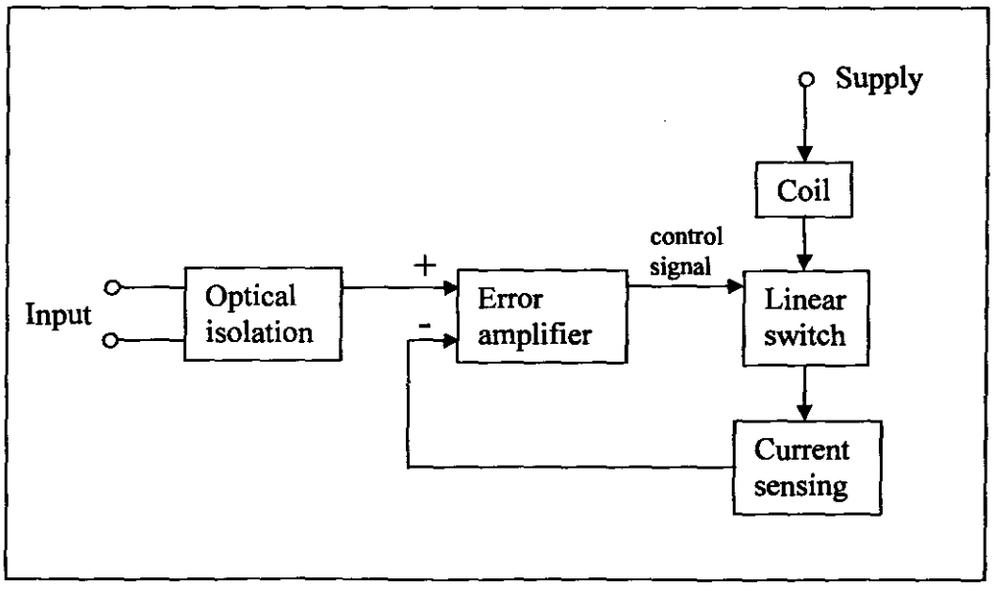

Figure 5.1: Power amplifier block diagram

5.1.3. Control circuit

The control circuit constitutes three basic parts: 1) optical isolation between the input signal and the power amplifier 2) a current sensing circuit and 3) an error amplifier. Current sensing is done to ensure that the power amplifier controls the current correctly at the desired value. This makes it a current mode amplifier. The error amplifier subtracts the current sense signal from the control signal and amplifies it with a certain gain. The output of the error amplifier drives the switching elements.

A 4N25 opto-coupler is used for the optical isolation. A linear configuration is used as shown in Figure 5.2. Values for the resistors can be calculated from the current transfer ratio (CTR) which is the ratio between the diode current and the collector current. From the 4N25 datasheet the CTR was chosen as 2 for a good linear relationship. The requirements for the opto-coupler are:

- input voltage range between 0 and 10 V
- output voltage range between 0 and 12 V
- maximum input current (I_f) of 5 mA,

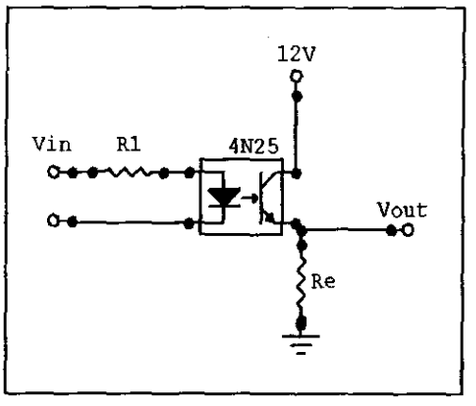

Figure 5.2: Opto-coupler in linear mode

By selecting $R1$ bigger than 2 kΩ the input current will be less than 5 mA. The CTR can be used to obtain the ratio of R_e to R_1:

$$\frac{I_f}{I_c} = 0.7 \tag{5.1}$$

$$I_f = 0.7 I_c$$

$$\frac{V_{in} - V_{diode}}{R_1} = \frac{0.7 V_{out}}{R_e}$$

$$\frac{10-1.2}{R_1} = \frac{0.7(12)}{R_e}$$

$$\frac{R_e}{R_1} = \frac{8.4}{8.8} = 0.95$$

The values for both R_e and R_1 are chosen as 15 kΩ.

The current sensing circuit measures the voltage across a resistor at the source of the switching element (Figure 5.3). This signal passes through a low-pass filter and is then used in the error amplifier. The total current (I_{tot}) of the amplifier flows through this resistor. Therefore a small resistor with a high power rating must be used. The maximum output voltage across the sense resistor (V_{sense}) is chosen as 1 V so that the value of the resistor and the maximum power that the resistor must dissipate is calculated in (5.2).

$$\begin{aligned} R_{sense} &= \frac{1}{2.5} \\ &= 0.5\,\Omega \longrightarrow \text{use } 0.39\,\Omega \end{aligned}$$

$$\begin{aligned} P_{sense} &= I_{tot}^2 R_{sense} \\ &= (2.5)^2 0.39 \\ &= 2.44\,\text{W} \longrightarrow \text{use } 5\,\text{W} \end{aligned} \qquad (5.2)$$

The error amplifier is one non-inverting operational amplifier with the control signal connected to the positive input and the current sense signal connected to the negative input (Figure 5.4). The gain can be adjusted be changing the input or feedback resistors in the circuit. From simulation and practical testing the gain was chosen as 1. The transfer function for the circuit is:

$$V_{out} = \frac{R_2}{R_1}(V_{in} - V_{sense}) \qquad (5.3)$$

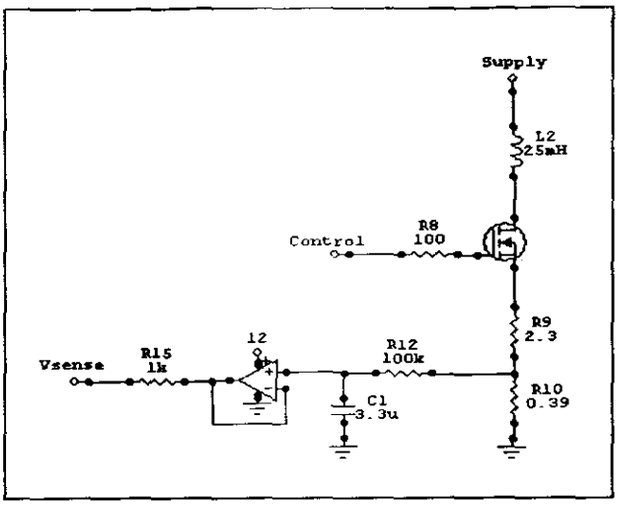

Figure 5.3: Current sensing circuit

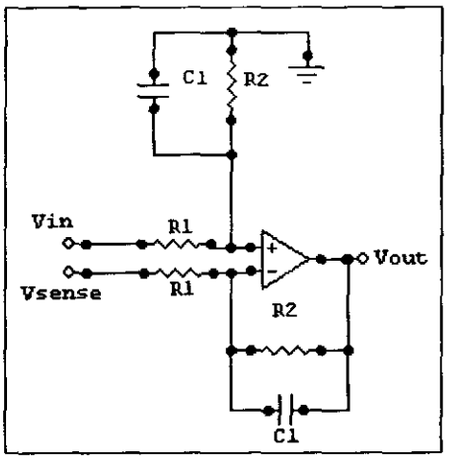

Figure 5.4: Error amplifier

5.1.4. Thermal design

The efficiency of the power amplifier is very low and most of the energy must be dissipated into the air. This is the most critical part of the amplifier design because too much heat will destroy the switching element. The design is done by simulation. The IRFP460 MOSFETS are used as switching elements. Four MOSFETS are used in parallel in the amplifier.

A resistor is placed in series with each MOSFET as shown in Figure 5.5. Each MOSFET has a different gate threshold voltage causing some MOSFETS to switch on before others resulting in unequal current distribution. When this happens the MOSFET will overheat. The series resistor prevents this from happening by decreasing the effective gate-source voltage and thus limiting the current.

There are four components that can dissipate heat in the power amplifier: the coil, the series resistors, the sense resistor and the MOSFETS. If the amount of heat that the heat sink must absorb is known, the size and type of heat sink can be determined. The resistance of the coil is 1.1 Ω, the series resistors are 2.2 Ω and the sense resistor is 0.39 Ω. The amount of power that the MOSFETS must dissipate can be calculated as follows:

$$\begin{aligned} P_{sink} &= P_{tot} - P_{coil} - P_{series} - P_{sense} \\ &= (50)(2.5) - 2.5^2(1.1) - 4\left(\frac{2.5}{4}\right)^2(2.2) - 2.5^2(0.39) \\ &\approx 113\ \text{W} \end{aligned} \tag{5.4}$$

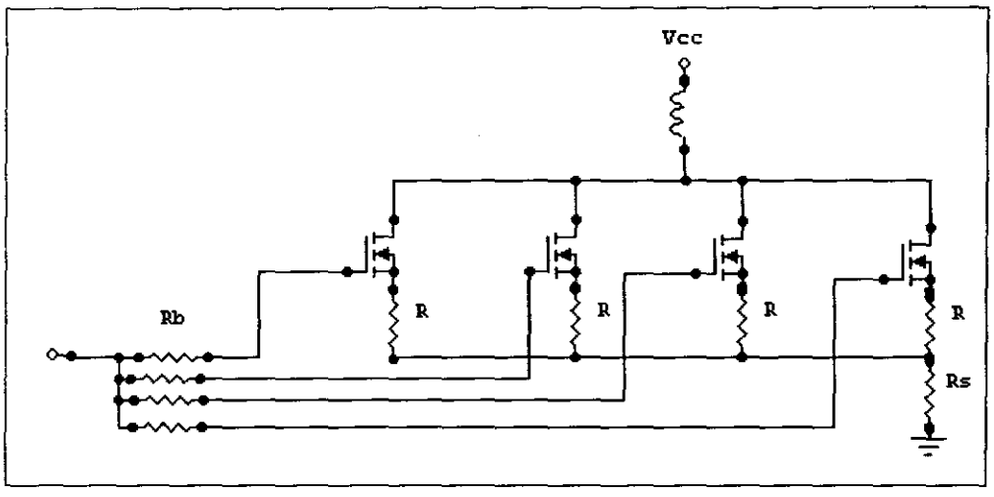

Figure 5.5: MOSFETS in parallel

The simulation of the thermal network constitutes current sources and resistors. Such a network is constructed in CircuitMaker® and the circuit (Figure 5.6) is used to determine the required thermal resistance of the heat sink. The four MOSFETS are represented as four current sources in parallel and the total power of 113 W is divided in four so that each MOSFET generates 28.25 W. The resistors are labelled as follows:

$R_{\theta jc}$ – thermal resistance of the junction to case obtained from the MOSFET's datasheet

$R_{\theta cs}$ – thermal resistance of the case to sink using a thermal conductive pad

$R_{\theta sa}$ – thermal resistance of the heat sink

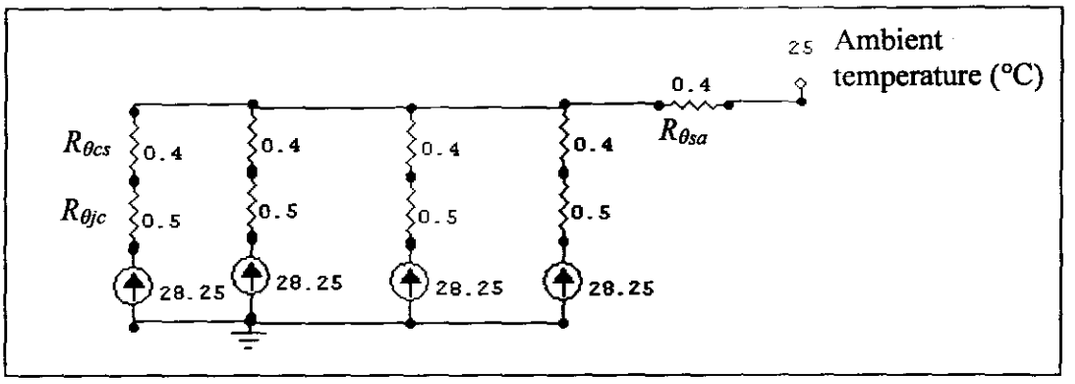

Figure 5.6: Simulation of thermal network

The maximum junction temperature for the MOSFET from its datasheet is 150 °C. When a heat sink with a thermal resistance of 0.4 °C/W is used a junction temperature of 95.6 °C is obtained. The heat sink temperature is 70.2 °C. The power efficiency of the power amplifier is calculated as the power dissipated in the coil, divided by the total input power:

$$\eta = \frac{P_{coil}}{V_{cc} i} \frac{100}{1} \tag{5.5}$$
$$= \frac{6.88}{125} \frac{100}{1}$$
$$= 5.5\%$$

5.1.5. Simulation results

The simulation was done in CircuitMaker® student version. Only 2 MOSFETs are used in parallel because only 50 devices can be used with the student version. This will however not affect the results very much because the choice to use four MOSFETs is only from a thermal point of view which is not simulated in this case. The three stages of the amplifier are indicated in Figure 5.7. A signal generator represents the input control voltage from dSpace®. The controlled output current through the coil is indicated with I_{out}.

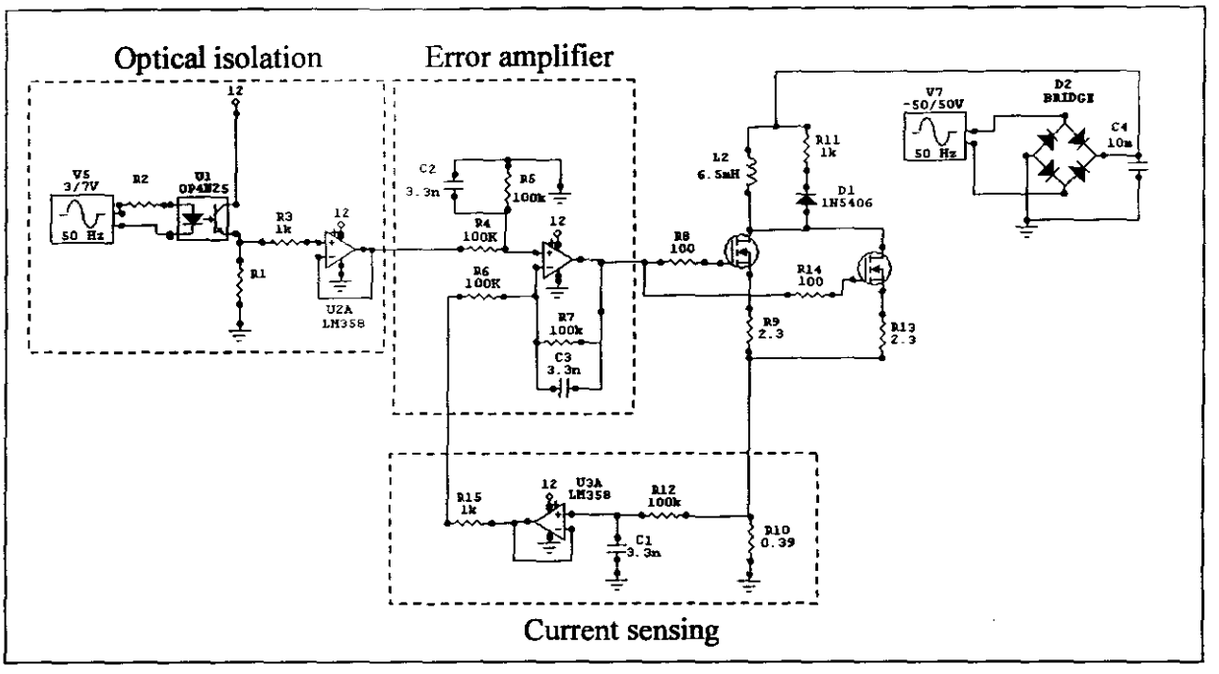

Figure 5.7: Power amplifier circuit

The simulation was done with an input signal of 50 Hz and 500 Hz. The required bandwidth of the power amplifier must be 500 Hz which is a factor 10 greater than the rotation speed of the rotor. Simulation results for the two cases are shown in Figures 5.6 and 5.7 respectively. At 500 Hz, a delay of 335 μs is measured. This delay is mainly caused by the opto-coupler. The gain of the power amplifier is 2.7 V/ 7 A which is 0.39 A/ V.

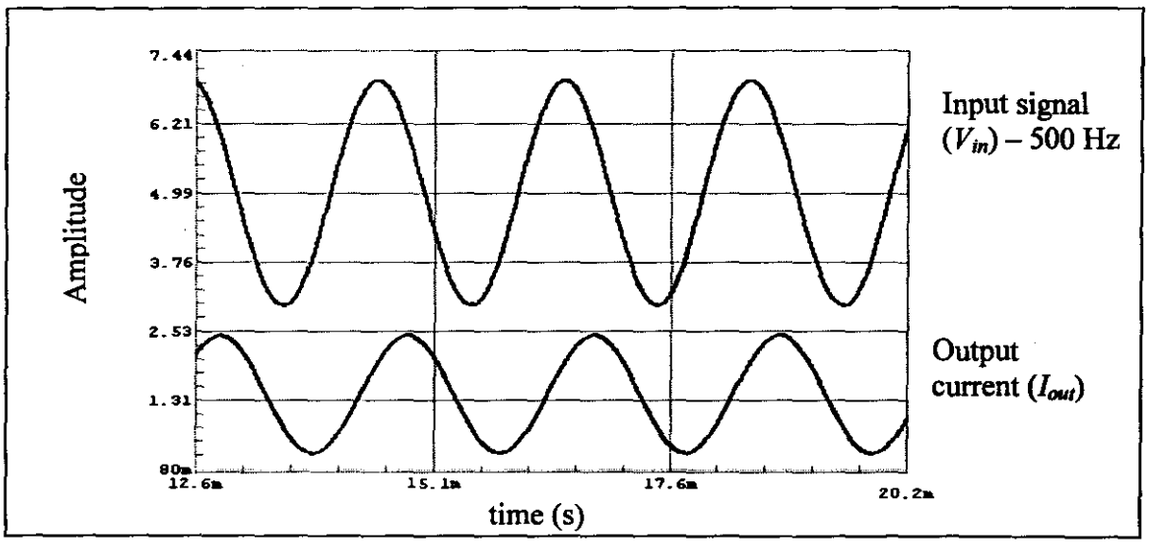

Figure 5.8: Simulation results at 50 Hz

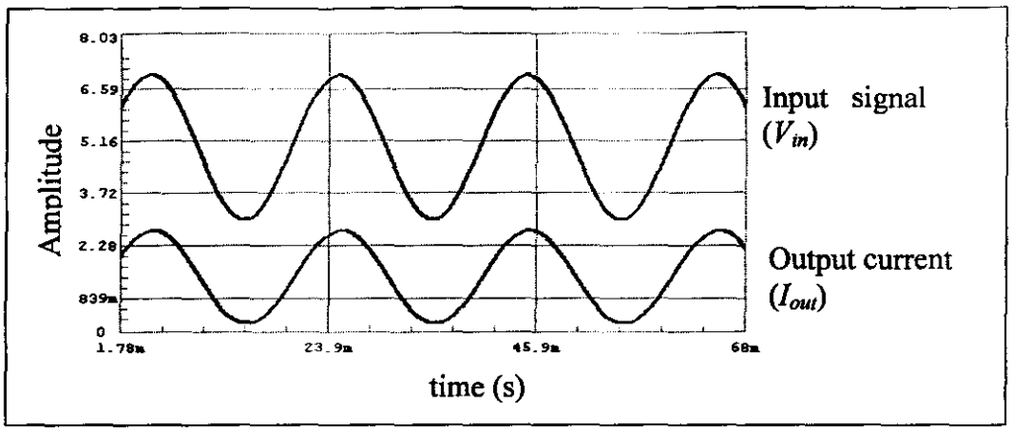

Figure 5.9: Simulation results at 500 Hz

5.1.6. Power amplifier results

The actual power amplifier is tested at 50, 250 and 500 Hz. A sine wave is given on the input of the opto-coupler and the current is measured. The results are shown in Figure 5.10. The current has a peak to peak value of 2.8 A. The bandwidth of the power amplifier is then 250 Hz. This will not have an effect on the system because it is still 5 times higher than the operating speed.

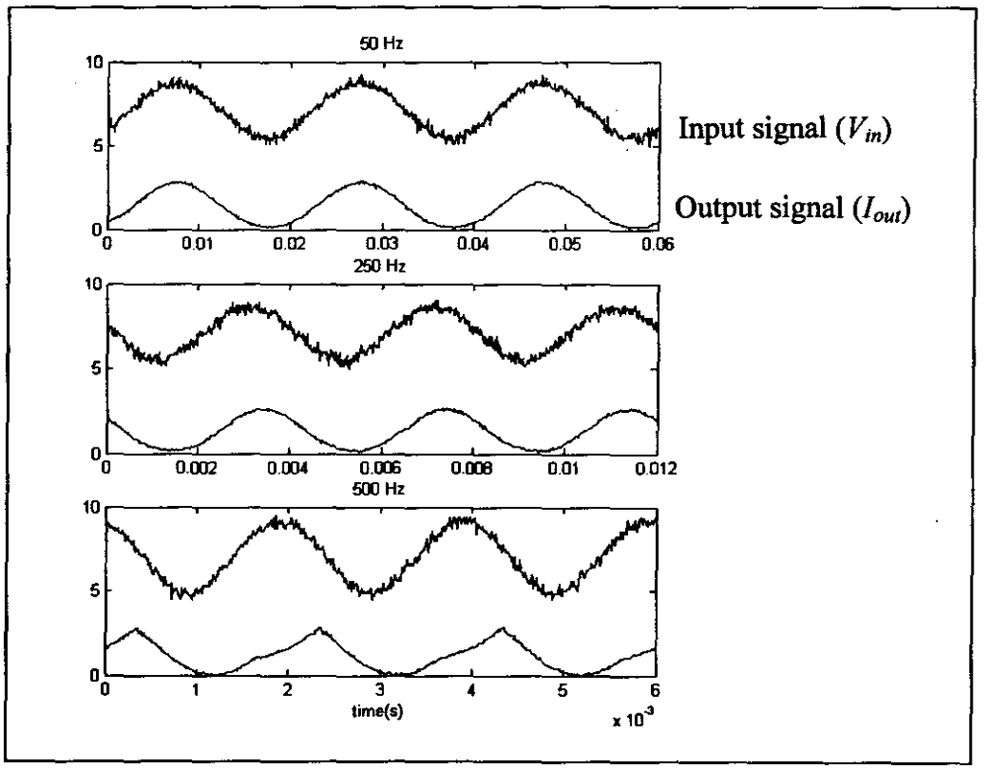

Figure 5.10: Power amplifier results

5.2. Sensors

The most important aspects to consider when selecting sensors are its sensitivity to electromagnetic noise, bandwidth, linearity and cost. In this project inductive sensors are used. This section will explain why inductive sensors are chosen and their operation will be discussed. A simulation of the electronic circuit is done and the results are given.

5.2.1. Operating principle

An inductive sensor constitutes two coils that work as a pair. A coil is placed on each side of the rotor and measure the rotor position. The coils are placed as close as possible to the rotor to achieve a good linear response. When the rotor position changes the impedances of the coils change.

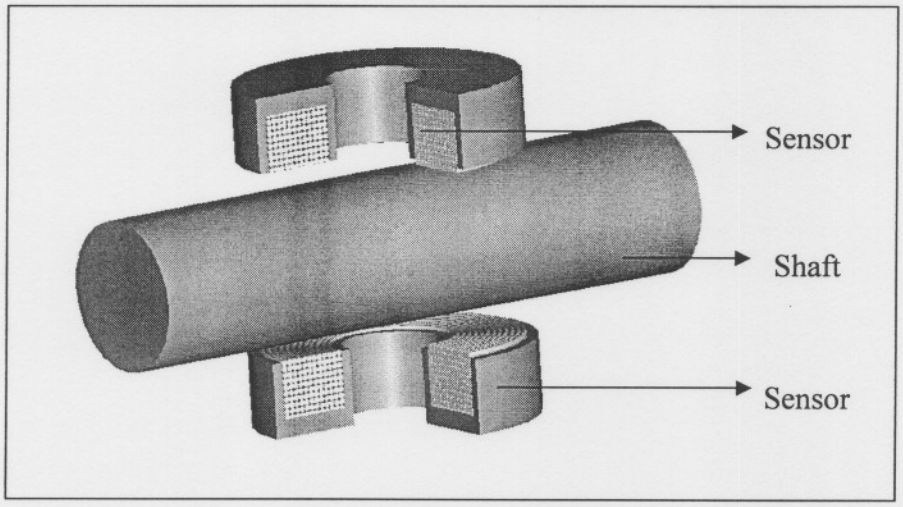

Figure 5.11: Inductive sensor

Consider two coils at opposite sides of the shaft. If the shaft is exactly in the middle the coils have the same inductance called L_0:

$$\begin{aligned} L_1 &= \frac{\mu_0 A_{core} N^2}{2(g_0)} \\ &= L_2 \\ &= L_0 \end{aligned} \tag{5.6}$$

If the shaft moves away from coil number 1 towards coil number 2 by a distance Δx the inductances of the coils are then given by:

$$\begin{aligned} L_1 &= \frac{\mu_0 A_{core} N^2}{2(g_0 + \Delta x)} \\ L_2 &= \frac{\mu_0 A_{core} N^2}{2(g_0 - \Delta x)} \end{aligned} \tag{5.7}$$

To find the inductance in terms of L_0:

$$\frac{L_1}{L_0} = \frac{\frac{\mu_0 A_{core} N^2}{2(g_0 + \Delta x)}}{\frac{\mu_0 A_{core} N^2}{2(g_0)}}$$

$$= \frac{g_0}{g_0 + \Delta x}$$

$$\therefore L_1 = L_0 \frac{g_0}{g_0 + \Delta x}$$

$$L_2 = L_0 \frac{g_0}{g_0 - \Delta x} \tag{5.8}$$

The two coils are connected in series and the output signal is found by using the voltage divider rule:

$$V_{out} = \frac{Z_2}{Z_1 + Z_2} V_{in}$$

$$= \frac{L_2}{L_1 + L_2} V_{in} \tag{5.9}$$

Substitute (5.7) in (5.9) to find the output voltage in terms of Δx:

$$V_{out} = \left[\frac{1}{2} + \frac{\Delta x}{2x}\right] V_{in} \tag{5.10}$$

Equation (5.10) shows that the output voltage is proportional to the deviation in the air gap around its nominal value of g_0. This result ignores the effect of hysteresis, eddy currents, fringing and coil resistance. These effects reduce the linear range of the sensor to a few millimetres.

5.2.2. Sensor circuit

The circuit constitutes three stages: an oscillator, band-pass filter and an ac to dc converter. The output of the inductive sensor is very susceptible to magnetic noise from the AMB's coils and the band-pass filter is used to filter out the noise and keep the oscillator signal of 33 kHz. The simulation was done in OrCad®. A block diagram of the sensor is shown in Figure 5.12.

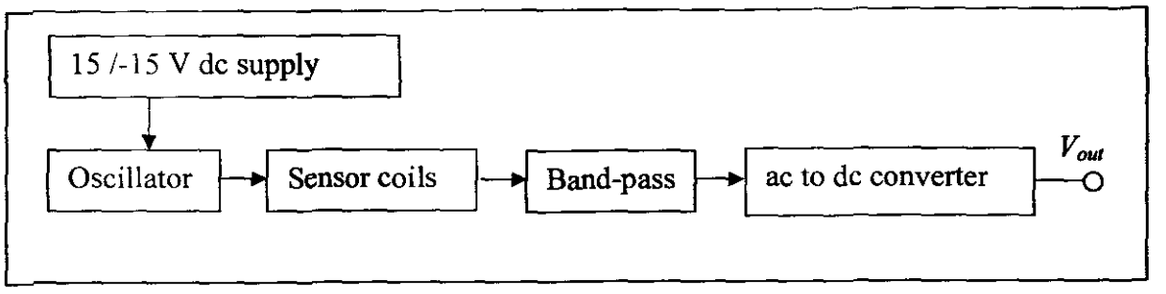

Figure 5.12: Block diagram of the sensor

For the oscillator an 8038 waveform generator is used to give a sine wave of 33 kHz. The circuit is very easy to implement with a low distortion in its output. The oscillating frequency (f) is determined by R_A, R_B and C (Figure 5.13). By choosing $R_A = R_B = R$ the frequency is given by (5.11). The variable resistance R_3 is for a precision adjustment of the frequency.

$$f = \frac{0.33}{RC} \tag{5.11}$$

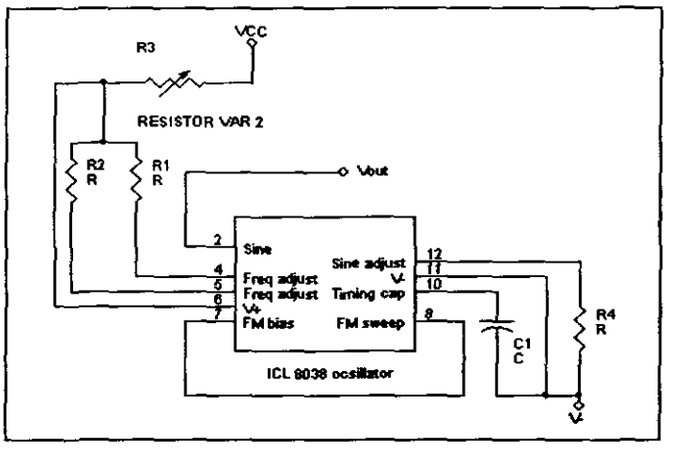

Figure 5.13: Oscillator circuit

The band-pass filter is implemented by using a third order high-pass Butterworth filter and a third order low-pass Butterworth filter. The top half of Figure 5.14 is the high-pass filter and the lower half is the low-pass filter. Standard values for the resistors and capacitors is chosen as near as possible to the required values. The chosen values are shown in Figure 5.14.

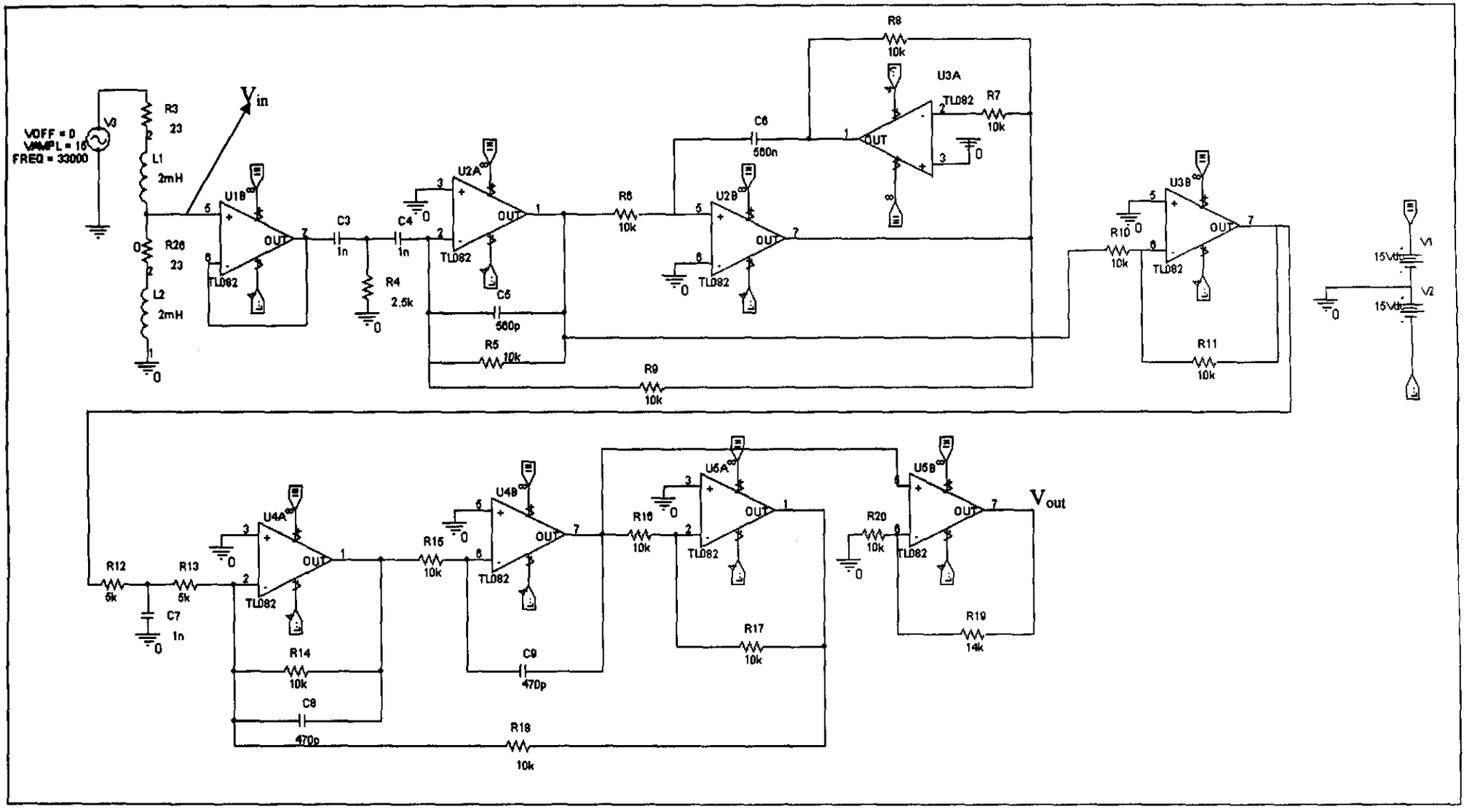

Figure 5.14: Band-pass filter

The filters are designed with the CAD program FilterSolutions®. The transfer function of the high-pass filter for a pass band frequency of 33 kHz is given by:

$$G(s)_{HP} = \frac{s^3}{s^3 + 4.147e+5s^2 + 8.598e+10s + 8.914e+15} \tag{5.12}$$

The transfer function of the low-pass filter for a pass band frequency of 33 kHz is given by:

$$G(s)_{LP} = \frac{8.914e+15}{s^3 + 4.4147e+05s^2 + 8.598e+10s + 8.914e+15} \tag{5.13}$$

The frequency response of the filter is obtained with OrCad®. The pass band with a frequency of 33 kHz is given in Figure 5.15. The last stage of the sensor is the ac to dc rectifier. An active rectifier was used as shown in Figure 5.16.

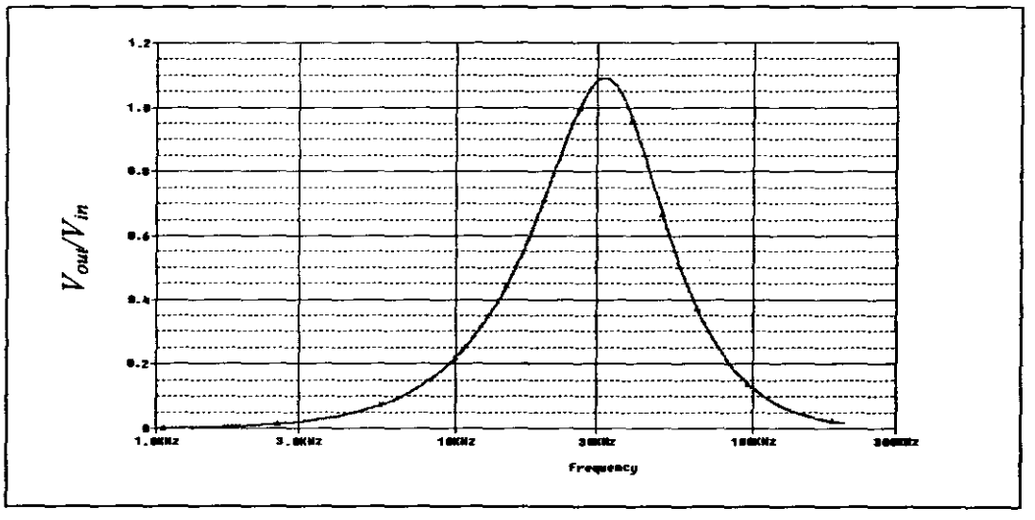

Figure 5.15: Frequency response of the band-pass filter

There is a trade of between the size of the ripple voltage on the output and the bandwidth of the system. From the simulation it is found that a 22 nF capacitor would be sufficient and the voltage ripple is then smaller than 10 mV peak to peak.

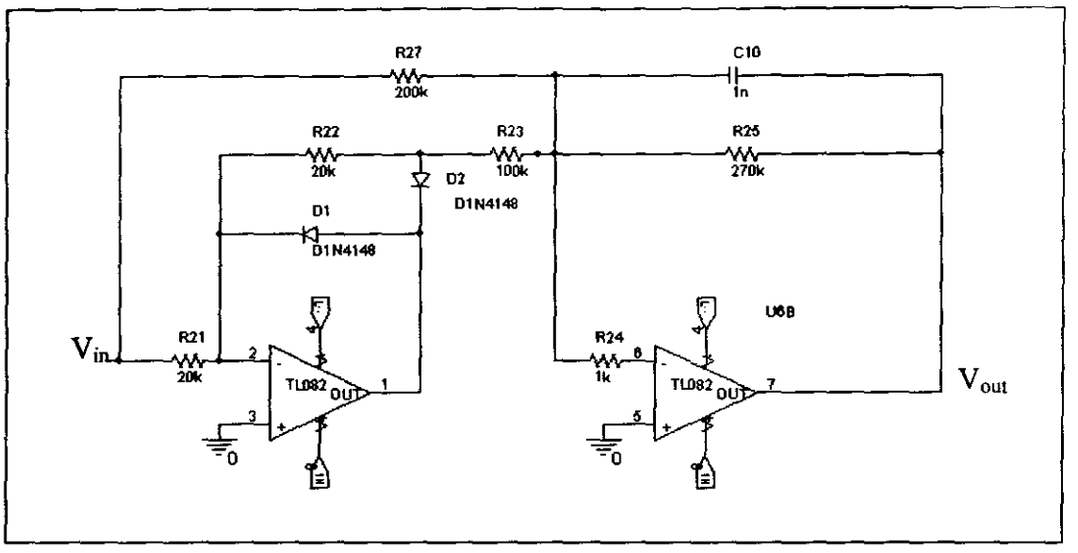

Figure 5.16: Ac to dc converter

5.3. Conclusion

In this chapter the design of the power amplifier and the sensor is discussed. The thermal design of the power amplifier proved to be the most challenging aspect because it is a linear amplifier with a low efficiency. Two power amplifiers are fitted onto one heat sink. The two can safely work together at the specifications of a 50 V, 2.5 A. The power amplifier is tested and has an actual bandwidth of 250 Hz.

The inductive sensor used in this design is a low cost sensor, but it is noise sensitive. A band-pass filter is built to reduce the noise. The dc output signal is scaled and an offset is added to the signal to improve the resolution when the value is read into dSpace®. The sensor can only really be tested when the complete system is finished. In Chapter 7 the linearity and accuracy of the sensor is tested and the results are given.

Chapter 6

System integration

The purpose of this chapter is to explain the integration of the different components that form the complete AMB system. As discussed in the previous chapters the system constitutes power amplifiers, sensors, a control system and actuators. The power amplifiers and sensors are respectively connected to D/A and A/D channels of the DS1104 dSpace® card. This chapter also discuss the control system that is implemented in Simulink®, the Graphical User Interface (GUI) of ControlDesk® software and the grounding of the system.

6.1. Interconnection of the sub-systems

The interconnection of the power amplifiers and sensors are shown in Figure 6.1. Four power amplifiers are used and numbered as shown in Figure 6.1. Power amplifiers one and two are built onto one heat sink and 3 and 4 onto another heat sink. Each power amplifier is connected to the DS1104 card via a dedicated 16-bit D/A channel. The sensors use two A/D channels with 12-bit resolution. An optical speed sensor is used to measure the speed of rotation. This sensor generates a 5 V pulse for each revolution of the rotor. It is connected to a bit I/O channel; 5 V represents a logical one and 0V a logical zero.

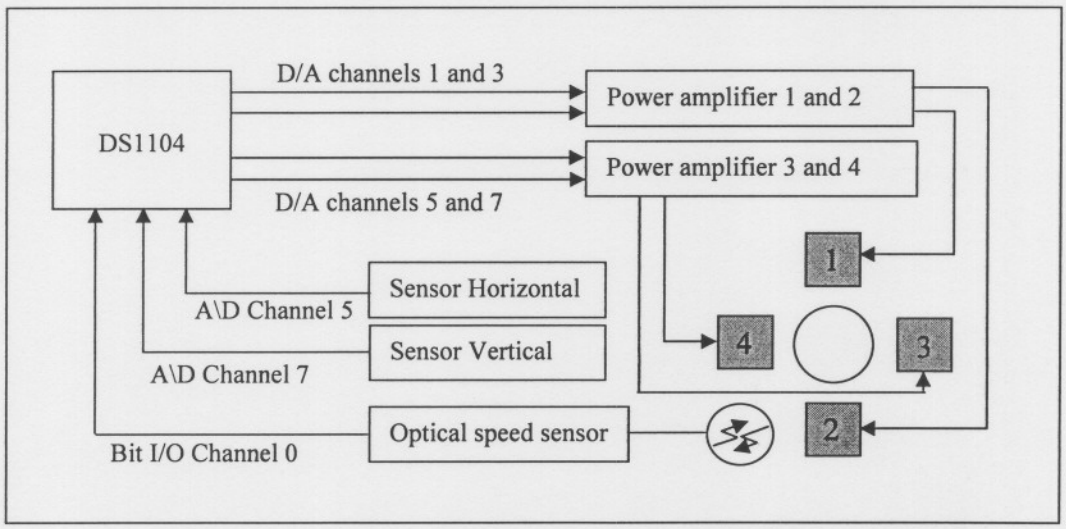

Figure 6.1: Interconnection diagram

6.2. Simulink® controller

The controller is developed in Simulink®. Two digital PID controllers are used; for the vertical and horizontal position respectively as shown in Figure 6.2. The sensor input is represented by a Simulink® block ADC. The channel number of the A/D can be selected from the block's properties. The signal is then subtracted from a reference signal. This reference signal can be a zero to indicate the centre position or a sine, block or saw tooth reference. A reference switch allows the user to switced between the zero reference and the waveform reference. The frequency and the amplitude of the waveform can be changed. The error signal is passed through a Butterworth low-pass filter with a cut-off frequency of 2 kHz to minimise the noise.

The PID controller has two inputs, the filtered control signal, and a reset value. The reset value must be set to 1 and back to zero each time the system is re-started. This resets the value of the integrator. If the system outputs are switched off, the integrator value keeps on increasing. When the outputs are switched on again the integrator must be reset. The output of the PID is the input to a differential driving mode. Two signals are formed and a bias value is added. The two signals are written out through the D/A converter to two opposing electromagnets.

The Simulink® model is developed so that a user has control over most of the important parameters of the controller. The output to each of the four electromagnets can be disabled individually. The PID parameters can be changed, the integration can be reset and the user can choose between the different reference input signals. With the help of dSpace® software the controller is downloaded onto the DS1104 board and a GUI is developed in ControlDesk®.

An optical speed sensor is used to measure the rotation speed of the shaft. The sensor gives a 5 V pulse for each revolution and the signal is read through the bit I/O port on the DS1104 card. To calculate the rotation speed in rpm, a Simulink® model is developed. The block diagram is shown in Figure 6.3. The model detects rising and falling edges and counts the number of pulses in 2 seconds. The value is multiplied by 15 to obtain the speed in rpm.

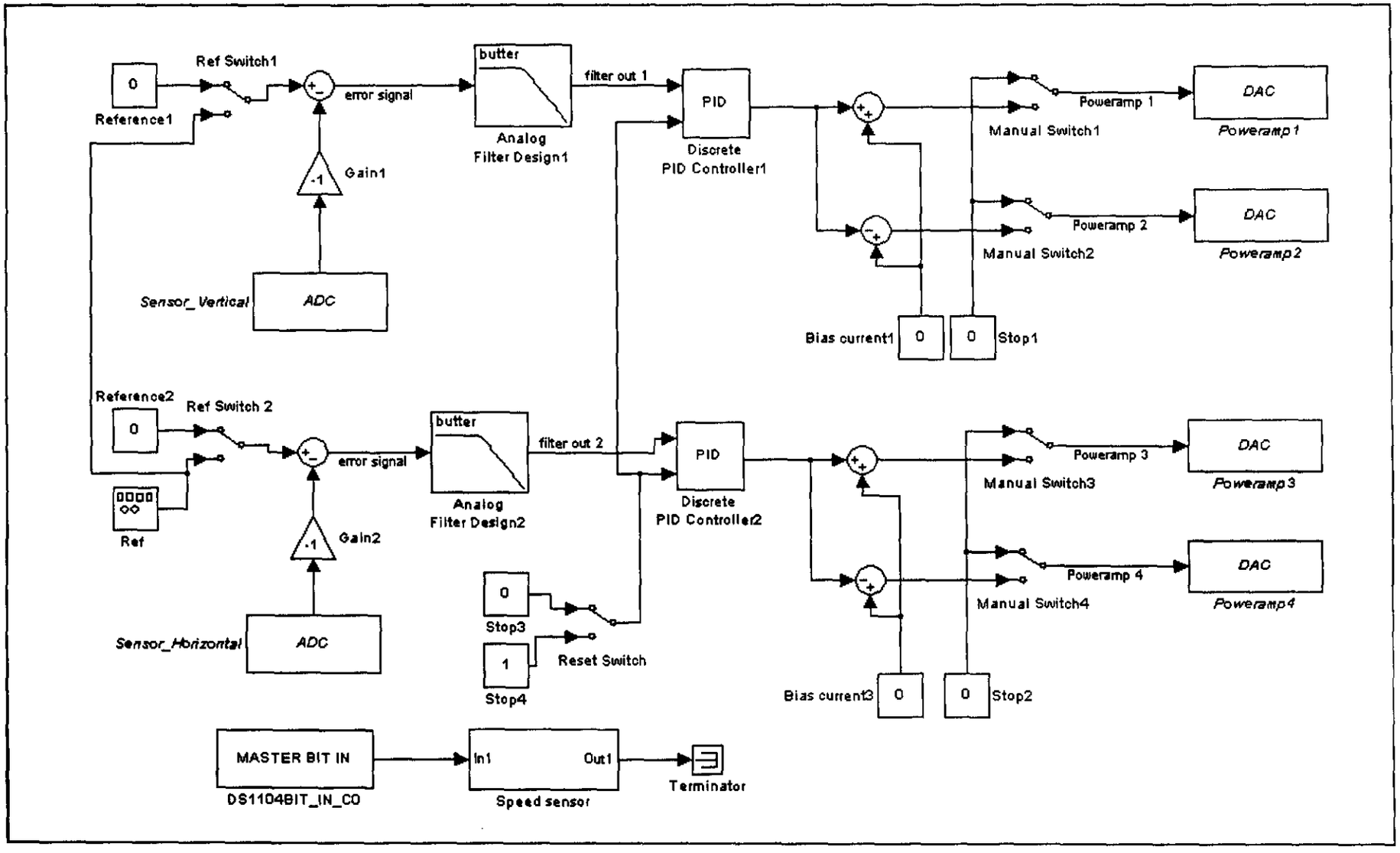

Figure 6.2: Simulink® controller

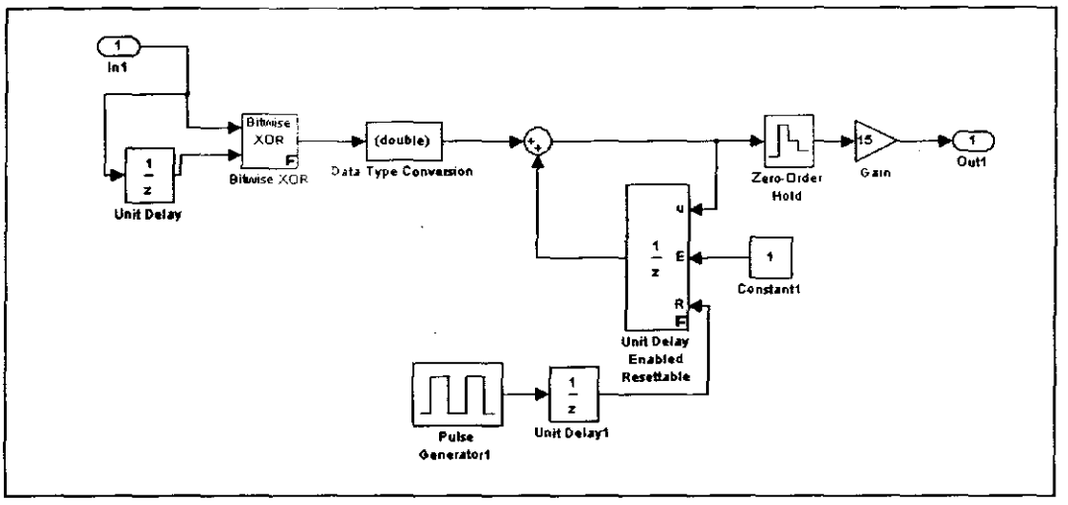

Figure 6.3: Speed sensor in Simulink®

6.3. The Graphical User Interface in ControlDesk®

A graphical user interface is created in ControlDesk® with two layouts. The first layout is a control layout where the different control parameters of the system can be changed. The outputs to the electromagnets can be disabled from this layout. The second layout is named the result layout. It shows position graphs and reference graphs and the numerical values of the PID parameters are displayed. The capture setting can be changed on this layout. With the capture function data can be saved to an external file for further analysis.

The control layout is shown in Figure 6.4. This layout displays the sensor input for the vertical and horizontal position in graphical and numerical form. Each power amplifier can be turned on and off by using switches 1 to 4. The outputs of power amplifier 3 and 4 are displayed in two graphs. The PID parameters can be changed with the use of slider bars and the amount of bias current can also be controlled. A reset switch is used to reset the integrator output to zero. The reference signal for each axis is zero by default. This is the centre position. A sine, block or saw tooth waveform can be used as reference by using two switches, one for each axis. The amplitude and the frequency can be changed by using slider bars. The speed in rpm is displayed in the lower right hand corner; this reading is updated every 2 seconds and has a resolution of 15 rpm.

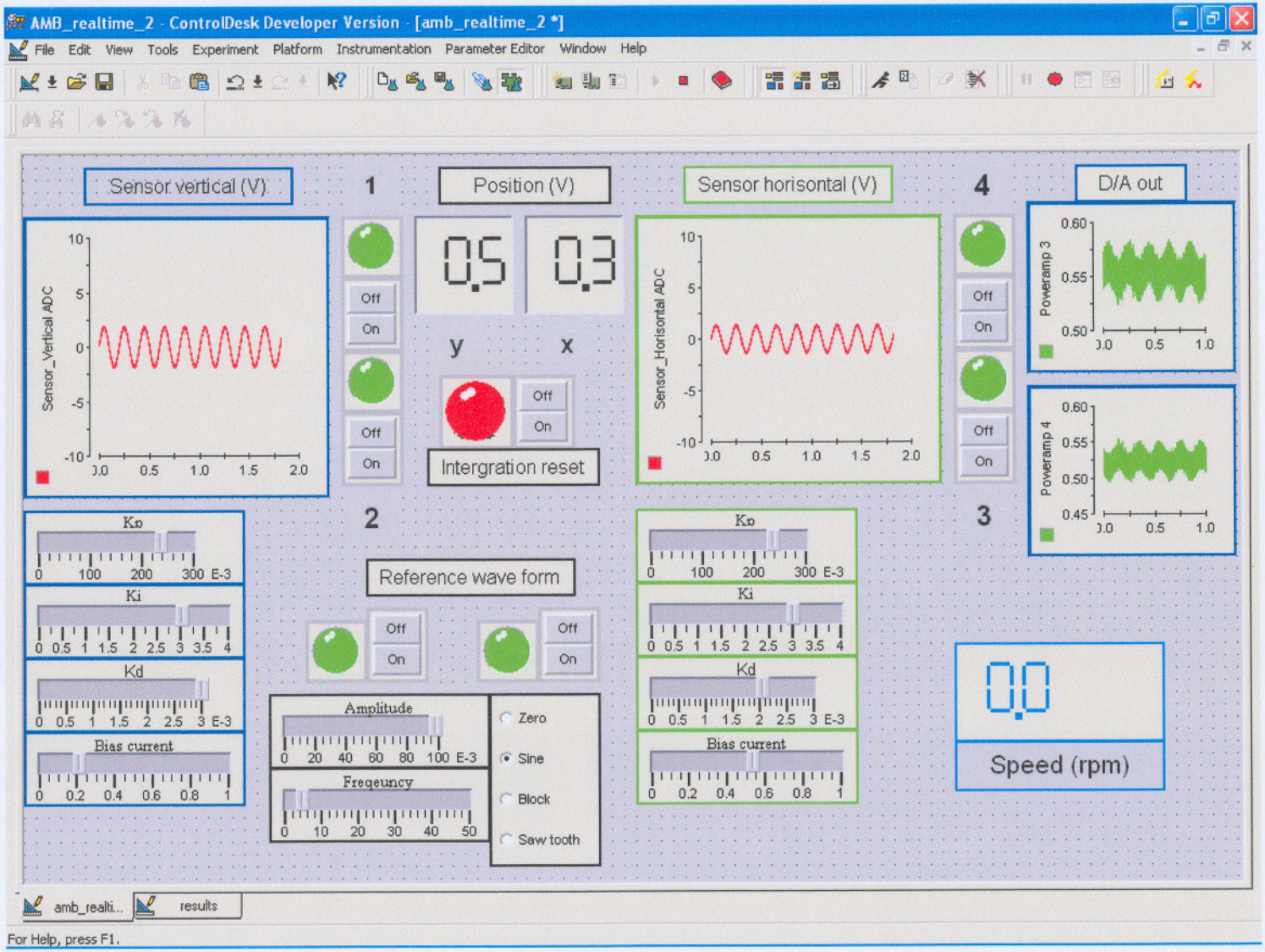

Figure 6.4: Control Layout in ControlDesk®

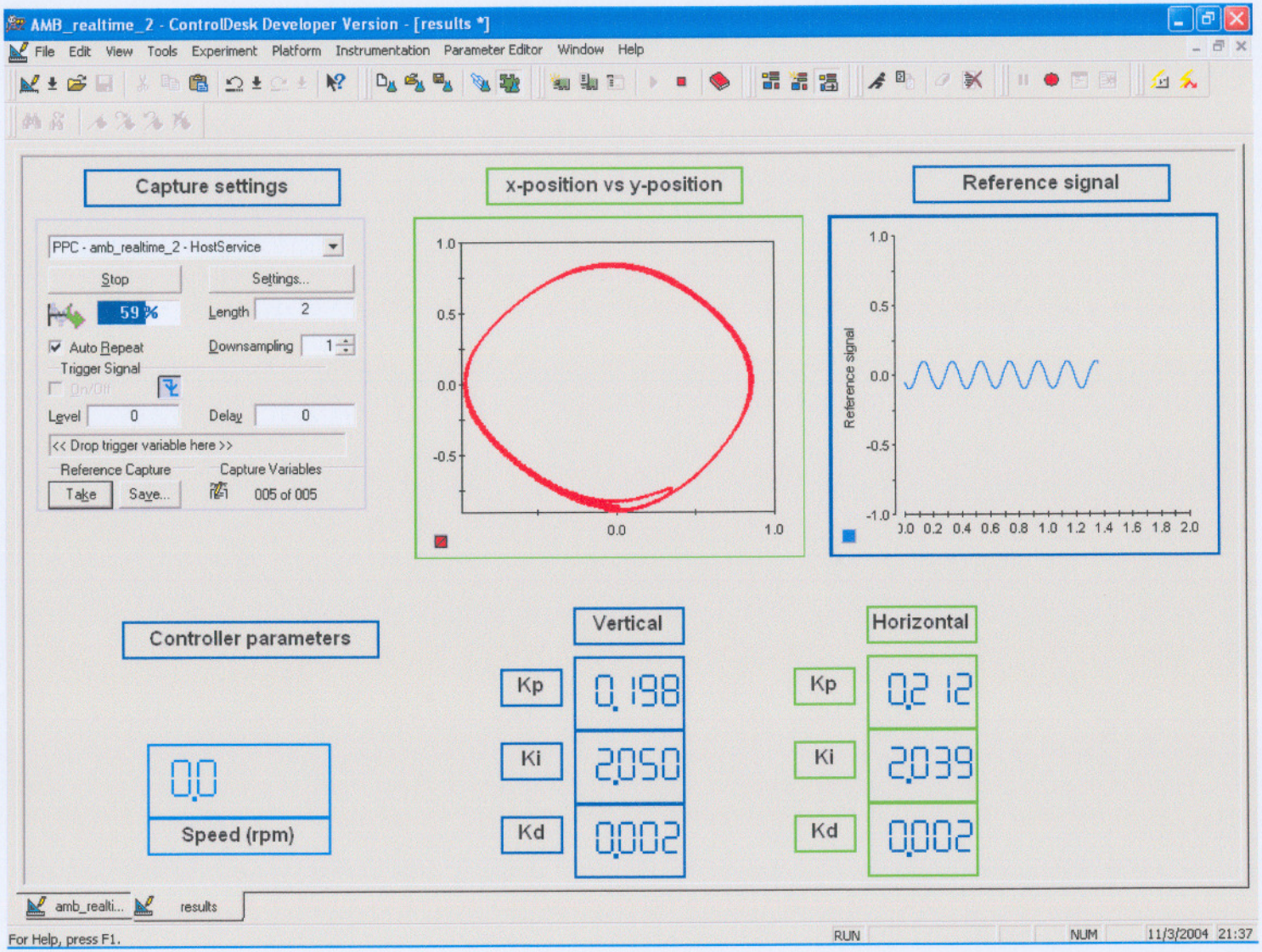

Figure 6.5: Results layout in ControlDesk®

The results layout is shown in Figure 6.5. Capture settings can be changed in this layout. The variables, time, file and file type can be selected. The values of the PID controller are shown with a digital display. To display the position of the rotor a graph is used with the horizontal position on the x-axis and the vertical position on the y-axis. This graph is very illustrative in terms of rotor position. At high rotation speeds the graph forms an elliptical shape. This will be discussed further in more detail in Chapter 7.

6.4. System grounding

To minimise noise and for protection against shock the model and the heat sinks of the system are connected to mains earth of the power grid. The connection reduced the noise levels but there is still a small 50 Hz noise signal on the power amplifiers. This noise signal is troublesome since its frequency falls in the required control bandwidth of the system. The noise signal originates on the output of the opto-coupler between the dSpace® card and the power amplifier and causes the current in the coils to have a 50 Hz noise component. It was found that a capacitor between the ground level of the input and the 0 V of the power amplifiers reduces this noise signal significantly. The connection of this capacitor is illustrated in Figure 6.6.

6.5. Conclusion

All the components of the AMB are integrated to form the final AMB system. The sensors and power amplifiers are connected to D/A channels and A/D channels respectively. These signals are displayed in ControlDesk®. A digital PID controller is implemented and the control parameters can be changed from ControlDesk®. An optical speed sensor is used to measure the speed.

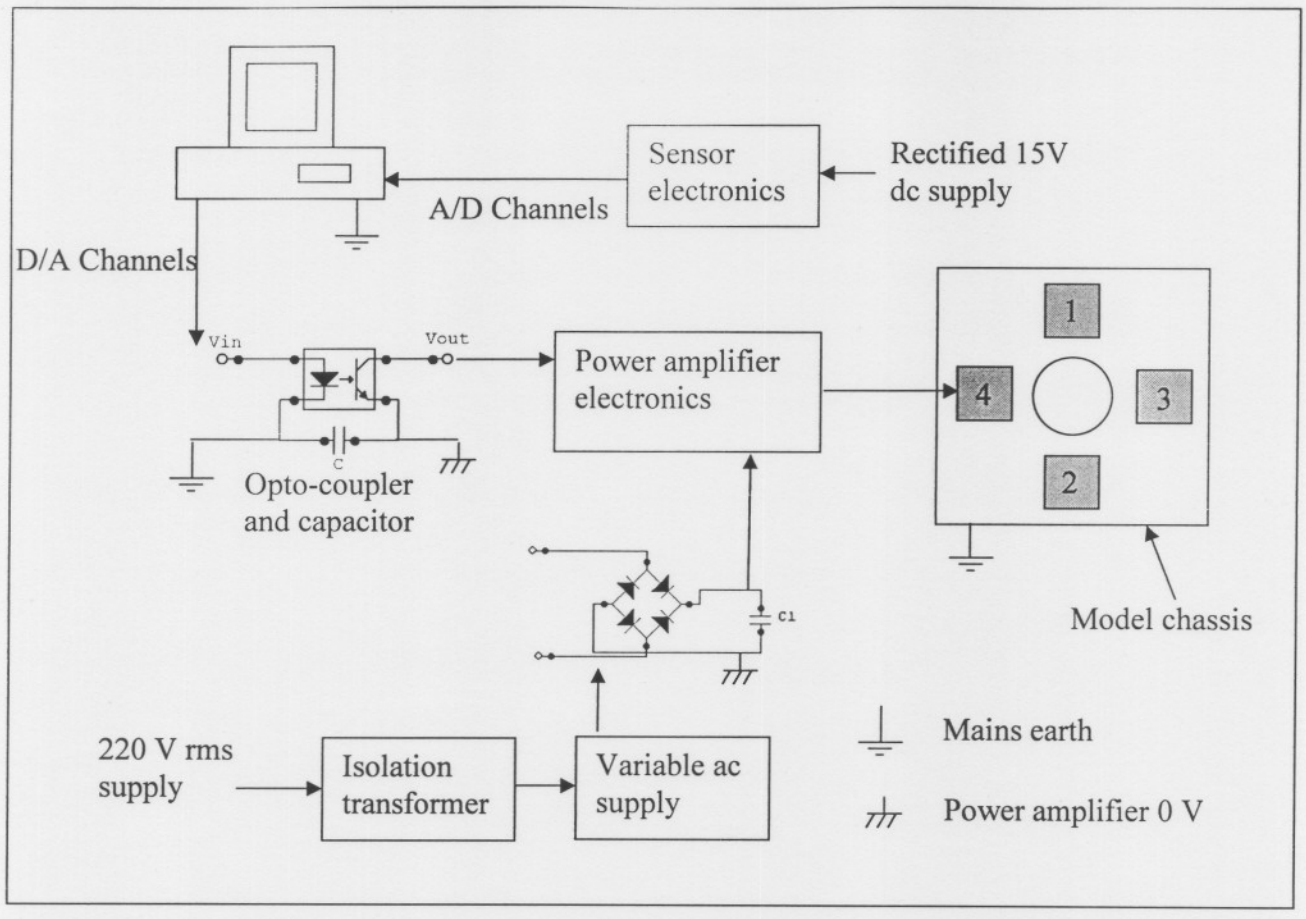

Figure 6.6: System grounding concept

Chapter 7

System characterization

In this chapter the AMB system is characterised. The control system is successfully implemented and a stable suspension is achieved. The control parameters of the actual system are compared to that of the simulation. To characterize the system different tests are performed. The first test is a step response in both the vertical and horizontal axes. From the results the percentage overshoot and settling time are determined and compared to what is predicted by the simulation.

With the help of the air turbine the rotor is propelled up to 3000 rpm, which is the design speed. A stable suspension is still achieved at speeds of 5000 rpm. From measurements of position and current the resulting force on the shaft is calculated. The imbalance of the shaft is also investigated and weights are added to reduce the imbalance on the shaft. The dynamic stiffness and damping of the AMB are determined by applying an impulse disturbance to the shaft at different speeds.

7.1. Control parameters

The first step to achieve a stable suspension is to find the correct PID parameters. The values of the simulation are used as a guideline as to what to expect for *Kp*, *Ki*, and *Kd*. Once a stable suspension is achieved the parameters are adjusted to give an optimum response. This is done by analysing the step response of the system. The final parameters are chosen where the overshoot and the settling time of the step response is the smallest. One other requirement is that the system must be stable when an impulse force is applied to the shaft. An impulse force is applied to the shaft so that the it almost touches the back-up bearing. It must then return to the centre.

The values used in the simulation and in the actual controller are shown in Table 7.1. Only the vertical values for the simulation are given because the simulation is done in the vertical axis. The PID values are not exactly the same as the values obtained from the simulation. The reason is that the actual actuator has non-linear characteristics that are not taken into account in the simulation such as: 1) non-linearities in the material of the electromagnet and rotor, 2) leakage and fringing 3) hysteresis and eddy current losses. The parameters are also sensitive to different operating points. The AMB system is a non-linear system and any small difference in bias current and position between the simulation and the actual system leads to a different operating point.

There is a difference between the bias value and the bias current as shown in Table 7.1. The bias value is the value that can be set in ControlDesk®. The bias current is the dc current of the electromagnets in Ampere. The bias currents are measured when the shaft is suspended and not rotating. The top electromagnet has a larger bias current because it has to overcome the weight of the rotor. Theoretically the bias currents of the left and right hand side electromagnets must be the same but there is a 100 mA difference between the two. This difference can be an indication that the rotor is not precisely in the middle and is closer to the left hand side.

Value	Simulation (vertical axis)	Actual controller (vertical axis)	Actual controller (horizontal axis)
K_p	0.6	0.175	0.21
K_i	2	2	2
K_p	0.012	0.002	0.002
Bias value	0.65	0.65	0.55
Bias current (A)	1.1 (top)	1.2 (top)	0.7 (left)
Bias current (A)	0.6 (bottom)	0.55 (bottom)	0.8 (right)

Table 7.1: PID parameters

7.2. Sensor scaling

The maximum deviation of the shaft is 0.5 mm to each side when it touches the back-up bearing. The position is represented by a -6 V to +6 V dc signal from the sensors. 0 V represents the centre position of the rotor. When the value is read in through the A/D converter the value is scaled by a factor of 0.1. To find the relation between position in mm and the value displayed in ControlDesk® a clock gauge is used. A low frequency sine reference for the position is given from ControlDesk® and the actual peak-to-peak position is measured in mm for different reference values. This relation is shown in Figure 7.1. The sensor has a good linearity and the relation between position and the value in ControlDesk® is:

$$\text{Deviation in mm} = \frac{\text{value in Simulink}}{1{,}11} \qquad (7.1)$$

This scaling factor also has an effect on the PID parameters. To prevent this scaling error between the simulation and the actual system's PID parameters, the exact same scaling factor is built into the simulation.

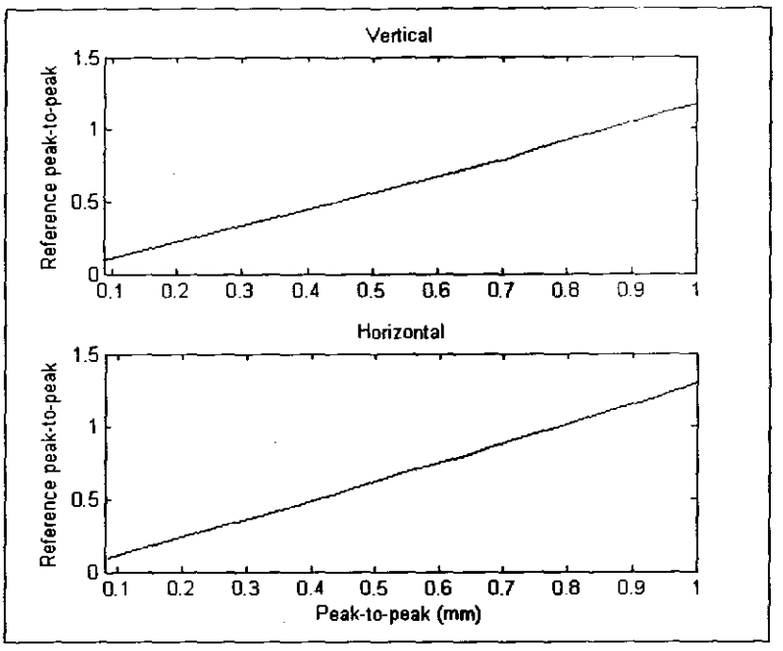

Figure 7.1: Sensor position

7.3. Step response

A step input of 0.05 is given to the system from ControlDesk®. This value converts to 0.045 mm. Step response analysis for the vertical and horizontal axes are done. Position and current are measured. The data is passed through a low-pass filter with a cut-off frequency of 30 Hz. This is to filter out the high frequency noise in the system so that a more realistic assessment can be made of the percentage overshoot and the settling time. The step response in the horizontal axis is shown in Figure 7.2. The top signal is the original position signal sampled at 50 kHz and the bottom signal is the output of the band-pass filter. The percentage overshoot and the settling time are calculated and given in Table 7.2.This is then compared to the simulation.

The currents in the horizontal electromagnets are also measured for a step response and are shown in Figure 7.3. As expected the currents are out of phase, oppose each other and the maximum peak value is 1.9 A. The step response results for the vertical axis are shown in Figure 7.4. There is more overshoot in the vertical axis than in the horizontal axis. The weight of the rotor works in on this axis, which makes it more difficult to control.

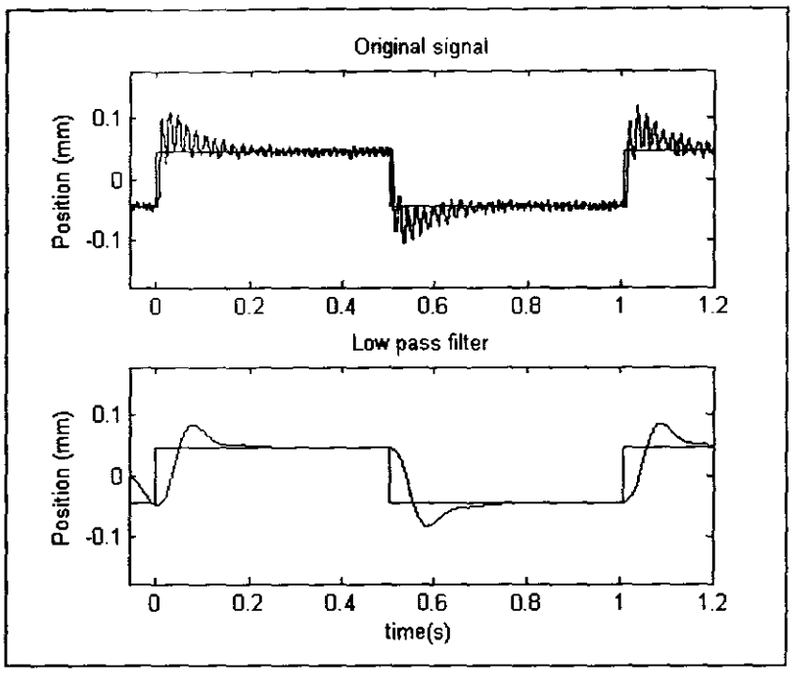

Figure 7.2: Step response in the horizontal axis

Theoretically the stiffness of the AMB is infinite. Stiffness is calculated as the deviation in force divided by the corresponding deviation in position. The system has no steady state error so the deviation in position is zero and this gives an infinite stiffness. Therefore the stiffness of an AMB is rather defined to be frequency dependent. It can be calculated at different speeds by applying an impulse disturbance by measuring the exponential decay of the position signal.

The percentage overshoot and the settling time of the step response can normally be used to calculate the stiffness and damping of the system. In this case however the percentage overshoot is greater than 100 %. This leads to a contradiction because for second order systems with a percentage overshoot greater than 100 % the system is unstable. To calculate the stiffness and damping using the percentage overshoot and settling time is therefore not meaningful.

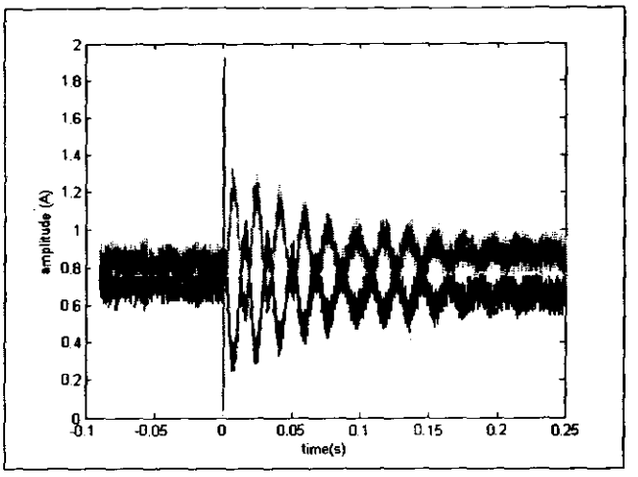

Figure 7.3: AMB currents for a step input in the horizontal axis

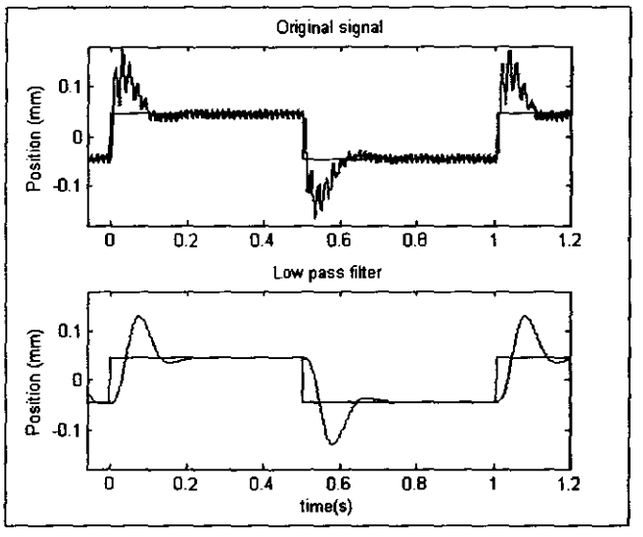

Figure 7.4: Step response in the vertical axis

Value	Simulation (vertical axis)	Actual controller (vertical axis)	Actual controller (horizontal axis)
Percentage Overshoot (%)	91	284	150
Settling time (s)	0.9	0.4	0.3

Table 7.2: Percentage overshoot and settling time

7.4. Rotation results

The rotor is propelled up to 1000, 2000 and 3000 rpm. At the different speeds the position and current is measured. To better visualise the effect of the different speeds on the position, a special graph is used with the horizontal position on the x-axis and the vertical position on the y-axis. Figure 7.5 shows the response for the three speeds mentioned. The maximum deviation is 0.11 mm for the vertical axis and 0.08 mm for the horizontal axis. In this graph the point (0,0) represents the centre position. The deviation increases as the speed increases. This is because of the increase in the centrifugal force.

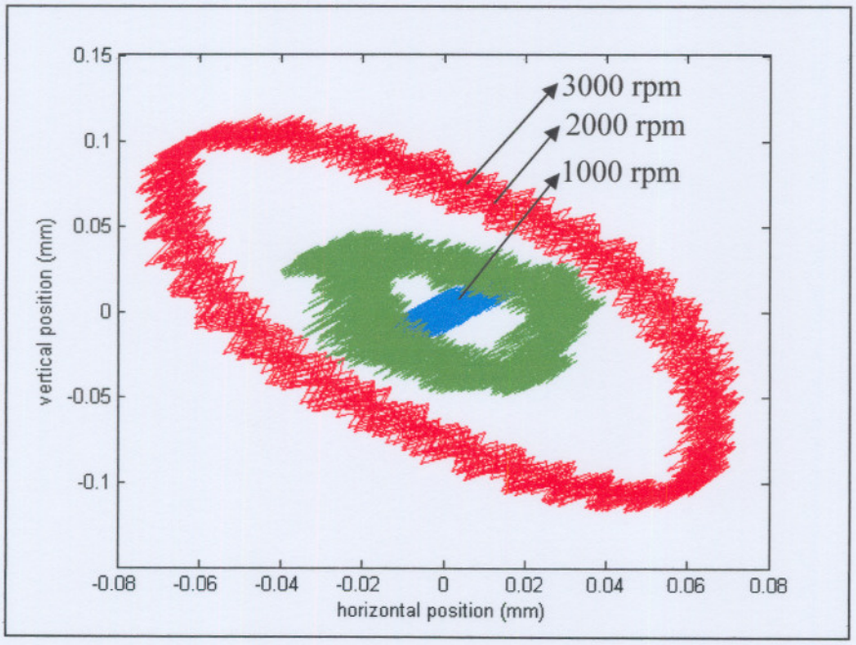

Figure 7.5: The vertical and horizontal position for different rotation speeds

The horizontal position against time is shown in Figure 7.6 for 3000 rpm. The period of one rotation is 20 ms and can clearly be seen. There is also high frequency noise present on the signal. The current for the horizontal axis is shown in Figure 7.7. The currents are also sinusoidal with a period of 20 ms.

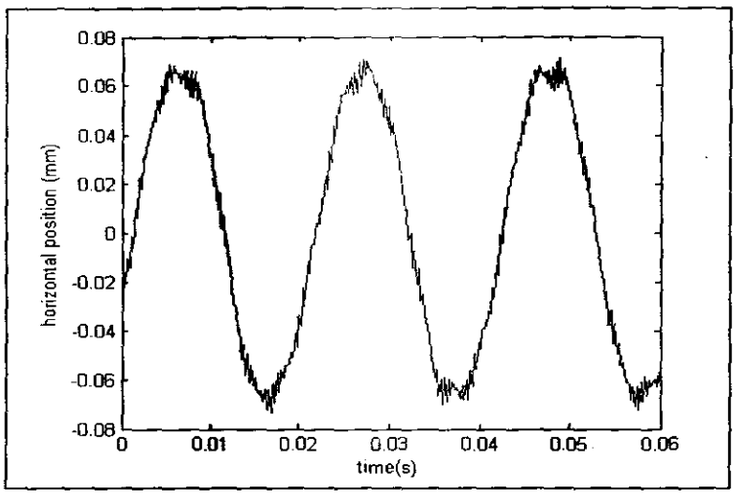

Figure 7.6: Position in horizontal axis at 3000 rpm

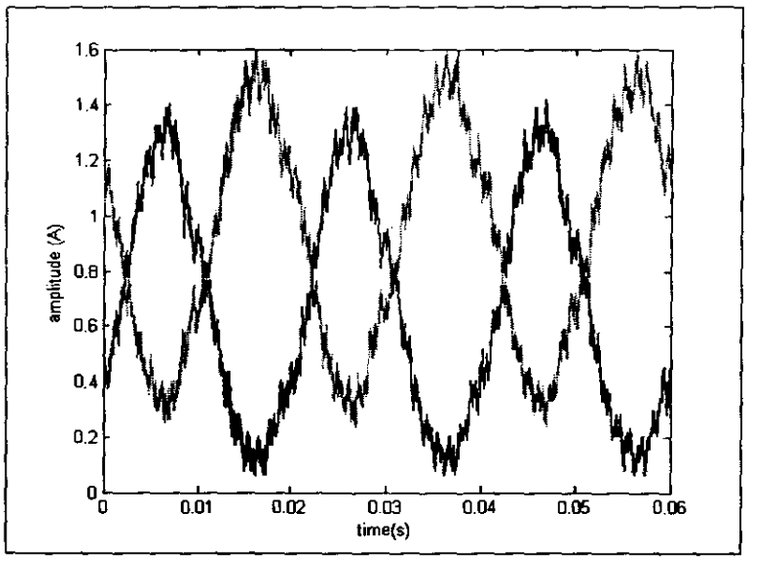

Figure 7.7: Currents in the horizontal axis at 3000 rpm

An estimation of the resulting force on the shaft in the horizontal axis is done by using the peak values for the position and currents. The peak force is then:

$$
\begin{aligned}
F_{res} &= F_3 - F_4 \qquad (7.2)\\
&= k\left(\frac{i_1^2}{x_1^2} - \frac{i_2^2}{x_2^2}\right)\\
&= k\left(\frac{1.5^2}{\left(0.94\text{x}10^{-3}\right)^2} - \frac{0.1^2}{\left(1.06\text{x}10^{-3}\right)^2}\right)\\
&= 31.6\,\text{N}
\end{aligned}
$$

with:

F_{res}	-	resulting force on the shaft
F_3	-	force of the right electromagnet
$F4$	-	force of the left electromagnet two
k	-	electromagnet constant

7.5. Balancing the rotor

The shaft has a certain imbalance and by measuring the shaft position relative to the pulses of the speed sensor, the position of the imbalance on the rotor can be determined. Weights can be attached to the shaft to reduce the imbalance on the shaft. Figure 7.8 shows a side view of the rotor. Every time the 0° mark passes the optical sensor, the sensor gives a pulse. The vertical position of the imbalanced shaft and the pulses of the speed sensor for 2000 rpm are shown in Figure 7.9. The position and the pulse are nearly 180° out of phase. A negative position value means that the position is towards the top electromagnet and the 0° point is at the bottom electromagnet. To counter the effect of the imbalance a weight thus has to be added on the 0° point of the shaft. The position of the balanced rotor is shown in Figure 7.10.

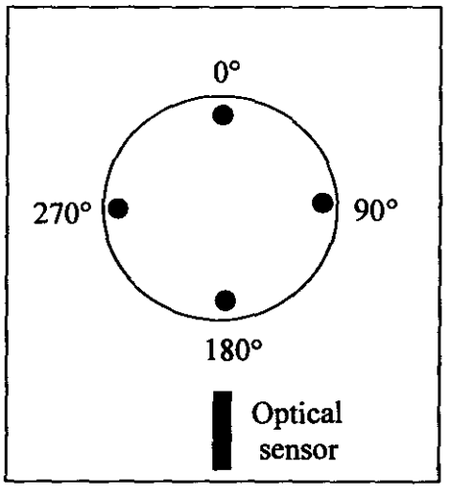

Figure 7.8: Rotor balancing

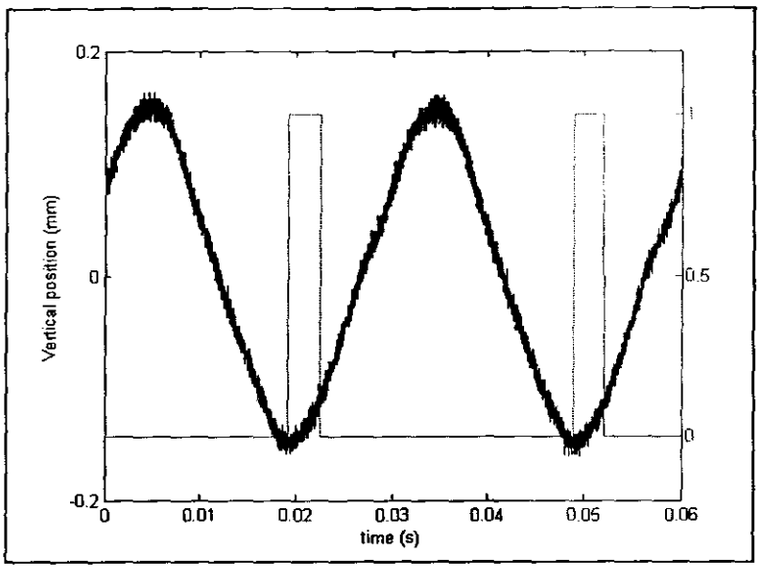

Figure 7.9: Imbalanced shaft

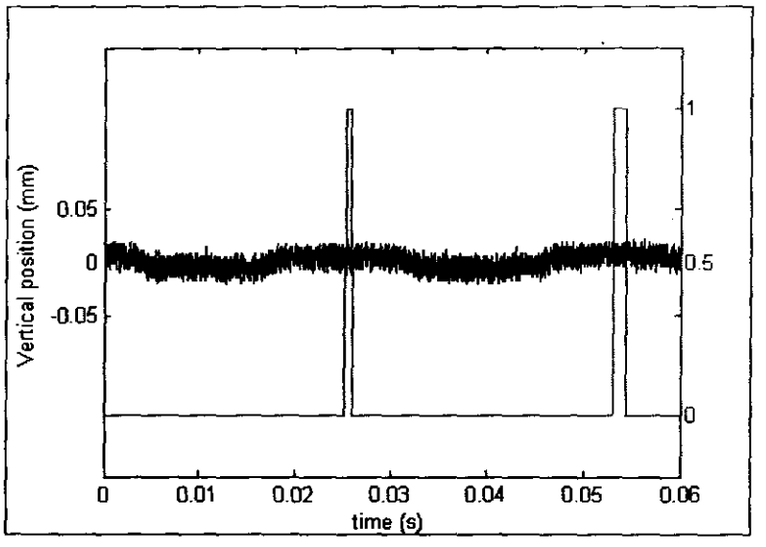

Figure 7.10: Balanced shaft

7.6. Dynamic stiffness and damping

The stiffness and damping for the AMB are not fixed values but rather frequency dependent. In order to estimate the stiffness and damping the rotor is balanced at 1000, 2000 and 3000 rpm. A small impulse is then applied to the shaft while the shaft is rotating. An exponential model is then fitted on the position and from the time constant and the damped frequency the stiffness and damping can be calculated.

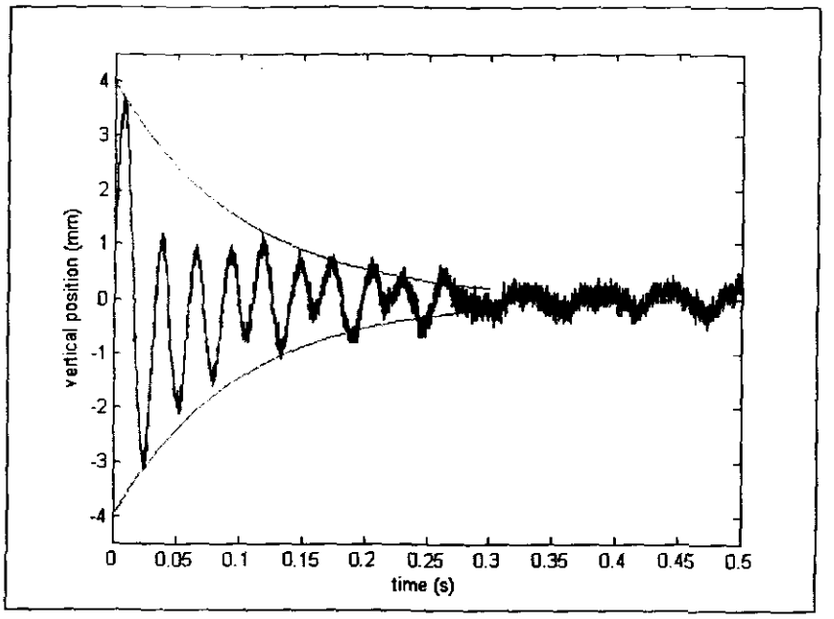

Figure 7.11: Exponential decay at 1000 rpm

The exponential function has the general form:

$$y = Ae^{\frac{-t}{\tau}} = Ae^{-\zeta\omega_n t} \tag{7.3}$$

with

ω_n - natural frequency of the system

ζ - damping factor

τ - time constant

The values for ζ and ω_n are calculated by solving the two simultaneous equations:

$$\tau = \frac{1}{\omega_n \zeta}$$
$$\omega_d = \omega_n \sqrt{1-\zeta^2} \tag{7.4}$$

The variable ω_d is the damped frequency of the system and is determined by measuring the frequency of the oscillation. A second order differential equation for a damped-spring-mass system is used to calculate the effective stiffness and damping:

$$y(s) = s^2 + 2\varsigma\omega_n s + \omega_n^2$$
$$= s^2 + \frac{b_{eq}}{m}s + k_{eq} \tag{7.5}$$

The stiffness and damping are calculated for three rotation speeds and shown in Table 7.3. The damping increases while the stiffness decreases. These values are only approximations.

Speed (rpm)	1000	2000	3000
Stiffness(N/m)	8 100	7 950	7 270
Damping(Ns/m)	30	33	37

Table 7.3: Stiffness and damping

7.7. Critical frequencies

When the shaft passes through a certain rotation speed the deviation in position would increase and then decrease again once the shaft has passed that certain speed. This is the first natural frequency of the total system. It is found that the natural frequency of the horizontal axis is at 2100 rpm and it differs from the vertical axis, which is at 2700 rpm. Figure 7.12 shows the critical speeds for both the vertical axis (2100 rpm) and the horizontal axis (2700 rpm). For comparison the position at 3000 rpm is also given. Note that the deviation is bigger at the critical frequencies than at 3000 rpm.

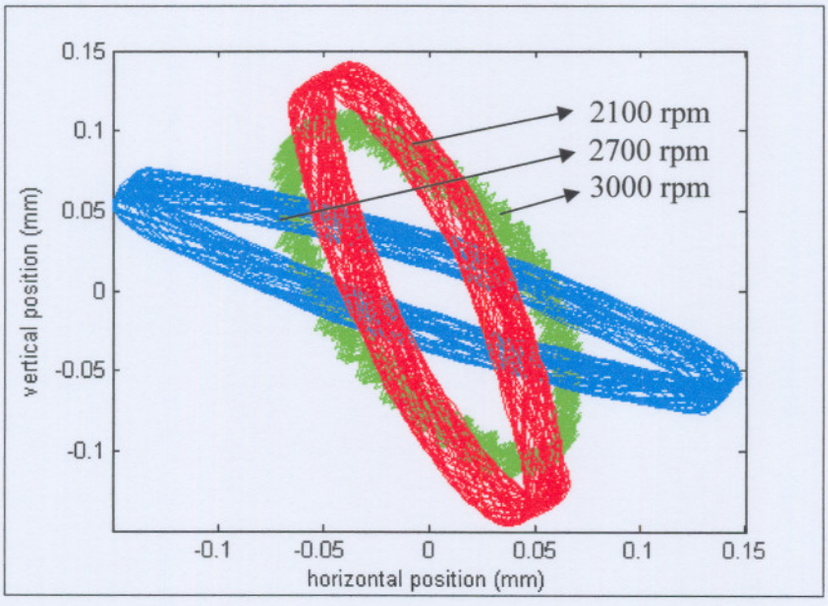

Figure 7.12: Critical frequencies

The stiffness is therefore lower in the vertical axis than in the horizontal axis. This is because of the lower K_p value in the vertical axis. It is found that when the value is increased the system becomes unstable. The stiffness is also lower than the designed stiffness. Further investigation will have to be done on this matter.

7.8. Conclusion

In this chapter the AMB is successfully suspended with rotation speeds up to 5000 rpm. There is a difference between the simulation and the actual system control parameters. This difference is discussed and is mainly because of unmodelled non-linearities in the actuator. Step response tests are conducted and the percentage overshoot and settling time are obtained. The values are compared to that of the simulation.

The shaft is balanced with the help of the speed sensor to minimise the deviation in position. An impulse is applied to the shaft at certain rotation speeds to measure the dynamic stiffness and damping. By fitting an exponential curve on the position the natural frequency and the damping factor can be calculated. The chapter ends by discussing the critical frequencies of the AMB and shows the results in each axis.

Chapter 8

Conclusion and recommendations

8.1. Aim of the project

The aim of this project was to develop a radial AMB and to suspend the shaft at rotation speeds of up to 3000 rpm with a 1 mm air gap between the shaft and the electromagnets. The power amplifiers, sensors and actuator of the AMB had to be designed and manufactured. A Matlab® simulation of the system had to be done to find the PID control parameters. All the components had to be integrated to form the final AMB system.

A stable suspension was achieved with the final AMB system at rotation speeds of up to 5000 rpm. At 3000 rpm the maximum deviation was found to be less than 0.11 mm from the centre position. The reference position signal was changed to a block waveform. The step response of the AMB was then measured. The settling time was less than 0.4 s with zero steady state error.

8.2. Project phases

The project constituted 6 phases: 1) Detail background study of AMB design and control, 2) electromechanical design of the AMB, 3) AMB simulation, 4) power amplifier and sensor design, 5) system integration and 6) system characterization.

A detail background study of AMBs was done to understand its basic principles. The force equation that relates the current and the position to the amount of force on the bearing is probably the most important equation for AMBs. From this equation the non-linear nature of AMBs could clearly be seen. The different types of electromagnet configurations were investigated as well as the different amplifiers and sensors available for AMBs.

The electromechanical design proved to be the most challenging part of this project. First a rigid shaft had to be designed and the centrifugal force because of rotor imbalance had to be calculated. The electromagnet was then designed. A heteropolar configuration was used without laminations on the shaft and the electromagnets. The design was verified in a finite element package.

The AMB system was simulated in Matlab®. A PID controller was implemented and proved to be sufficient to control the AMB system. From the simulation the specifications for the power

amplifier were obtained as well as the values for the PID control parameters. The unbalance force due to shaft imbalance was also simulated.

It was decided to use linear power amplifiers and inductive sensors. The inductive sensors have low costs but are sensitive to noise. Therefore linear power amplifiers were used instead of switched mode power amplifiers. The thermal design of the power amplifier was a critical part of the design because of the low efficiency of this type of power amplifier.

The power amplifiers and sensors were connected to the A/D channels of the dSpace® card. A graphical user interface was created in ControlDesk®. From this interface the position and control output can be monitored and the data can be captured to files on the hard drive of the computer. The PID control parameters can be changed and each power amplifier can be turned on or off.

The last phase of the project was to characterise the AMB system. It was found that the dynamic stiffness in the vertical axis was lower than that in the horizontal axis. The positions of both axes were measured and shown on a graph with the horizontal position on the x-axis and the vertical position on the y-axis. This graph gave good insight into the behaviour at different rotation speeds. The deviation in position increased with an increase in speed. The maximum deviation in the horizontal axis occurred at 2700 rpm while for the vertical axis it was at 2100 rpm.

8.3. Recommendations

The following recommendations are given to improve the AMB systems and for further studies in this field:

- The developed AMB system has a relatively low dynamic stiffness. Future studies can be done to find the effect that each PID parameter has on the dynamic stiffness.

- The control system of the AMB is implemented on the dSpace® card. It is recommended that the controller be implemented on a microcontroller chip, to eliminate the computer and the dSpace® card.

- Machines must sometimes work at rotation speeds that are higher than its natural frequencies. The third critical frequency of the rotor is a bending mode and special care

has to be taken to place the actuators and sensors at the correct place on the rotor. A future study could be to develop an AMB that allow the machine to work at frequencies above its natural frequencies. A good understanding of rotor dynamics is essential for this study.

- There is a 50 Hz noise on the system. This noise signal originates at the power amplifiers. An investigation can be conducted on how to eliminate it.

- The filters of the sensors are analog filters. These filters can be changed to digital filters and implemented on the dSpace card or microcontroller.

Appendix A

The first critical frequency of the shaft

The aim is to calculate the first natural frequency of the shaft shown in Figure A.1. The point at the ball bearing will be used as the fixed position. The shaft is divided into two parts: the journal and the rod. The inertia of each part must be calculated about an axis through its centre of mass parallel to the y-axis. Then the moment of inertia must be calculated about a parallel axis through the fixed point indicated by the triangle.

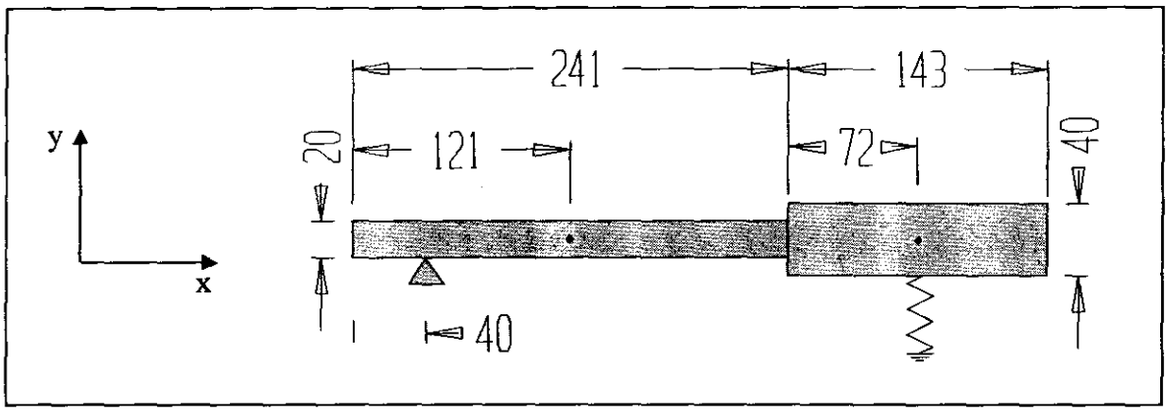

Figure A.1: Shaft dimensions

The inertia of the journal (I_j) and the rod (I_r) are:

$$I_j = \frac{m_j (3d_j^2 + 4l_j^2)}{48}$$

$$I_r = \frac{m_r l_r^2}{12} \qquad \text{(A.1)}$$

with

m	-	mass
d	-	diameter
l	-	length

The dimensions and mass values are substituted:

$$I_j = 2.54\text{x}10^{-3}$$
$$I_r = 2.86\text{x}10^{-3}$$

To relate this inertia values to the fixed point the parallel-axis theorem [23] is used:

$$I'_j = I_j + s_j{}^2 m_j$$
$$I'_r = I_r + s_r{}^2 m_r \qquad \text{(A.2)}$$

with:

s - the distance between the centre of mass and the fixed point

The total inertia (I_t) of the system is:

$$I_t = I_j' + I_r' \qquad \text{(A.3)}$$

To calculate the natural frequency the stiffness of the system must specified. The stiffness of the system is specified as 630 000 N/m. The natural frequency is now given by A.4. The distance s is now the distance between the fixed point and the centre of AMB journal.

$$\omega = \sqrt{\frac{630000 s^2}{I_t}} \qquad \text{(A.4)}$$
$$= 641\,\text{rad/s}$$
$$f = 102\,\text{Hz}$$

Appendix B

Derivation of the force that the electromagnet can exert

The force that the electromagnet in Figure B.1 with a flat surface A_g can exert, neglecting leakage and fringing as well as iron losses, is given by:

$$F_{flat} = \left(\frac{B_{air}^2}{\mu_0}\right) A_g \qquad \text{(B. 1)}$$

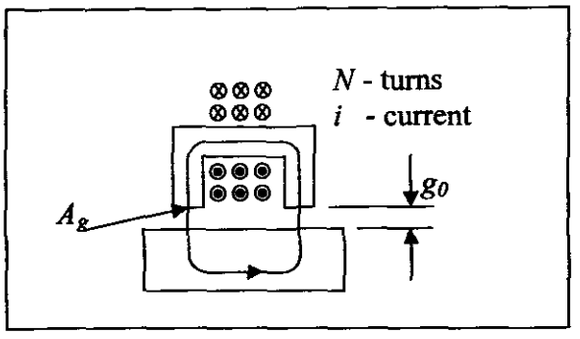

Figure B.1: Electromagnet with a flat surface

Consider now an electromagnet with a rounded surface as seen in Figure B.2.

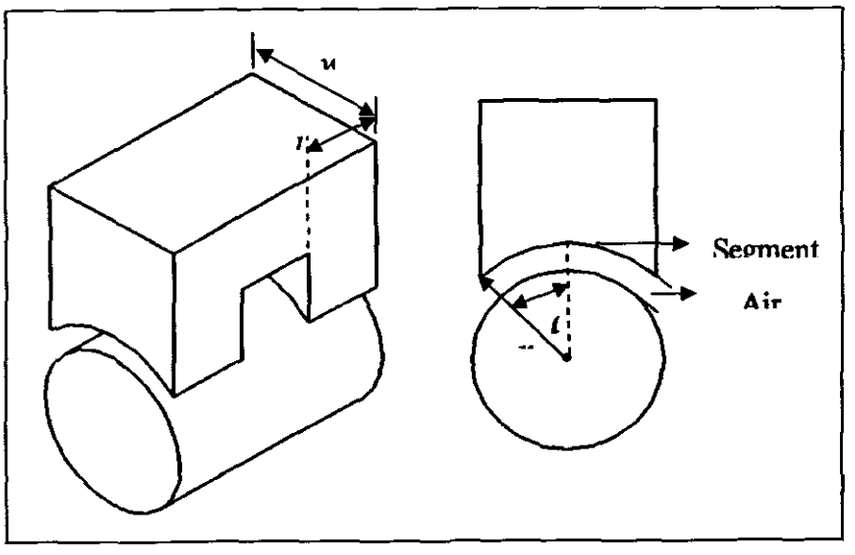

Figure B.2: Electromagnet of a radial AMB

The perpendicular area of one leg is

$$A_{iron} = wl \tag{B. 2}$$

The segment s makes an angle of 2θ with the centre of the shaft. To calculate the force that one leg of the electromagnet can exert, divide the segment s into very small segments ds. The effective area of the surface between the airgap and the iron is then

$$dA_{gap} = w\,ds$$

The distance ds can be expressed in terms of the angle θ and the radius of the segment r so that

$$ds = r\,d\theta$$

and

$$dA_{gap} = w\,r\,d\theta$$

The force is perpendicular to the area A_{gap} so that for a small area dA_{gap} the force is

$$dF = \frac{B_{gap}^2\,dA_{gap}}{2\mu_0} = \frac{B_{gap}^2\,w\,r\,d\theta}{2\mu_0}$$

The force in the upwards direction is then

$$dF = \frac{B_{gap}^2\,w r d\theta}{2\mu_0}(\cos\theta)$$

To complete the calculation integrate over the whole sector to find the total force in the upwards direction.

$$F = \int_{-\theta}^{\theta} dF = \int_{-\theta}^{\theta} \frac{B_{gap}^2\,wr}{2\mu_0}\cos(\theta) = \frac{B_{gap}^2\,wr}{2\mu_0}\sin(\theta)\Big|_{-\theta}^{\theta}$$

$$
\begin{aligned}
&= \frac{B_{gap}^2 wr}{2\mu_0}\left(\sin(\theta) - \sin(-\theta)\right) \\
&= \frac{B_{gap}^2 wr}{2\mu_0}\left(\sin(\theta) + \sin(\theta)\right) \\
&= \frac{B_{gap}^2 wr}{\mu_0}\left(\sin(\theta)\right)
\end{aligned}
\qquad \text{(B. 3)}
$$

The flux density in the air gap (B_{gap}) and in the iron (B_{iron}) is not the same because the effective areas are different. It is useful to find an expression in terms of B_{iron} because the saturation iron flux density is known for different kinds of materials. By using the fact that magnetic field lines do not begin or end anywhere (divergence of a magnetic field is zero), all the field lines in the iron must go through the air gap so that:

$$
\begin{aligned}
&B_{iron} A_{iron} = B_{gap} A_{gap} \\
&\therefore B_{gap} = \frac{A_{iron} B_{iron}}{A_{gap}}
\end{aligned}
\qquad \text{(B. 4)}
$$

Substitute (B. 4) in (B. 3):

$$
\begin{aligned}
F &= \left[\frac{A_{iron} B_{iron}}{A_{gap}}\right]^2 \frac{wr}{\mu_0 g}\left(\sin(\theta)\right) \\
&= \frac{B_{iron}^2 A_{iron}}{\mu_0 g}\left[\frac{A_{iron}}{A_{gap}^2} wr\left(\sin(\theta)\right)\right]
\end{aligned}
\qquad \text{(B. 5)}
$$

Using trigonometry the areas in the iron and the air gap is

$$
\begin{aligned}
A_{iron} &= w\, 2r \sin(\theta) \\
A_{gap} &= w\, 2r\theta
\end{aligned}
$$

Substitute A_{gap} and A_{iron} in (B. 5):

$$F = \frac{B_{iron}^2 A_{iron}}{\mu_0}\left[\frac{w2r\sin(\theta)}{(w2r\theta)^2} wr(\sin(\theta))\right]$$
$$= \frac{1}{2}\frac{B_{iron}^2 A_{iron}}{\mu_0}\frac{\sin^2(\theta)}{\theta^2}$$

For two air gaps the force is twice this value so the total force that the bearing can exert is

$$F_t = \frac{B_{iron}^2 A_{iron}}{\mu_0}\frac{\sin^2(\theta)}{\theta^2} \qquad \text{(B. 6)}$$

Appendix C

Imbalance quality grades

Imbalance quality grade	Product of (e x ω) in mm/s	General rotor types
G4000	4000	Crankshaft of rigidly mounted slow marine diesel engines with uneven number of cylinders
G1600	1600	Crankshafts of rigidly mounted large two-cycle engines
G630	630	Crankshafts of rigidly large four-cycle engines
G250	250	Crankshafts of rigidly mounted fast four-cylinder diesel engines
G100	100	Crankshafts of fast diesel engines with six or more cylinders
G40	40	Car wheels, crankshafts of engines of cars
G16	16	Drive shafts with special requirements, Parts of crushing machines
G6.3	6.3	Fans, flywheels and pump impellers
G2.5	2.5	Gas and steam turbines and turbo compressors
G1	1	Tape recorder drives, small electric armatures with special requirements
G0.4	0.4	spindles, discs and armatures of precision grinders, Gyroscopes

Table C.1: Imbalance quality grades

Appendix D

Cadkey Drawings

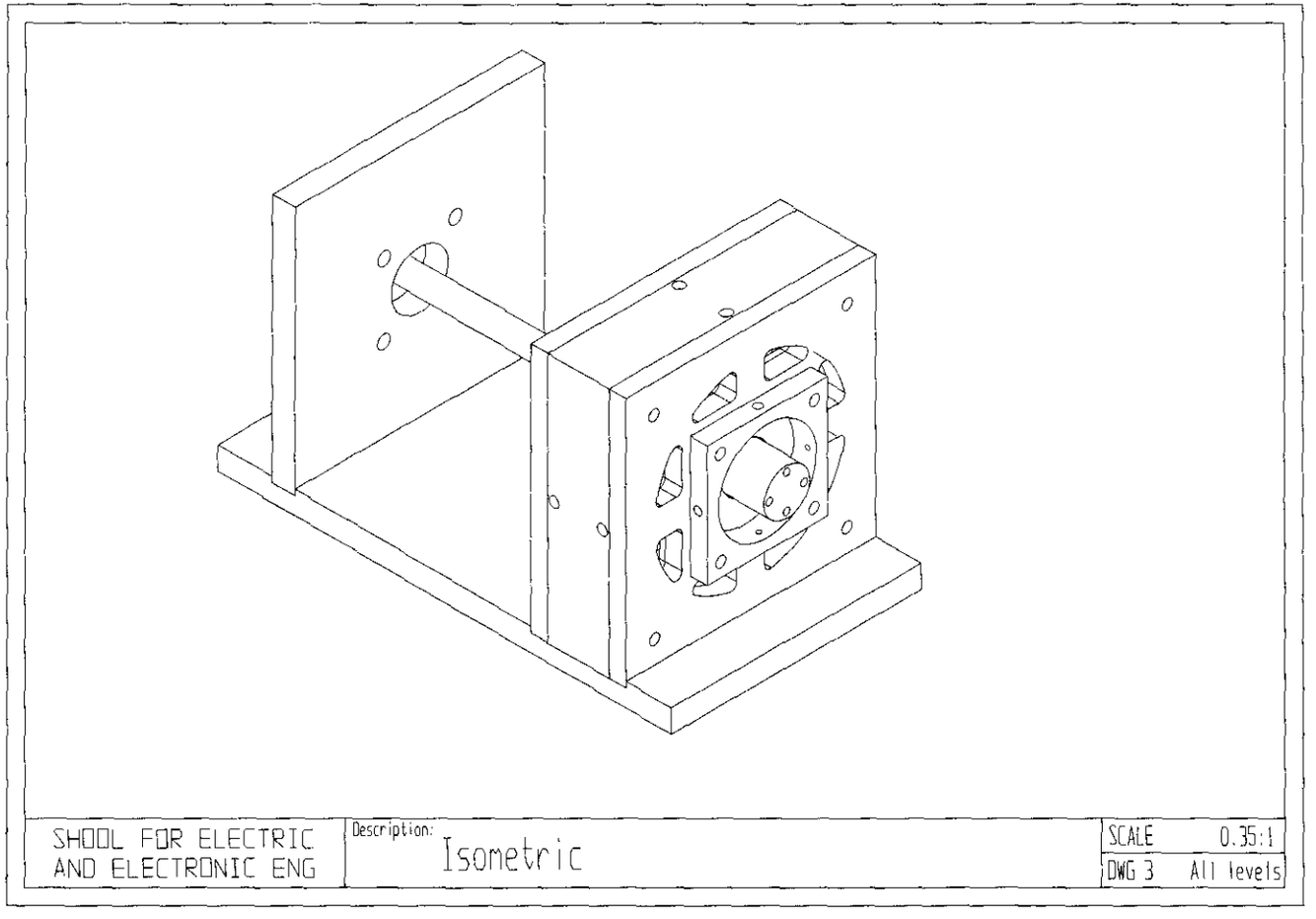

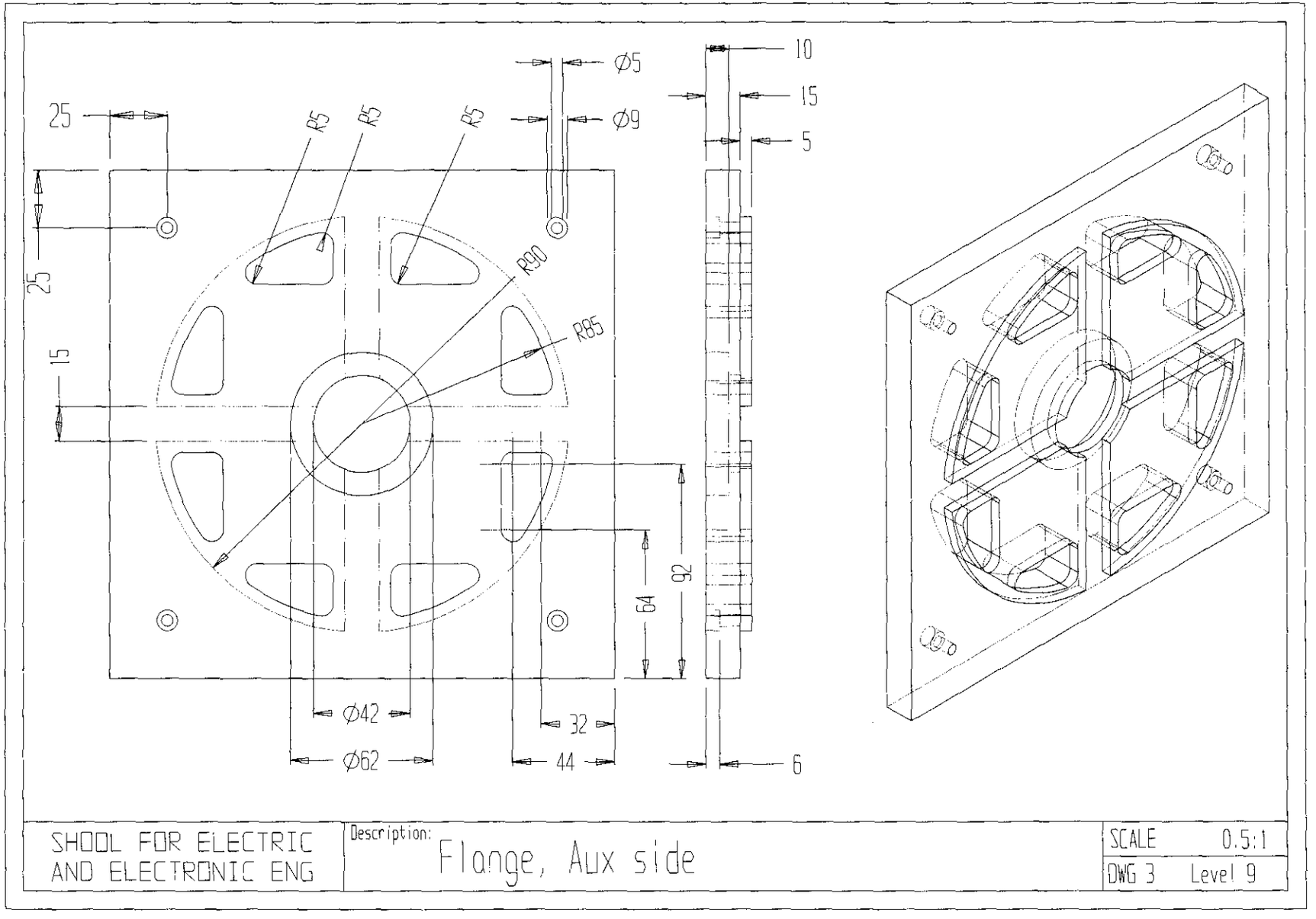
25
25
15
R5
R5
R5
R90
R85
Ø5
Ø9
10
15
5
92
64
Ø42
Ø62
32
44
6
SHOOL FOR ELECTRIC
AND ELECTRONIC ENG
Description:
Flange, Aux side
SCALE 0.5:1
DWG 3 Level 9

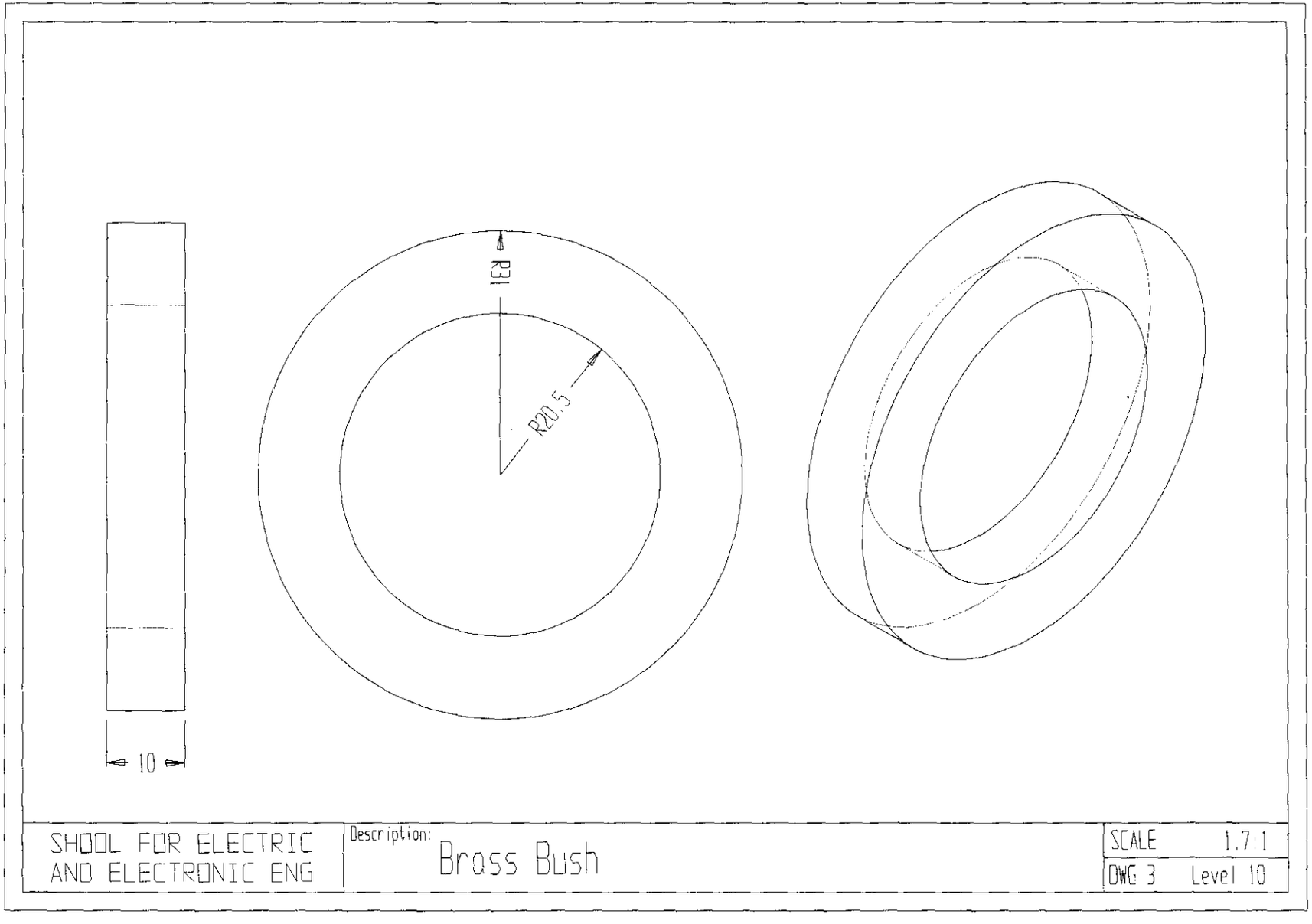
R1
R20.5
10
SHOOL FOR ELECTRIC
AND ELECTRONIC ENG
Description:
Brass Bush
SCALE 1.7:1
DWG 3 Level 10

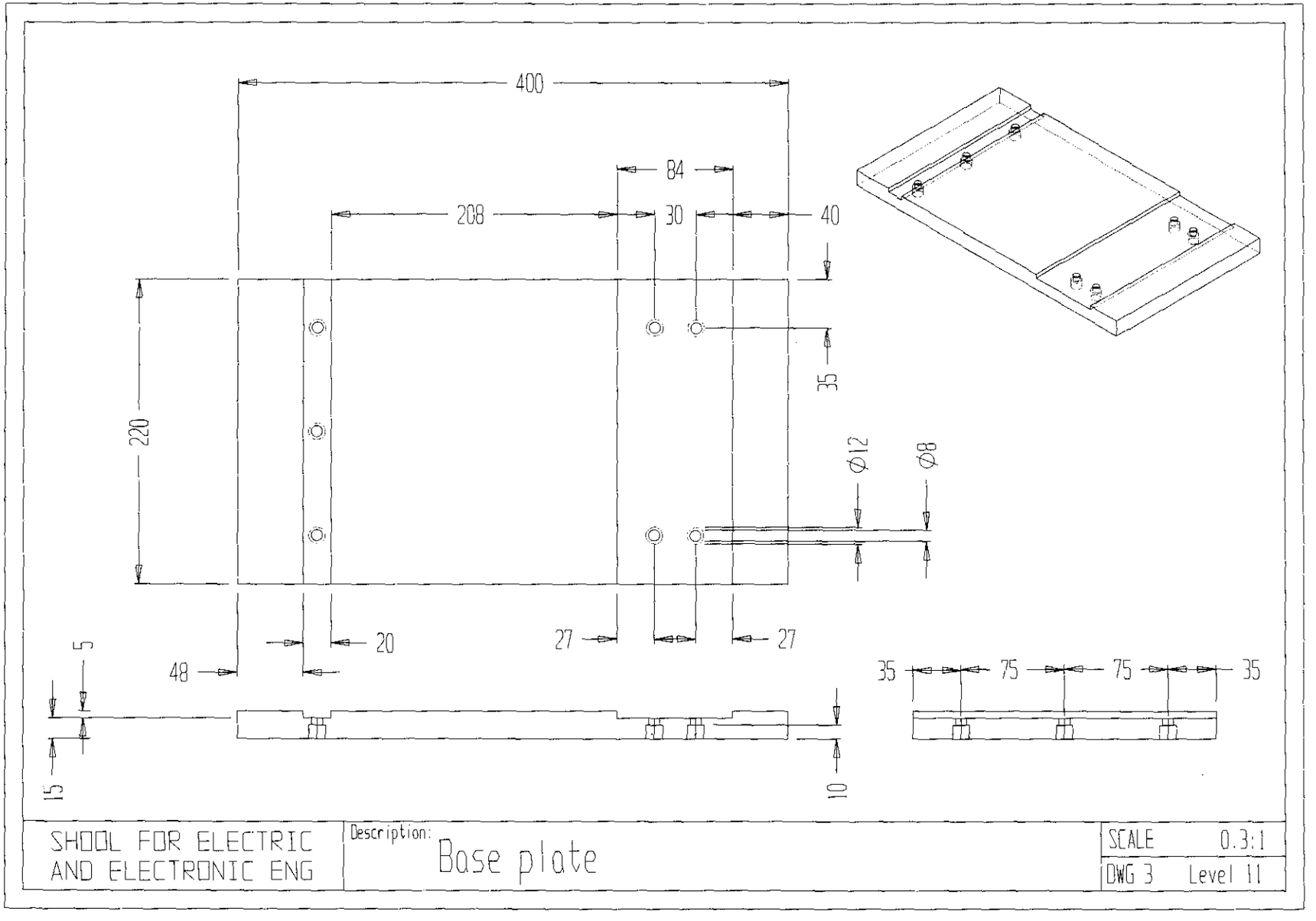
400
84
208
30
40
35
220
Φ12
Φ8
20
27
27
48
5
15
10
35
75
75
35
SHOOL FOR ELECTRIC AND ELECTRONIC ENG
Description:
Base plate
SCALE 0.3:1
DWG 3 Level 11

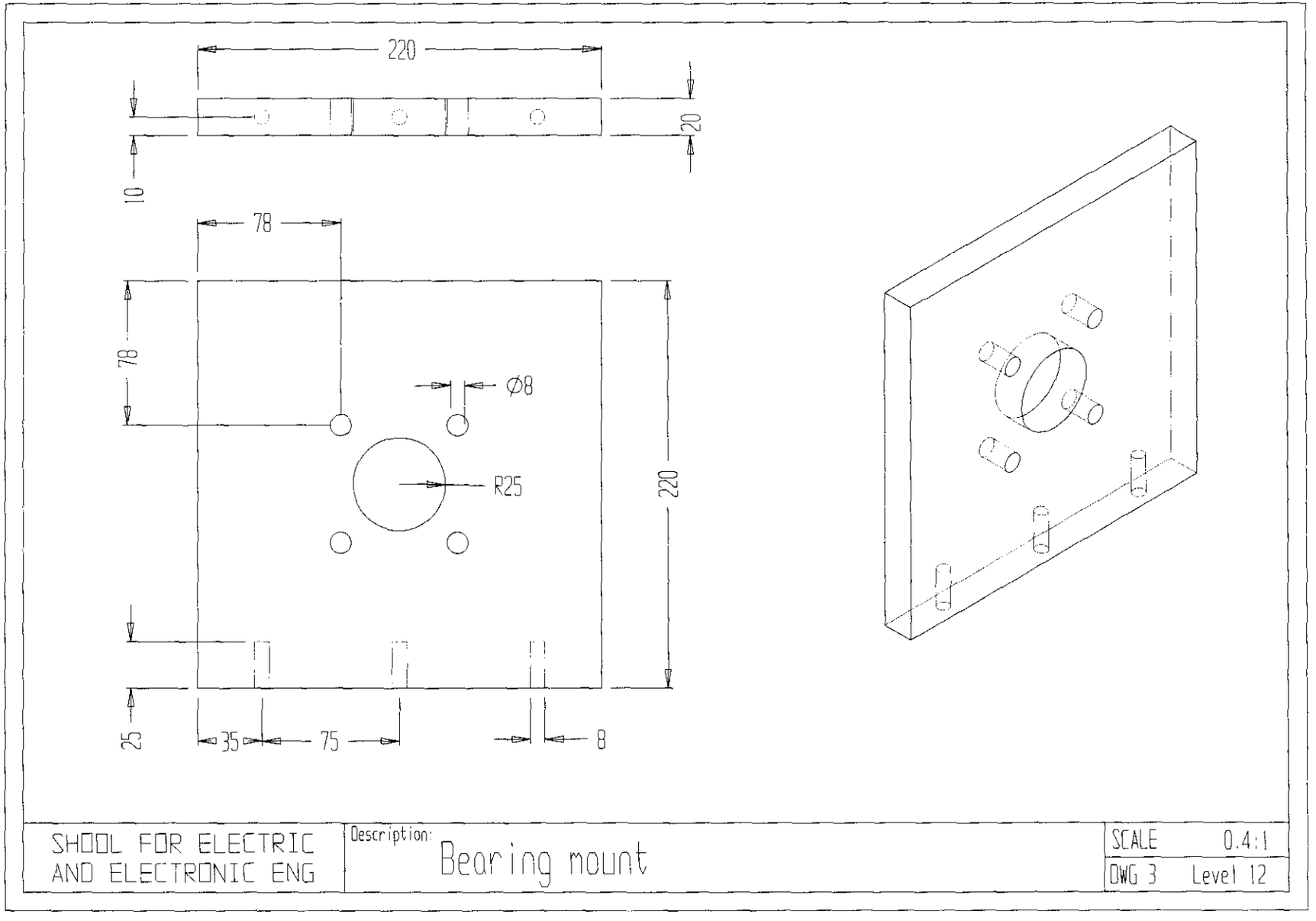
220
20
10
78
78
Ø8
R25
220
25
35
75
8
SHOOL FOR ELECTRIC
AND ELECTRONIC ENG
Description:
Bearing mount
SCALE 0.4:1
DWG 3 Level 12

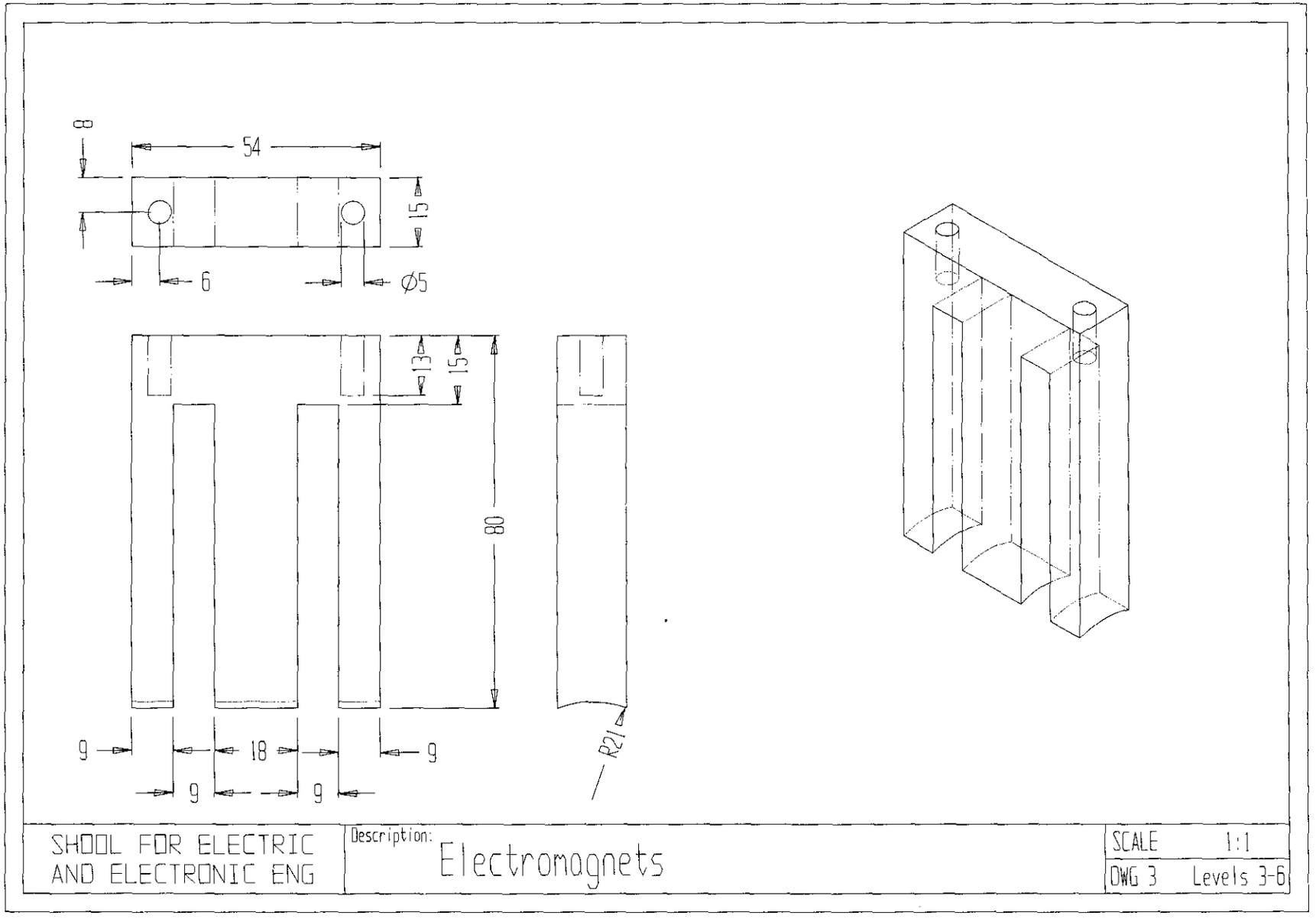
8
54
15
6
Ø5
13
15
80
9
18
9
9
9
R21
SHOOL FOR ELECTRIC
AND ELECTRONIC ENG
Description:
Electromagnets
SCALE 1:1
DWG 3 Levels 3-6

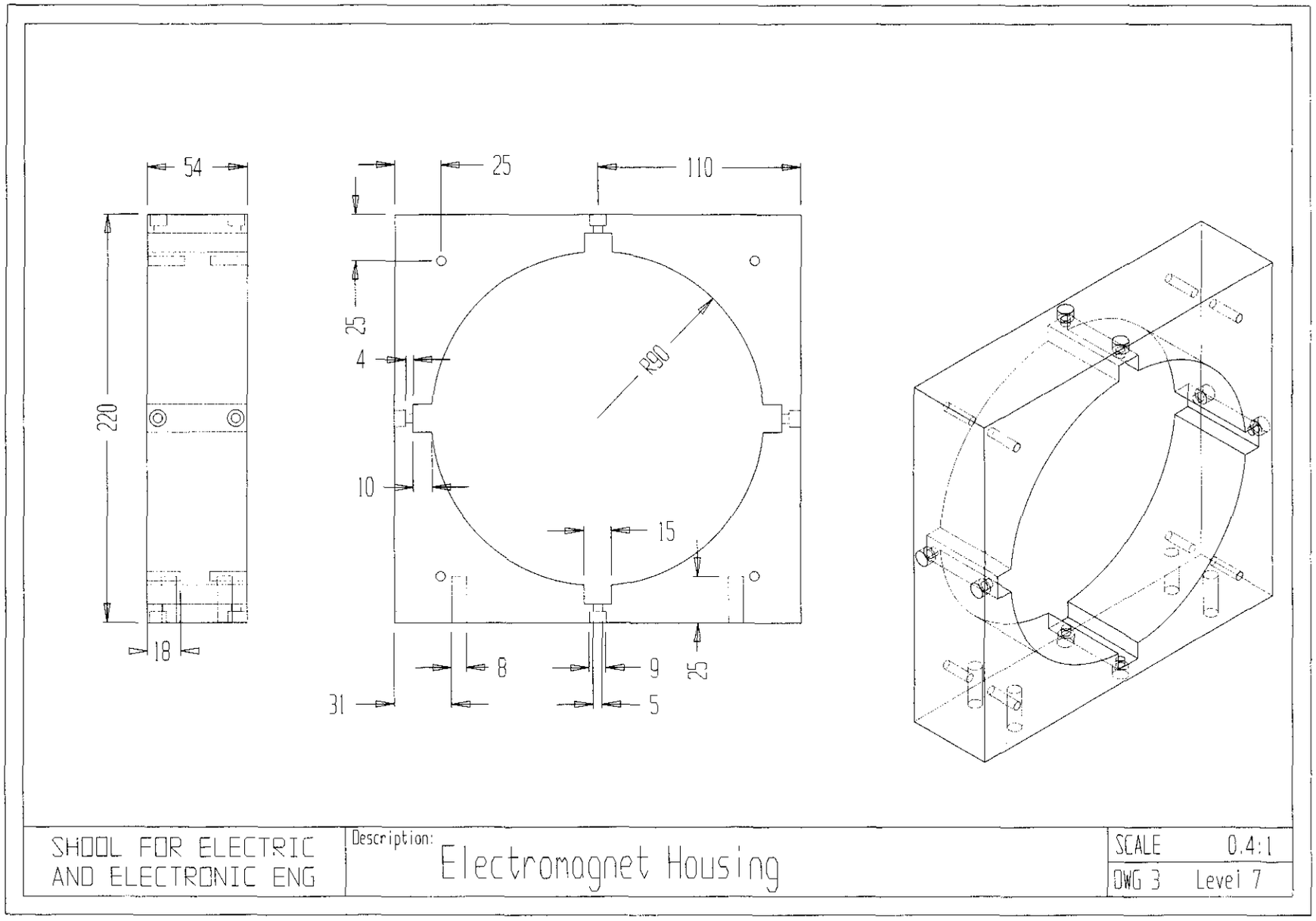

SHOOL FOR ELECTRIC AND ELECTRONIC ENG	Description: Electromagnet Housing	SCALE 0.4:1 DWG 3 Level 7

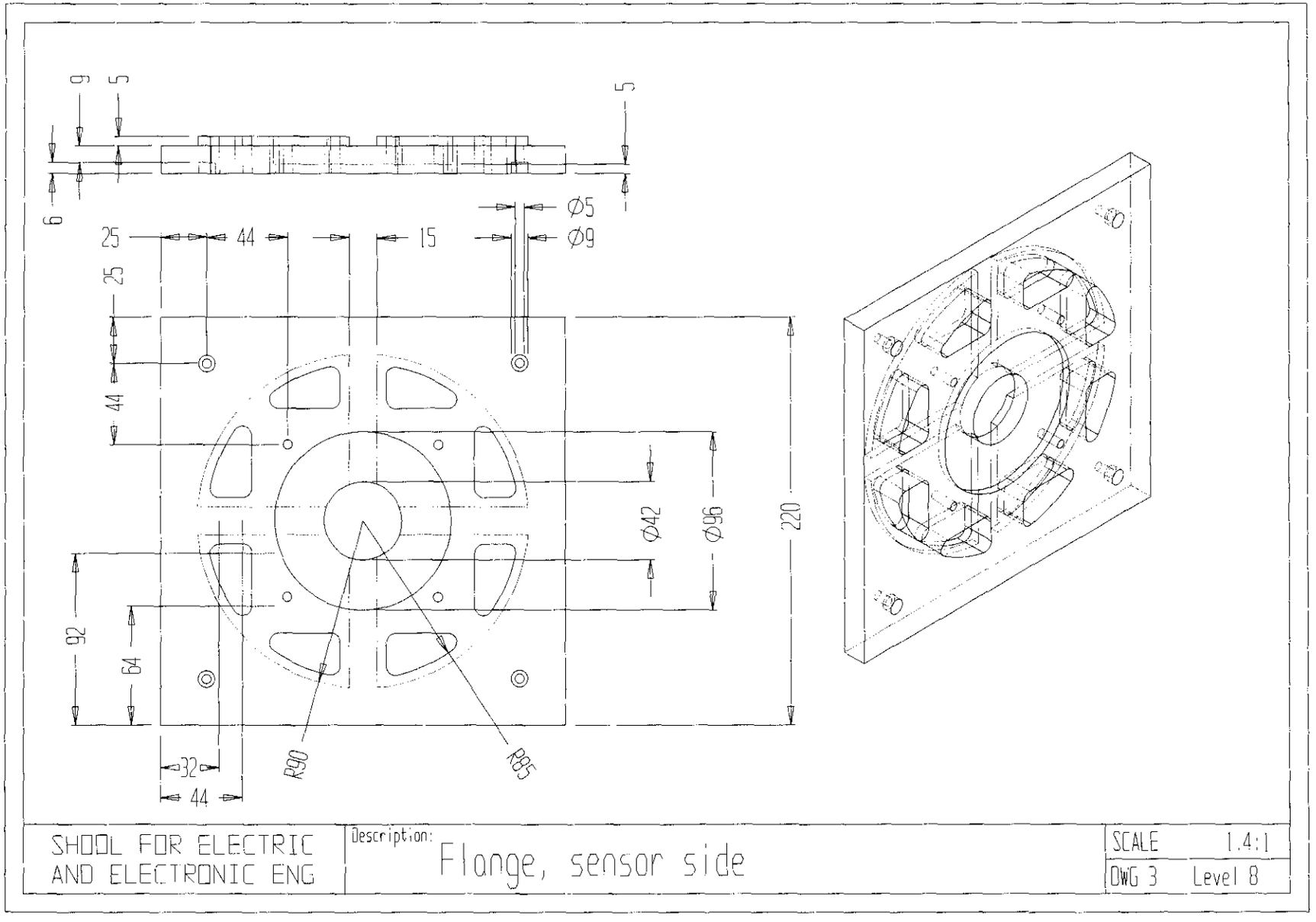

SHOOL FOR ELECTRIC AND ELECTRONIC ENG	Description: Flange, sensor side	SCALE 1.4:1
		DWG 3 Level 8

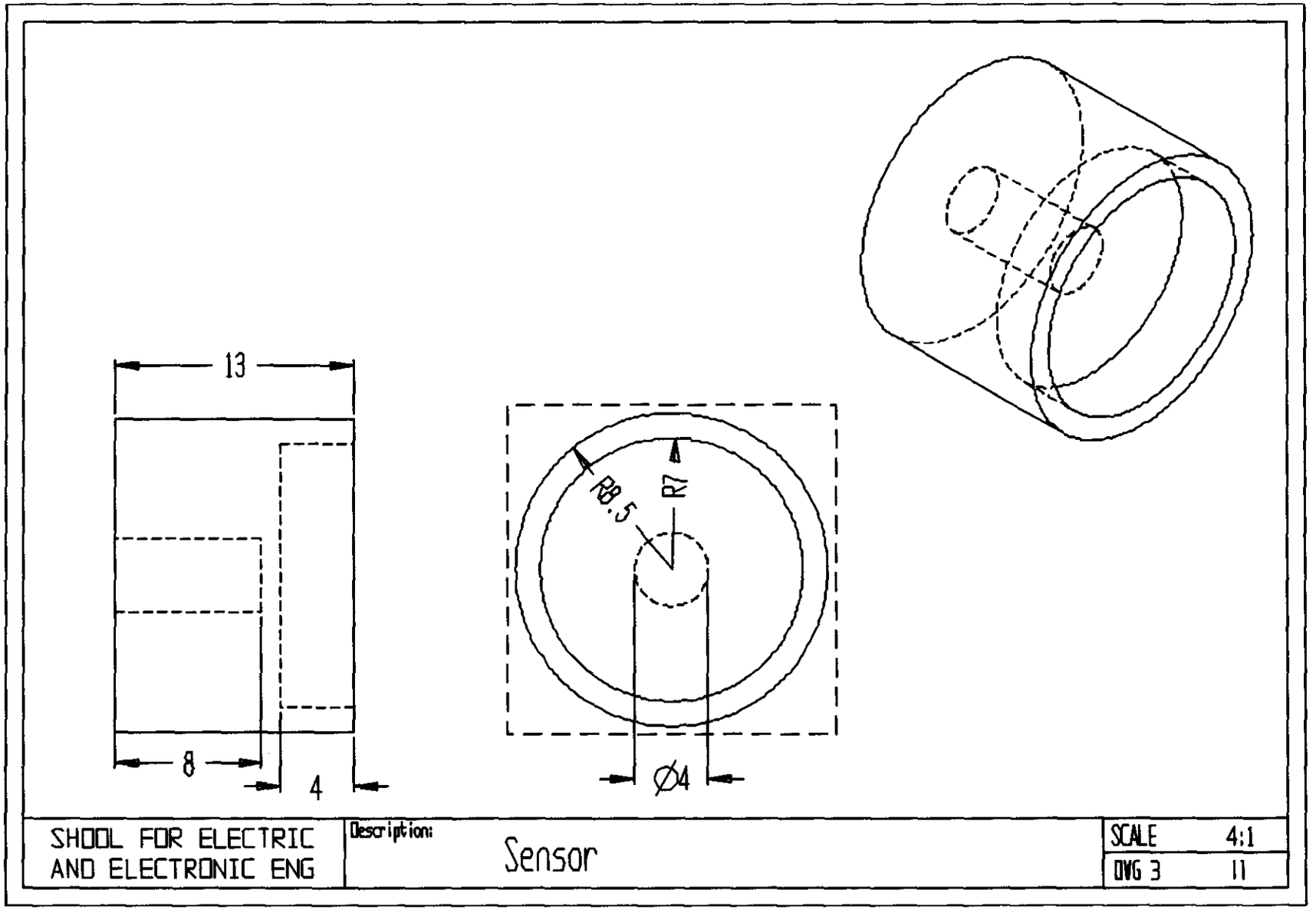
13
8
4
R8.5
R7
Ø4
SHOOL FOR ELECTRIC
AND ELECTRONIC ENG
Description:
Sensor
SCALE 4:1
DWG 3 11

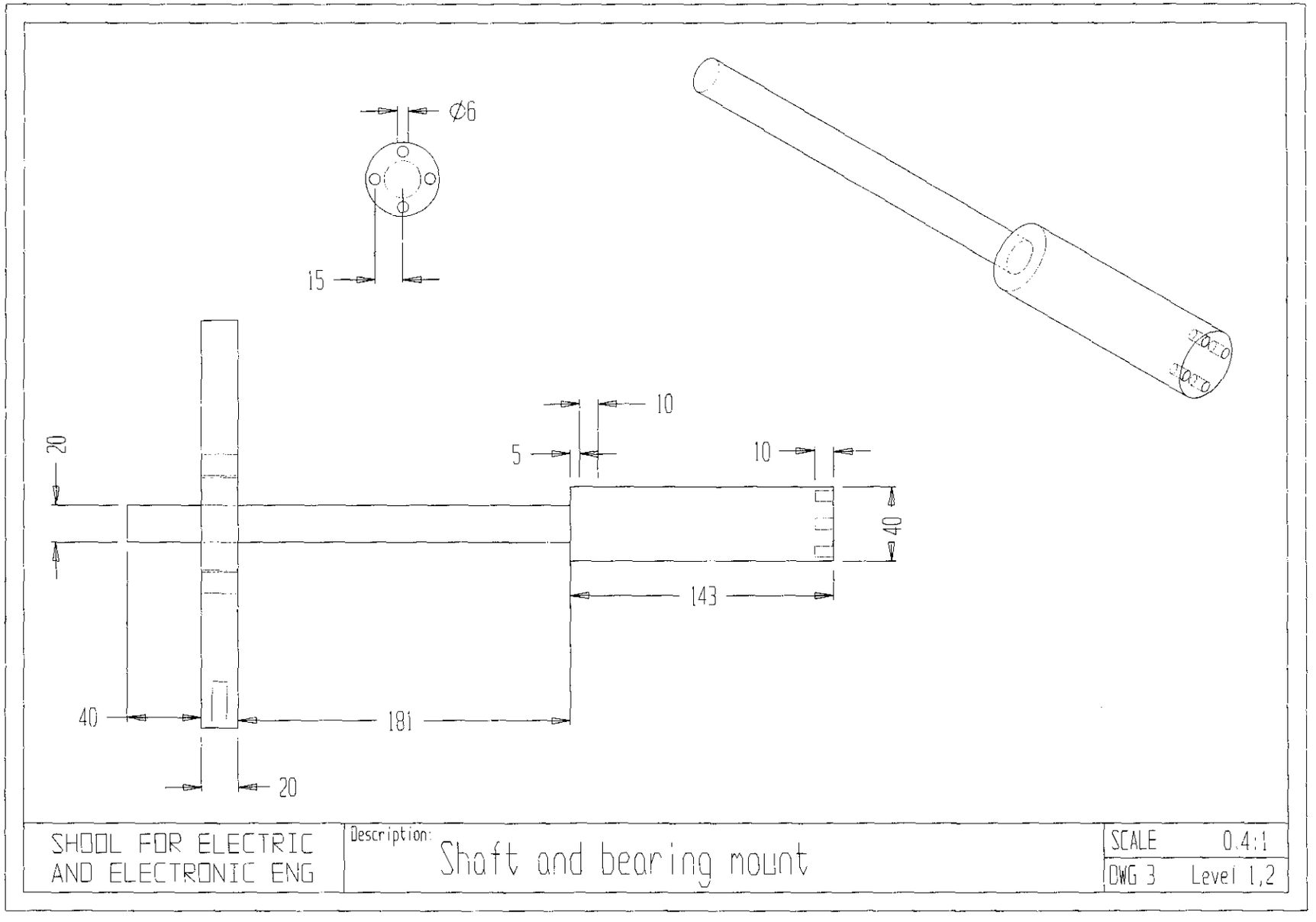
Ø6
15
10
5
10
20
40
143
40
181
20
SHOOL FOR ELECTRIC AND ELECTRONIC ENG
Description:
Shaft and bearing mount
SCALE 0.4:1
DWG 3 Level 1,2

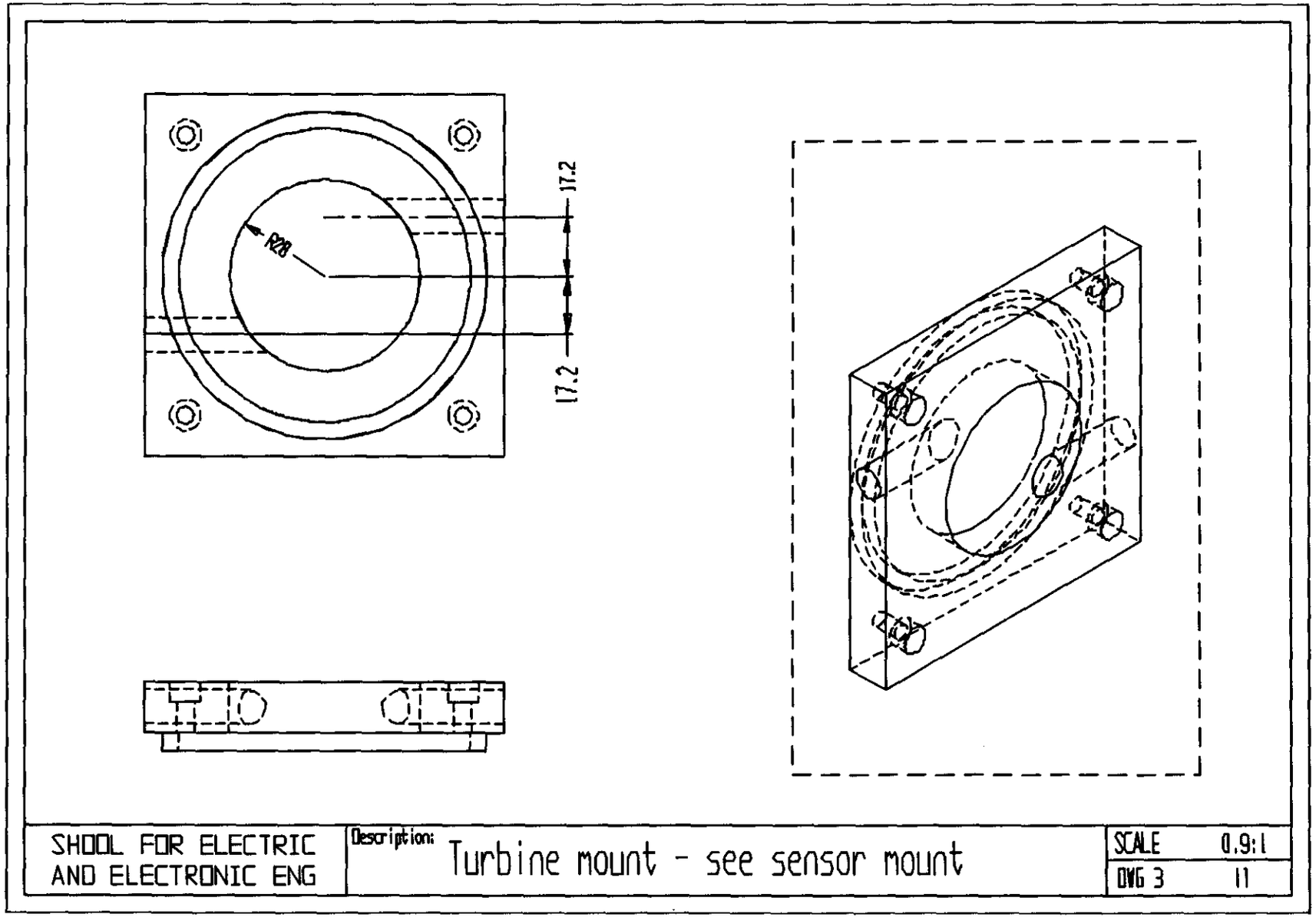
R28
17.2
17.2
SHOOL FOR ELECTRIC
AND ELECTRONIC ENG
Description:
Turbine mount - see sensor mount
SCALE 0.9:1
DWG 3 11

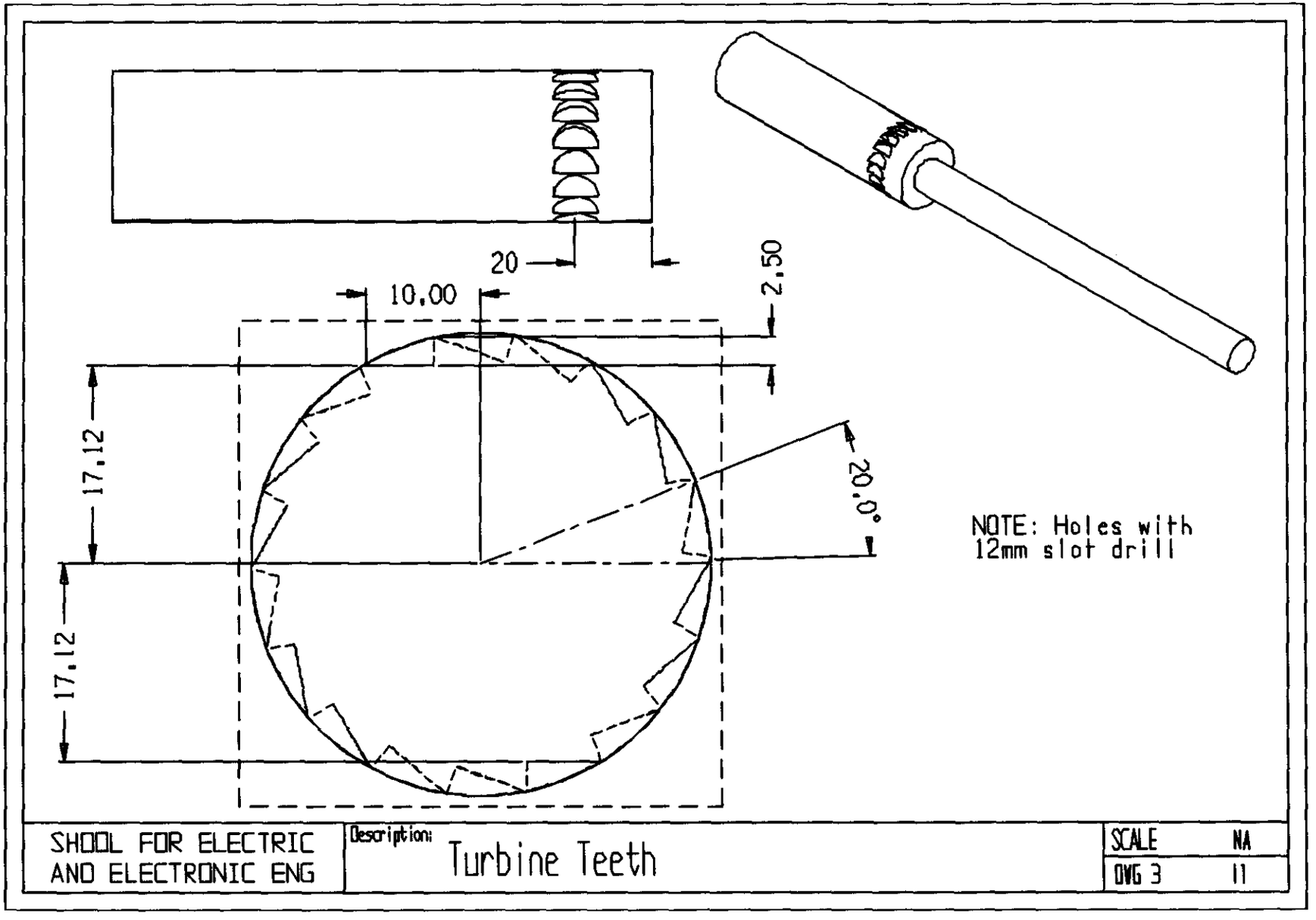
20
10,00
2,50
17,12
17,12
20,0°
NOTE: Holes with
12mm slot drill
SHOOL FOR ELECTRIC
AND ELECTRONIC ENG
Description:
Turbine Teeth
SCALE NA
DWG 3 11

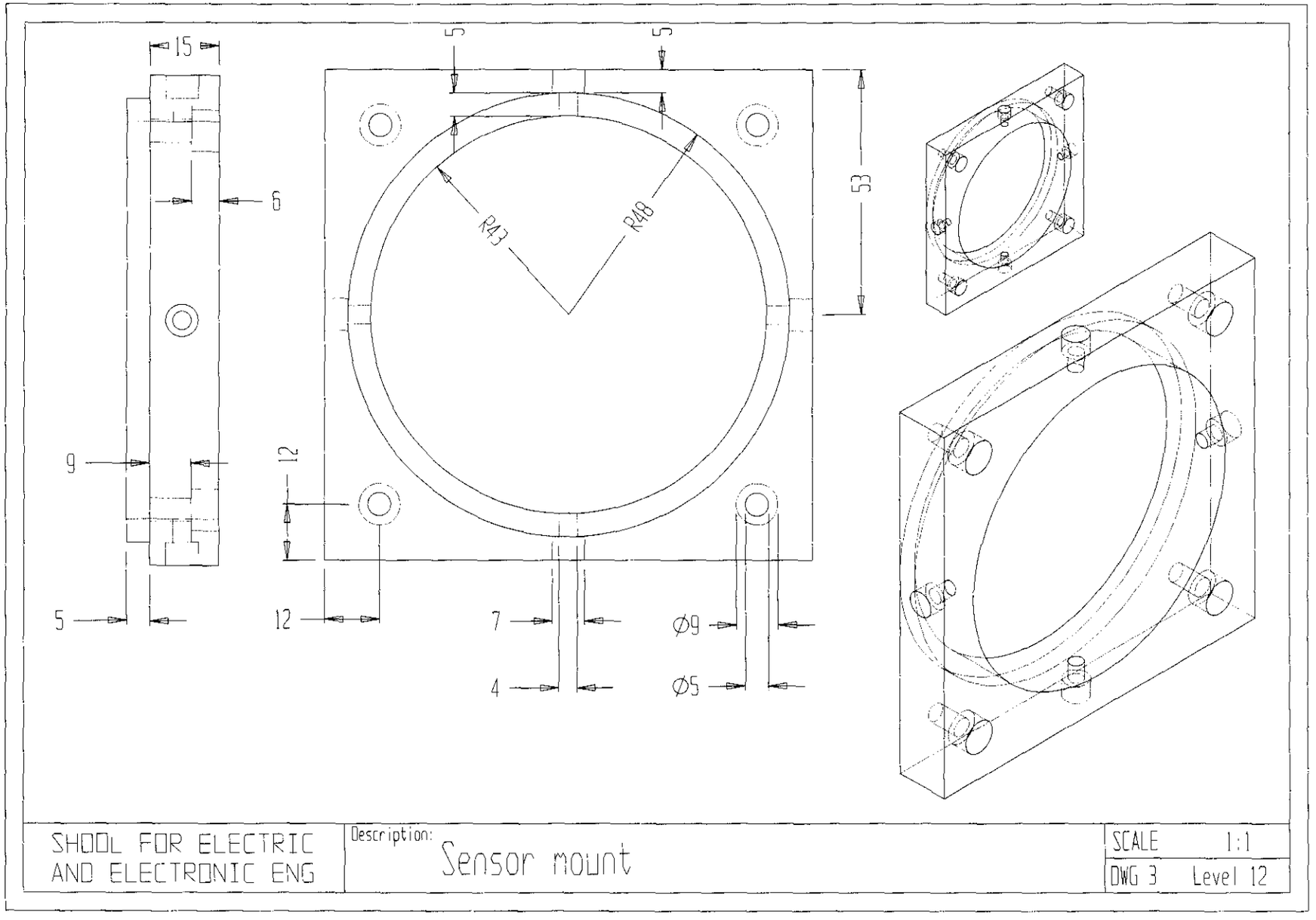
15
6
9
5
12
5
5
R43
R48
53
12
7
4
Ø9
Ø5
SHOOL FOR ELECTRIC AND ELECTRONIC ENG
Description:
Sensor mount
SCALE 1:1
DWG 3 Level 12

Appendix E

Photos

This appendix contains photos of the AMB system. The first two photos are a back and front view of the AMB (Figure E.1). The sensors are situated on the front as well as the holes where unbalance weights can be added. At the back side is the ball bearing. Figure E.2 shows the complete AMB system with the computer and the power amplifiers. The optical speed sensor is situated between the ball bearing and the AMB. The turbine and the back-up bearing are shown in Figure E.3. The back-up bearing is the brash bush in the middle. The end plates have grooves that the electromagnets fit into.

In Figure E.4 the four homopolar electromagnets and the sensors are shown. Each sensor is exactly aligned with an electromagnet. Figure E.5 shows the power amplifiers and the shaft. Two power amplifiers are built on one heat sink. The picture of the shaft shows the journal and the teeth of the turbine.

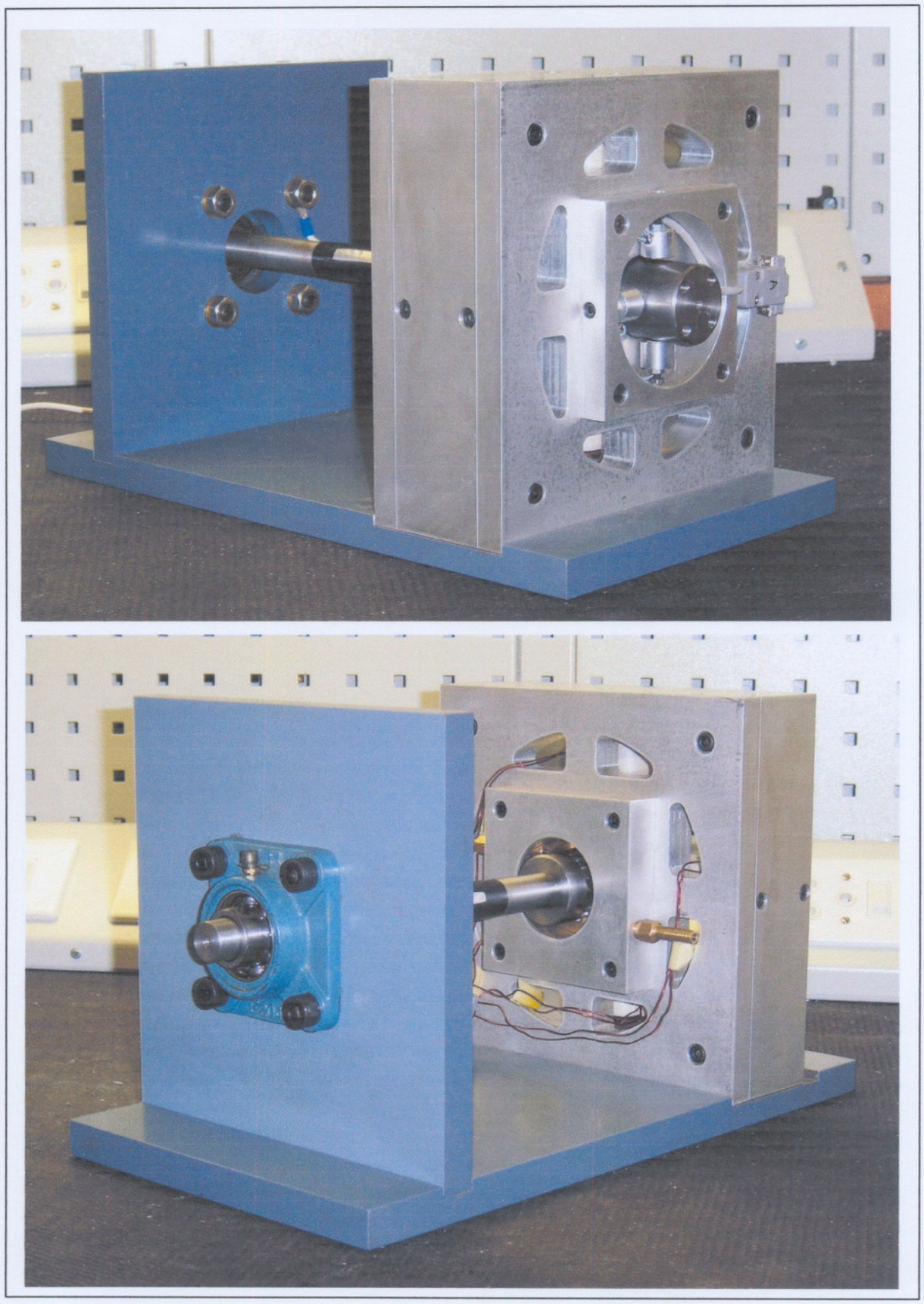

Figure E.1: Front and back view of the AMB

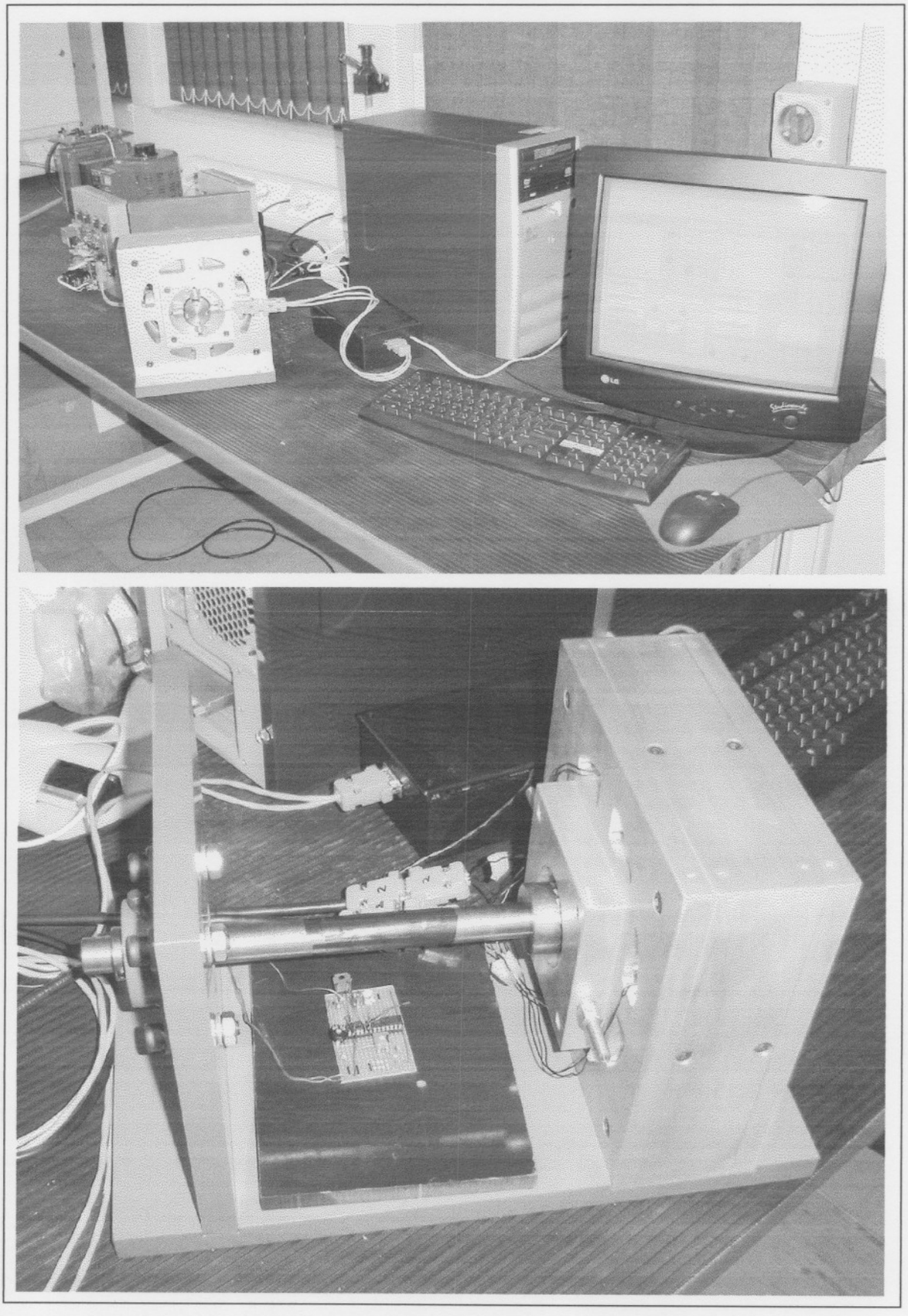

Figure E.2: The complete system and speed senor

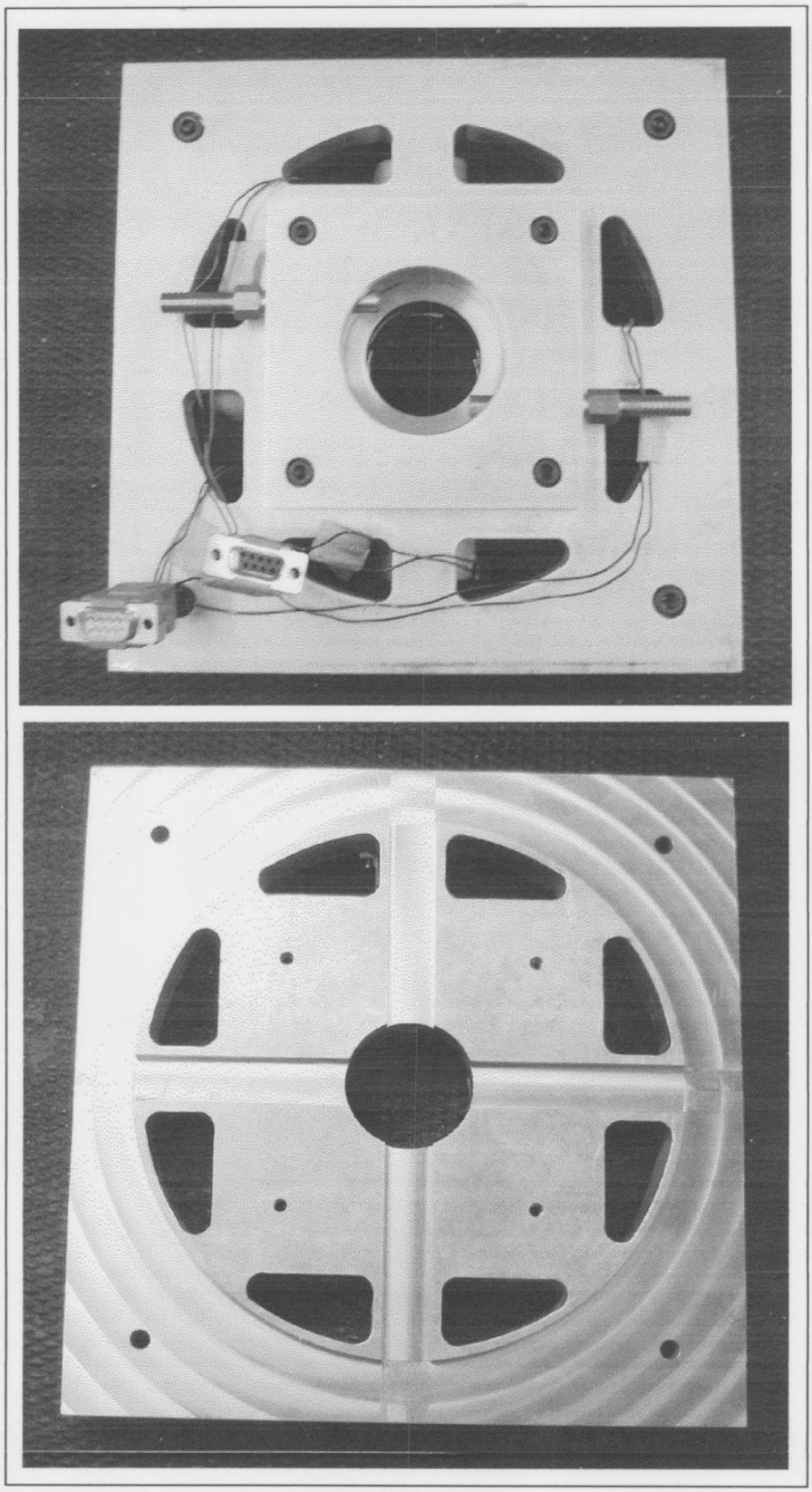

Figure E.3: Turbine side end plates

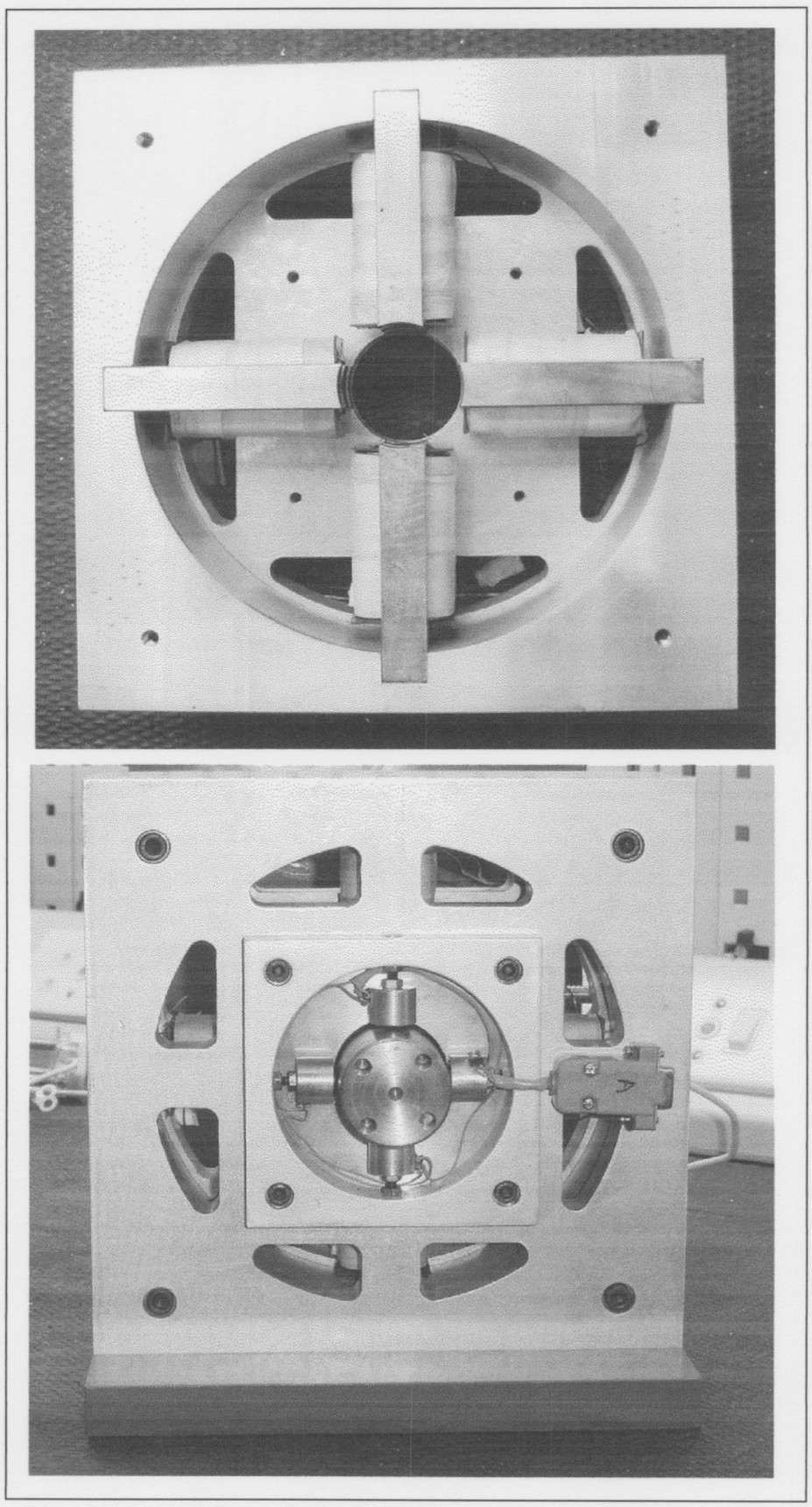

Figure E.4: Electromagnets and sensors

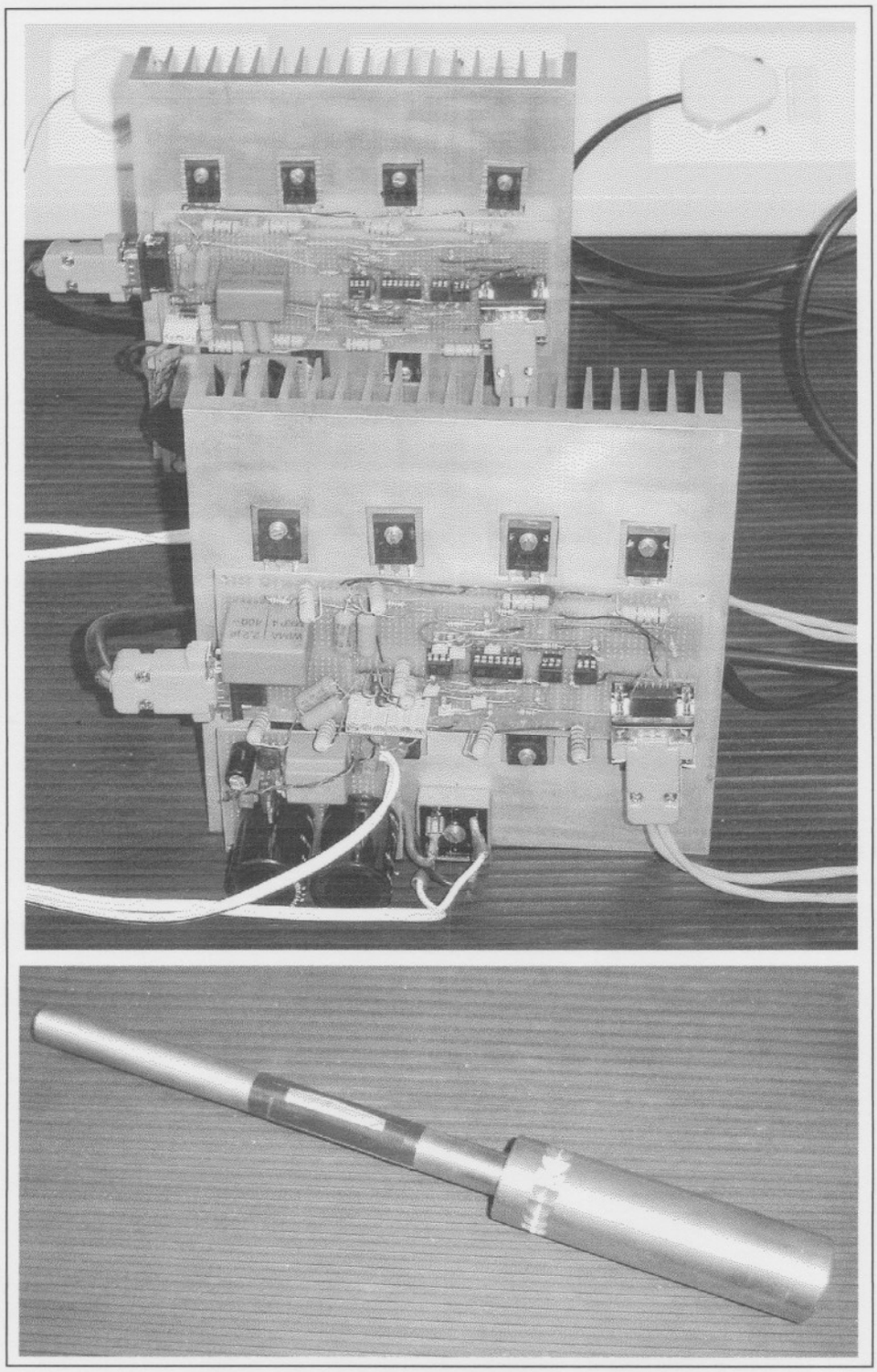

Figure E.5: Power amplifiers and shaft

Appendix F

Dissertation in MS Word format

Matlab® simulation

MathCad® electromagnetic design

dSpace® experiment files

References

[1] A.P. George, "Introduction to the Pebble Bed Modular reactor (PBMR)," PBMR, Pretoria, Tech. Rep., 2001.

[2] M.C. Nieuwoudt and W. Kriel, "PBMR operability summary," PBMR, Pretoria, Tech. Rep. Revision: 2D, 2001.

[3] P.K. Sinha, "Electromagnetic suspension, dynamics and control," IEE control engineering series, vol. 30,New York: Peter Peregrinus Ltd, 1987.

[4] M.E.F. Kasarda, " An overview of active magnetic bearing technology and applications," *The Shock and Vibration digest,* Vol. 32, no.2, pp 91-99, March 2000

[5] P.E. Allaire and E.H. Maslen, "Introduction to magnetic bearings," Mechanical and Aerospace Engineering Dept., University of Virginia, Charlottesville, 1997

[6] P. Allaire, C.R. Knospe, *et al.* "Short course on magnetic bearings," University of Virginia, United States of America, 1997.

[7] D.J. Peel, C.M Bingham, *et al.* "Simplified characteristics of active magnetic bearings," *Journal of Mechanical Engineering Science,* Vol. 216, Issue C5, pp 623-628.

[8] J.Y. Hunh and N.G. Albriton, *et al.* "Non-linear control of magnetic bearing systems," *Mechatronics,* vol. 13 no.6. pp 621-637, 2003 [Online] Available: http:\\www. sciencedirect.com [Date of access: March 2003].

[9] M.T. Thompson. "Electrodynamic Magnetic Suspension – Models, Scaling Laws and Experimental Results," *IEEE Transactions on Education*, vol. 43, no. 3 August 2000

[10] A. Dimarogonas, "Vibration for Engineers," 2nd edition, New Jersey: Prentice-Hall, 1996.

[11] G. Schweitzer, H. Bleuler and A, Traxler, "Active Magnetic Bearings," Zürich :Authors working group, 2003

[12] J.M. Vance, " Rotordynamics of turbomachinery," Texas: John Wiley and Son Inc.,1988

[13] R. Gouws,"The development of an axial active magnetic bearing," Dissertation M.Ing., North-West University, Potchefstroom 2004.

[14] M.E.F. Kasarda and P.E. Allaire, "The measurement and characterization of power losses in high speed magnetic bearings," School of Engineering and Applied Science, University of Virginia, Romac report no 4071997, 1997

[15] T. McCloskey, "Guidelines for the use of magnetic bearings in turbo machinery," Technology insights, San Diego, Calafornia, February 1996

[16] N Mohan, "Power Electronics, Converters, applications, and design," Second edition,New York: Jogn Wiley & Sons, 1995

[17] M.H. Rashid, "Power electronic handbook," California: Academic Press, 2001

[18] J.M.A. Scherpen, "Non-linear control for Magnetic Bearings in Deployment Test Rigs:Simulation and Experimental results," Faculty of Information Technology & systems, Dept. of Electrical Engineering, USA, pp2613-2618,1996

[19] R.C. Dorf and R.H. Bishop, "Modern control systems," 9th edition, Prentice-Hall Inc, 2001

[20] E.Oberg, F.D. Jones, *et al.* "Machinery's handbook," 25th edition, New York: Industrial Press Inc, 1996.

[21] L. Li,T. Shinshi, *et al.*(2002). "Compensation of rotor imbalance for precision rotation of a planar magnetic bearing rotor". *Precision Engineering.* No 5320, pp 1–11 Available: http:\\www. sciencedirect.com [Date of access: March 2003].

[22] R Hertzog, P. Bühler, *et al.* Unbalance compensation using generalized notch filters in the multivariable feedback of magnetic bearings. *IEEE Transactions on control systems technology: Special issue on magnetic bearing control.* Vol. 4, no.5, pp 580-585, Sept. 1996.

[23] R.C.Hibbeler, "Engineering Mechanics Dynamics," SI edition, Prentice Hall 1997.